Applied Physics Reviews REVIEW pubs.aip.org/aip/are

Multi-material additive manufacturing of energy storage and conversion devices: Recent progress and future prospects

Cite as: Appl. Phys. Rev. **12**, 011330 (2025); doi: 10.1063/5.0235864
Submitted: 30 August 2024 · Accepted: 11 February 2025 ·
Published Online: 12 March 2025

Naimul Arefin,[1] Hur-E-Jannat Moni,[1] David Espinosa,[1] Weilong Cong,[2] and Minxiang Zeng[1,a)]

AFFILIATIONS

[1]Department of Chemical Engineering, Texas Tech University, Lubbock, Texas 79409, USA
[2]Department of Industrial, Manufacturing, and Systems Engineering, Texas Tech University, Lubbock, Texas 79409, USA

Note: This paper is part of the APR Special Topic on Frontiers in energy materials research: novel measurement, modelling and processing approaches.
[a)]**Author to whom correspondence should be addressed:** minzeng@ttu.edu

ABSTRACT

The ever-increasing energy demand has highlighted the need for sustainable, low-carbon, and multi-functional energy solutions. Recently, multi-material additive manufacturing (MMAM) has become an emerging processing approach to prototype energy storage and conversion devices by enabling the fabrication of complex systems in a single, streamlined process while offering design freedom to customize end-product properties at precise, user-defined patterns and geometries. Moreover, it provides opportunities to fine-tune interfaces and material compositions at the microscale, opening new avenues for next-generation energy storage and conversion devices. As MMAM is still in its early stages, a comprehensive understanding of the interplay between material chemistry, processing methods, and device design is fundamental to fully realize its potential for developing high-performance energy materials. This review proposes a framework to bridge the gaps between the fundamental principles of processing physics and the practical implementation of various MMAM techniques in fabricating advanced energy storage and conversion devices, highlighting research challenges and future opportunities.

TABLE OF CONTENTS

I. INTRODUCTION

Energy is arguably one of the most critical resources in modern society, as it powers economic growth, technological advancements,

and daily life.[1] On the one hand, estimates suggest that energy demand in the US alone is projected to be between 100 and 115 quadrillion British thermal units (Btu) by 2050;[2] on the other hand, current energy systems are bulky and rigid, often lacking the flexibility needed for customized energy solutions such as self-powered wearable energy technologies.[3] These challenges underscore the need for the development of next-generation energy devices. In past decades, a wide range of energy conversion and storage devices (e.g., batteries, capacitors, fuel cells, energy harvesters) have been extensively studied, which not only provides flexible solutions toward various energy needs/applications but also helps decrease vulnerability to global supply chain disruptions associated with fossil fuels by diversifying energy sources and localized energy production.[4] Although significant advances have been made in different energy materials (e.g., photovoltaics, piezoelectric, thermoelectric, magnetoelectric materials), challenges remain in manufacturing and processing approaches due to the high cost, low stability, and poor efficiency.

Energy devices are traditionally manufactured using blade coating,[5–7] pressurized sintering,[8,9] and injection molding.[10,11] While effective, these methods are often limited by low design freedom and high material waste.[12] Additive manufacturing (AM) has emerged as a promising solution that enables the customized production of energy devices with complex geometries and integrated functionalities. In particular, multi-material additive manufacturing (MMAM) enables the deposition of multiple materials to create compositionally complex systems, including functionally graded materials (FGM),[13] multicomponent segmented materials (MSM),[14] high-entropy ceramics/alloys,[15] and compositionally complex composites (CCC).[16] Most energy devices have at least three components: functional materials, electrodes (current-collecting materials), and packaging materials. The functional material (e.g., piezoelectric material, thermoelectric material) is the heart of the device. Conductive electrodes facilitate the flow of electric current, and the insulating packaging provides structure and houses the other components. Thus, many energy devices can be classified as multi-material (MM) systems. Ideally, MM systems should synergistically integrate multiple materials with different properties (e.g., strength, flexibility, conductivity, thermal resistance) and ensure compatible interfaces for customized functionalities across different fields.[17]

MMAM techniques can be broadly categorized into ink-based and ink-free methods, each offering distinct advantages for fabricating advanced energy storage and conversion devices. Ink-based techniques, such as direct ink writing (DIW), inkjet printing (IJP), and aerosol jet printing (AJP), allow controlled extrusion or jetting of inks with tailored rheological and functional properties, enabling the on-demand fabrication of complex MM energy devices.[18,19] One key advantage of ink-based techniques is the ability to mix and switch between different inks on the fly, which allows the manufacturing of engineered interfaces and graded compositions necessary for optimizing the performance of energy devices.[20] Additionally, ink-based techniques are often compatible with room-temperature deposition/processing and thus are compatible with thermal-sensitive energy materials like chalcogenides (reducing the risk of degradation).[18] In contrast, ink-free techniques like powder bed fusion (PBF) and directed energy deposition (DED) are well-suited for manufacturing MM systems with high density and mechanical properties, making them highly suitable for nuclear energy applications where structural integrity is critical.[21–23] New technologies like two-photon polymerization (TPP) can expand the capabilities of MMAM by enabling micro- and nano-scale fabrication, achieving resolutions as low as 100 nm. To further push the limits of MMAM, some printing modules can be combined to build hybrid platforms to overcome the limitations of individual processes, optimize material composition and structures at a system level (all-print process without the need for further manufacturing),[24] and accelerate the scalable processing of energy materials.

Although there have been notable advancements in 3D printing for energy devices, a comprehensive understanding of the interplay among materials chemistry, processing methods, and device designs in the context of MMAM is still lacking. This review proposes a foundational framework to investigate the correlation between material physics, design methodologies, printing techniques, and applications. We begin with an overview of key fundamental physics related to multi-material processing, such as mixing phenomena and interfacial interactions. Next, we introduce various printing methods and summarize recent developments in post-processing approaches like sintering and annealing to enhance device performance. Following this, our discussion extends beyond traditional device applications and highlights how MM printing enables the development of novel high-performance structures that are otherwise challenging to manufacture using conventional methods. Finally, research challenges are identified, and future opportunities for MM printing technologies are discussed. It is important to note that this review does not aim to cover all types of energy devices; instead, it focuses primarily on electronic energy materials and devices (Table I summarizes the energy systems covered in this review with the performance metrics). Topics like thermal energy storage and chemical energy conversion are beyond the scope of this work and can be found in other literature reviews.[25–27]

II. OVERVIEW OF FUNDAMENTAL THEORY

When it comes to multi-material systems, how different materials connect, distribute, diffuse, and interact at the microscale is a key consideration in MMAM. During this process, common phenomena include material mixing, interface formation, and defect growth. For example, insufficient mixing of nanofillers in FGM can lead to non-uniform local compositions, resulting in sharp interfacial transitions that may introduce defects. These factors are especially critical in fabricating energy devices, where consistent electrical/electrochemical transport and desired contact structures are often needed to maintain device reliability.[36,37] Thus, knowledge regarding the principles governing the mixing process and interfacial bonding is fundamental for achieving the maximum energy output and long-term durability of MMAM-fabricated energy systems.

A. Mixing theory

MMAM involves processing multiple materials in a single build process at different length scales, and thus, the interaction between dissimilar materials is an essential consideration. Mixing different materials can be important for MMAM because it directly affects the composition and properties of the non-segmented devices, such as MMAM of composites and alloys. Proper mixing ensures uniform distribution of the materials, which helps achieve the desired mechanical, thermal, and chemical properties.[38] Inadequate mixing in composites can lead to defects, weak interfaces, and non-uniform properties,

TABLE I. Examples of energy materials and their key performance indicators (KPI). Abbreviations: ITO: indium tin oxide, ABS: acrylonitrile butadiene styrene, CNT: carbon nanotube, LSM: lanthanum strontium manganite, MMA: methyl methacrylate, PLA: polylactic acid, P(VDF-TrFE): poly(vinylidene fluoride-trifluoroethylene), PZT: lead zirconate titanate, rGO: reduced graphene oxide, $Ti_3C_2T_n$: titanium carbide MXene, TPU: thermoplastic polyurethane, YSZ: yttria-stabilized zirconia.

Category	Devices	Examples of metrics	Examples of MM systems
Energy conversion	Solar cells	Power conversion efficiency (PCE), fill factor (FF)	ITO/NiO_x/perovskite/ZnO/Ag[28] (PCE∼26.47%)
	Fuel cells	Area-specific resistance (ASR), power density, and open circuit voltage (OCV)	LSM/YSZ[29] (ASR∼2.1 Ω cm^2)
	Piezoelectric harvester	Output voltage and power density	Carbon/TPU/PZT[30] (output voltage∼20 V)
	Thermoelectric harvester	Figure of merit (zT), power factor, power density	$Bi_xSb_{2-x}Te_3$[31] (zT∼0.94)
	Magnetic harvester	Power density	P(VDF-TrFE)/Ag/$CoFe_2O_4$[32] (power density∼9.7 mW cm^{-3})
	Triboelectric harvester	Power density	Nylon/Ti6Al4V/ABS/PLA/MMA[33] (power density∼4.52 kW m^{-3})
Energy storage	Capacitor	Energy density, power density, capacitance, cycle life	$CoSe_2$-$Ti_3C_2T_n$/Carbon[34] (cycle life∼6000)
	Battery	Energy density, output voltage, cycle life	rGO/CNT/$Ni(OH)_2$/α-Fe_2O_3[35] (energy density∼28.1 mWh cm^{-3})

compromising the performance and reliability of the manufactured parts.[39,40]

The mixing index (MI) is a quantitative measure of the degree of mixing in a system of two co-flowing streams, indicating how uniformly different substances are distributed in a mixture. A higher MI represents greater homogeneity. One way to calculate MI is by using the standard deviation of the concentration of one component in a mixture and normalizing it with the maximum possible standard deviation. MI has been proposed as:[41,42]

$$MI = 1 - \frac{\sqrt{\frac{1}{N}\sum_1^N (C_i - \bar{C})^2}}{\bar{C}}, \quad (1)$$

where C_i and $\bar{C}$ are the concentration of species i and the average concentration of species i at the selected cross-sectional area, respectively, and N is the number of points in the selected cross section perpendicular to the flow. MI = 0 represents an idealized scenario of no mixing where the concentration variation is maximum, with each species in the system retaining its concentration profile as no diffusion or convection-driven mixing occurs at the molecular or bulk level.[43] In contrast, MI = 1 indicates complete homogeneity with zero concentration variance across the system. However, for a comprehensive evaluation of the mixing performance, the pressure drop across the inlet and outlet of the nozzle and the input power must be considered.[38] The mixing cost (MC), a ratio of input power and MI, can predict the performance of mixing based on the required input power to sustain the flow in geometrically complex micromixers.[44]

While the MI provides quantitative indicators for mixing, dimensionless parameters provide a qualitative measure of complex mixing systems by consolidating various factors into a single value.[45] Dimensionless parameters affecting mixing include Reynolds number (Re), Peclet number (Pe), Fourier number (Fo), Knudsen number (Kn), and Dean number (De).[46,47] For instance, the Re number indicates the ratio of inertial to viscous forces and whether the flow is laminar or turbulent, directly impacting the mixing efficiency. Microchannels, with dimensions in the micrometer range, typically exhibit low values of Re ($\ll$100), resulting in laminar flow.[48] Therefore, diffusion plays the dominating role at low values of Re. However, designing mixers with geometrical constraints and external energy sources can increase mixing efficiency by introducing chaotic convection.[46] Pe number represents the relative effects of convection and diffusion in the mixing process.[47] For uniaxial flow, the length of the mixing channel is proportional to the Pe number.[46] Fo number is important in MM mixing because it represents the ratio of average residence time (t_r) to average diffusive mixing time (t_m), indicating the mixing efficiency within a given timeframe.[49] When $Fo < 1$, t_r is sufficient for mixing.[50] When $Fo > 1$, complete mixing would be challenging for the given geometry and flow conditions, as fluid streams may not interact sufficiently.[51] Kn number determines the applicability of boundary conditions, such as no slip or slip, at the fluid-solid interface. $Kn < 0.01$ indicates a continuum regime with viscous forces dominating and negligible molecular effects in mixing.[52] At higher values ranging from 0.01 to 0.1, the no-slip boundary condition is no longer strictly valid, and additional factors such as velocity slip and temperature jump at the boundary can affect the mixing.[53,54] A transitional flow regime occurs when the value ranges from 0.1 to 10, leading to complex flow behaviors that can influence mixing.[55] The De number indicates the influence of curvature on the flow behavior in microchannels.[56] Additionally, De number can indicate the formation of counter-rotating vortices with fluid recirculation known as Dean vortices.[57–59] When $De > 150$, the secondary flow consists of 2 vortices.[60] When $De < 150$, the dean vortices can split into two additional loops.[60,61] Adding more loops improves mixing efficiency but also makes the design more complex. Thus, it is necessary to design high-efficiency mixers with a minimal number of loops. Jiang *et al.*[62] found that the critical De number is 140 and proposed a planar meander

mixer that induces chaotic mixing without requiring complex multi-step or 3D structures.

$$Re = \frac{\rho U D_h}{\mu}, \tag{2}$$

$$Pe = \frac{UL}{D}, \tag{3}$$

$$Fo = \frac{Dt_r}{L^2}, \tag{4}$$

$$Kn = \frac{\lambda}{D_h}, \tag{5}$$

$$De = Re\sqrt{\frac{D_h}{2R}}, \tag{6}$$

where ρ is the density of the fluid, D_h is the hydraulic diameter of the mixing channel, μ is the dynamic viscosity of the fluid, L is the characteristic length of the mixing channel, t_r is the residence time, D is the mass diffusivity, U is the average velocity, R is the average radius of the channel curvature, and λ is the mean free path for the molecules in the fluid.

Depending on the use of external energy sources, mixing can be broadly classified into active and passive. Active mixing uses external energy sources to induce fluid motion and enhance the mixing process, typically employing mechanical, electrical, or acoustic means to create turbulence or controlled flow patterns that improve the homogenization of the mixture.[63] For highly viscous liquids ($Pe > 10^6$), longer channels are required for adequate mixing, leading to greater pressure drops and sometimes making MM printing infeasible. In such cases, active mixers are more effective because the shear rate can be controlled independently from operating flow and channel geometry, minimizing volume, mixing time, and pressure drop. Ober *et al.*[64] developed a framework showing that a low L/D_h ratio is preferred to reduce dead volume for a fixed nozzle diameter, and an active mixer [Fig. 1(a)] at high impeller speed (Ω) can mix at low L/D_h and high Pe.

In contrast to active mixing with impellers, passive mixing can offer simpler designs and often relies on the channel's inherent flow dynamics and geometrical features to enhance mixing without external energy input. Passive mixing often introduces chaotic advection through twisted channels or staggered herringbone patterns and flow field manipulation by varying geometry.[67] Moreover, passive mixing has the potential to manufacture spatially graded structures efficiently with high throughput. For example, a plug-and-play MM chaotic printing method was developed [Fig. 1(b)] by Ceballos-González *et al.*[65] to produce radial and axial gradients in hydrogel filaments. This method utilized chaotic advection within printheads equipped with Kenics static mixing (KSM) elements and multiple inlet ports to achieve complex, well-defined graded microstructures. By adjusting the number of KSM elements, the positions, and the activation of top and lateral inlets, a variety of complex, multilayered patterns can be generated within a single hydrogel filament. Computational fluid dynamics (CFD) simulations help predict microstructures formed by different printhead configurations. Similarly, Wang *et al.*[66] developed a passive mixing method to generate compositional gradients in real-time. This system integrates a microfluidic chaotic mixer [Fig. 1(c)] to create continuous or discrete gradients of bio-inks on the fly by adjusting the flow ratios of the bioinks. The chaotic mixer, featuring a design with slanted ribs and barriers, ensures efficient and rapid bio-ink mixing, producing homogenous solutions with desired gradient levels. This method minimizes bio-ink waste during gradient transitions and enhances the time efficiency of the bioprinting process.

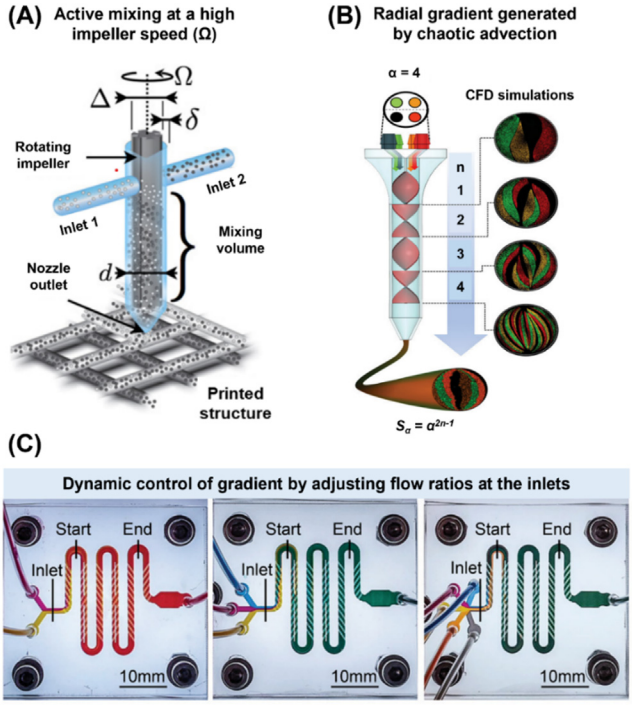

FIG. 1. Examples of mixing strategies in MMAM: (A) Schematic of an active mixer with dual inlets operating at constant impeller speed Ω. Reprinted with permission from Ober *et al.*, Proceed. Nat. Acad. Sci. **112**, 12293–12298 (2015).[64] Copyright 2015, licensed under a Creative Commons Attribution (CC BY) license. (B) Chaotic advection generated by geometrical obstacles along the mixing channel. Reprinted with permission from Ceballos-González *et al.*, Adv. Mater. Technol. **8**, 2202208 (2023).[65] Copyright 2023 Wiley-VCH GmbH. (C) Dynamic control of gradient by controlling the flow ratios of the 2, 3, and 5 inlets in a microfluidic chaotic mixer. Reprinted with permission from Wang *et al.*, Adv. Mater. **34**, 2107038 (2022).[66] Copyright 2022 Wiley-VCH GmbH.

B. Interfaces and defects

To design MM parts efficiently, it is important to understand the material and structural compatibility of the two phases. Compatibility depends on interfacial chemistry, lattice parameters, thermal expansion, and diffusion coefficients.[17] The adhesion at the interface can be influenced by the physical, chemical, and mechanical properties of the dissimilar materials.[68] Additionally, bonding strength and thermal stresses in printed materials depend on geometry, process parameters, post-treatment steps, and environmental conditions.[69] Table II summarizes some defects that typically arise in various MMAM techniques, while a detailed discussion of defects in AM can be found in other literature.[70,71]

Mechanical adhesion at the MM interface can be achieved through the interlocking of different phases with surface irregularities, such as microscopic bumps, pores, and grooves.[80,81] The adhesion between the two phases depends on how effectively the pores are filled. Partially filling the pores may lead to a lower interface strength.[82]

TABLE II. Types of defects that arise in different MMAM techniques and their potential solutions. Abbreviations: DIW: direct ink writing, IJP: inkjet printing, AJP: aerosol jet printing, BJ: binder jetting, FDM: fused deposition modeling, PBF: powder bed fusion, DED: direct energy deposition, VPP: vat photopolymerization.

Methods	Examples of defects	Reasons	Potential solutions
DIW	Layer delamination	Poor interlayer bonding	Introducing interlayer materials or compositional gradient[72,73]
IJP, AJP	Coffee-ring effect	Non-uniform ink drying	Temperature control[74,75]
BJ	Residual porosity, cracks	Low binder saturation	Fabrication of shelled geometries[76]
FDM	Interfacial delamination	Non-uniform thermal gradients	Annealing/Microwave irradiation[77]
PBF, DED	Micro-cracks	Thermal stress concentration	Addition of nucleating agents[78]
VPP	Voids	Trapped bubbles, resin underfill	Visual-guided *in situ* repair[79]

Moreover, interlayer diffusion can also increase the bonding strength. In polymeric MM systems, the polymer chains can diffuse and cause chain entanglement to enhance the interface strength. The diffusion model explains adhesion through the interdiffusion of polymer chains across the interface. Due to the interdiffusion of the chains, a transition zone is formed at the interface. The model is described by Fick's law, where the average penetration depth (x) is given for a certain range of contact time by:[83]

$$x \propto \exp\left(\frac{-E}{2RT}\right) t^{\frac{1}{2}}. \tag{7}$$

Here, E is the activation energy for diffusion, t is the contact time, R is the molar gas constant, and T is the temperature. It is evident from Eq. (7) that the interdiffusion is dependent on the energy input and contact time. Thus, higher printing temperature and reduced printing speed can increase diffusion and interface strength.[84,85] For extrusion-based MMAM methods, the interface strength can be predicted by the contact area of the interface and polymer diffusion between each subsequent layer. Coogan and Kazmer[86] predicted the interface strength of extruded layers by a modified form of Wool and O'Connor's polymer healing model.[87,88] According to the healing model, the maximum strength of the bonded layers is achieved when the polymers have reached maximum entanglement or bonding.

Wetting is another critical phenomenon that influences the interface between two materials. Conventionally, wetting has been used for designing coatings,[89] surfactants,[90–94] and oil-water separation.[95,96] The thermodynamic adsorption or wetting model is crucial for understanding the adhesion mechanisms between two materials.[97] This model emphasizes the significance of interfacial energies. Minimizing the total surface energy through wetting can improve adhesion between the two materials. When a liquid adhesive is placed on a solid substrate, it spreads out to minimize the system's overall surface energy. Surface energy determines the degree to which a liquid spreads. Young's equation describes the minimum surface energy at equilibrium:[98]

$$\gamma_{sv} = \gamma_{sl} + \gamma_{lv} \cos\theta. \tag{8}$$

Here, γ_{sv}, γ_{sb} and γ_{lv} are the surface energy of the solid-vapor, solid-liquid, and liquid-vapor interfaces, respectively, and θ is the contact angle. The liquid must wet the solid for good adhesion, meaning the total surface energy should be minimized. For macroscopic rough surfaces, the Wenzel model in Eq. (9) can be a beneficial tool for designing MM interfaces by maximizing the material contact area.[99]

$$\cos\theta^* = R\cos\theta. \tag{9}$$

Here, R is the roughness factor at the interface, and θ^* is the apparent contact angle. Conversely, the Cassie-Baxter model in Eq. (10) describes wetting on heterogeneous or composite surfaces, which can guide strategies to minimize interfacial tension in incompatible material combinations by inducing a composite wetting state.[99,100]

$$\cos\theta^* = f - 1 + f\cos\theta. \tag{10}$$

Here, f is the fraction of the interface in the composite. Equations (8)–(10) can be used to engineer interfaces for stable and durable MM composites.

Interactions between the materials, such as chemisorption, metallic bonds, van der Waals forces, or hydrogen bonds, can also increase the overall strength of the product interfaces. Chemisorption enhances adhesion by forming strong chemical bonds at the interface. In MMAM, chemisorption is observed in reactive printing methods that involve embedding reactive fillers.[101] Intermolecular forces enhance adsorption between the two phases if both materials are polar. Plasma treatment has often been used to introduce polar groups at the surface to induce adhesion.[102] Furthermore, if both phases can form hydrogen bonds, this effect is amplified, as hydrogen bonds are stronger than van der Waals forces.

At the interface, thermal stress reduction is critical. A mismatch in melting points or thermal expansion coefficients can lead to stress concentration.[103] For metal-ceramic MM systems, the difference in thermal properties at elevated temperatures can cause metal evaporation and promote delamination or cracks.[104] The formation of gradient composition at the interface can counteract the thermal stress concentration. Thus, it is possible to engineer interfaces by fabricating FGM structures.[105,106] The functional variation in FGMs depends on the gradual change in chemical composition, grain size, and physical or mechanical properties. Because of the smooth transition at the interface in FGMs, the residual stress is lowered compared to traditional composite materials.[107]

In MM systems, adding reinforcement materials can strengthen the interface of dissimilar materials. Filler materials such as CNT, graphene, or nano-silica can reinforce the matrix by enhancing the overall toughness and resistance to crack propagation.[108] Based on the matrix type, composites can be classified as polymer matrix composites (PMCs) like thermosets and thermoplastics, metal matrix composites (MMCs), generally with Al, Mg, Cu, and Ti matrices, and ceramic matrix composites (CMCs) using materials like SiC.[109,110] Reinforcement types further differentiate composites into fibrous (continuous and short fibers), particulate (particles like silica or alumina), layered materials (clay), and nanocomposites.[111–114] Three primary

mechanisms, crack deflection, pull-out, and crack bridging, can strengthen the composites' interface by dissipating energy during the embedding process.[115,116] Additionally, various surface treatments on the fibers with functional groups or coupling agents can enhance the adhesion between the matrix and the reinforcement.[117]

C. Design and modeling

In the MMAM workflow, defining and allocating the different materials for each layer, site, and/or voxel within the design is an important step. Thus, designing and modeling MM components requires a comprehensive understanding of material properties, interface interactions, and process parameters. The typical workflow involves creating a geometric model using computer-aided design (CAD), slicing the model into layers, converting it into the standard tessellation language (STL) file format, generating necessary supports, fabricating the component, and performing post-processing operations if required. However, the absence of guidelines and proper tools restricts the design of microstructures with transitioning phases.[118]

Designing FGM structures begins with visualizing geometry, but conventional CAD tools like boundary representation (B-rep),[119] function representation (F-rep),[120] constructive solid geometry (CSG),[119] and spatial decomposition[121] fail to define internal composition or interfaces.[122] Advanced methods such as topology optimization (TO), reverse image modeling, and voxel-based approaches address this gap.[123] TO algorithms, including density-based approaches, level set methods (LSM), and evolutionary structural optimization (ESO), optimize material distribution by iteratively updating density variables to meet performance objectives like stiffness, compositional gradients, or weight reduction.[124,125] For instance, Liu *et al.*[126] developed and optimized eight porous structures using penalized stiffness models and iterative algorithms, achieving final designs after 500 iterations. These designs were converted into CAD models, exported as STL files, and processed for 3D printing with precise layer slicing, enabling scalable and detailed FGM designs.

Furthermore, material attributes, compatibility, and composition of different phases must be considered when designing complex structures. Conventional CAD tools are limited to the 3D Euclidean space E^3.[123] When both geometrical and material attributes are considered, the modeling space can be expanded by a factor of E^k. Here, E^k is the material space, and the exponent k represents the number of materials present in the system.[123] Hence, the composition of the materials can be integrated into the model as:[123]

$$X = (X_g, X_m), \tag{11}$$

$$X_g = (x, y, z) \in \Omega_g \subset E^3, \tag{12}$$

$$X_m = (r_1, r_2, \ldots r_k) \in \Omega_m \subset E^k; \quad 0 \le r_i \le 1, \tag{13}$$

$$\sum_{i=1}^{k} r_k = 1; \quad 1 \le i \le k. \tag{14}$$

Here, X_g represents the coordinates in the geometrical domain Ω_g, X_m is the composition at the position X_g, Ω_m is the material domain, and r_i represents the volume fraction of the ith material. The scalars, r_i sum to one, ensuring that the composition X_m is physically valid.[127]

Optimizing process parameters for microstructures and interfaces conventionally relies on trial-and-error experiments, resulting in extended lead times and increased costs.[128] To date, several modular, cross-platform software packages have been proposed for the simulation of microstructures. For example, "DREAM.3D" is an effective tool for visualizing the interfacial phases.[129] The software supports a wide range of functionalities, including statistical analysis, synthetic microstructure generation, and finite element mesh creation, providing insights into the grain boundary networks, distribution of different phases, and the impact of microstructure on the material performance. Moreover, joining two dissimilar metals may sometimes result in brittle intermetallic phases (e.g., B2, Laves C14 phases) that may induce cracking and delamination.[130,131] The CALPHAD (Calculation of Phase Diagrams) approach is a powerful computational technique used to model the thermodynamic properties of multi-component systems. It involves creating thermodynamic databases from experimental data and theoretical calculations describing the Gibbs free energy of different phases. These databases allow CALPHAD to simulate phase diagrams for binary, ternary, or quaternary systems, providing detailed insights into phase stability, transformations, and equilibria. This method can effectively model the gradient paths and predict the arrangement of different phases at varying temperatures and compositions.[130,132] Bobbio *et al.*[133] utilized CALPHAD and Scheil-Gulliver simulations to design a compositionally stable pathway that avoids the formation of detrimental phases. The ternary phase diagram for the Cr-Fe-Ni-Ti-V system shown in Fig. 2(a) illustrates the composition regions for different phases and the gradient pathways designed for two-powder (red dashed line) and three-powder (blue dotted line) systems. Computationally designed gradient pathway transitions through intermediate compositions involving Ni-20Cr, Cr, and V to ensure a smooth and stable transition from SS316 to Ti-6Al-4V. The study validates the computational design through experimental fabrication and characterization, confirming the predicted phase transitions and the absence of detrimental phases. In addition, Moustafa *et al.*[134] introduced a novel technique for designing FGMs fabricated through high-temperature MMAM techniques (e.g., PBF, DED). The technique involves the creation of non-equilibrium Scheil Ternary Projection (STeP) diagrams that account for the rapid solidification occurring in high-temperature environments. Unlike traditional equilibrium phase diagrams, STeP diagrams provide a more accurate prediction of phase formation by integrating phase fields across a wide range of compositions and temperatures. This approach enabled the identification of optimal composition gradients in Fe-Cr-Al ternary FGMs that avoid the formation of brittle phases.

Various computational tools have been used to predict the final product performance, properties, and geometry of DED and PBF-manufactured components. Finite Element Analysis (FEA) tools, such as ANSYS and ABAQUS, can predict the strain distribution and linear gradient modulus.[136–138] CFD software packages, like FLOW-3D, simulate fluid motion, diffusion, and phase transition while conserving mass, energy, and momentum through nonlinear systems.[139] Additionally, multiphysics simulation platforms like COMSOL Multiphysics combine these analyses to comprehensively understand the thermal, fluid, and structural interactions.[140,141] However, most simulation methods still face challenges, such as high computational power requirements, lengthy computational times, increased costs, and difficulties in acquiring accurate MM data. To narrow the research gap, Rodgers *et al.*[135] proposed a modified kinetic Monte Carlo Potts model that significantly reduced the overall computational costs and time. This approach models the microstructural changes within and around the molten zone during manufacturing. Figure 2(b) illustrates

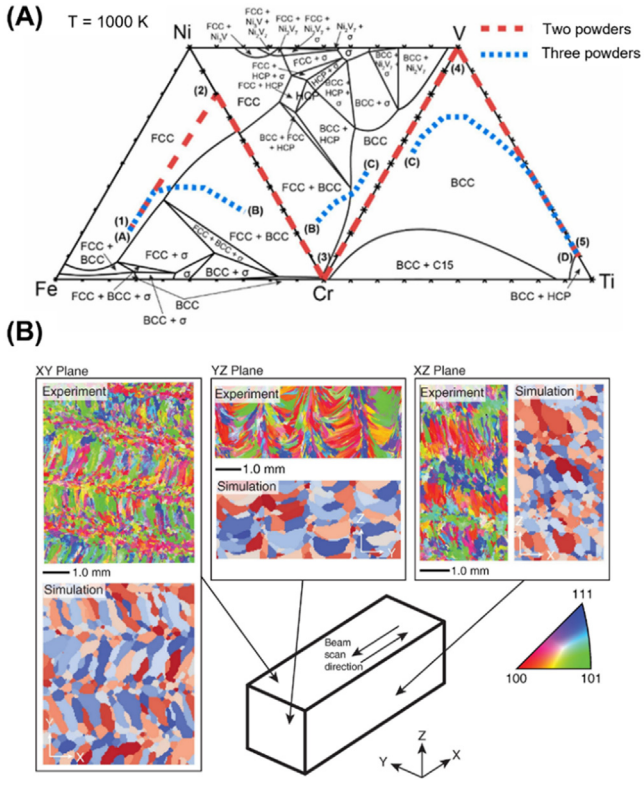

FIG. 2. Examples of thermodynamic analysis and computational modeling on the composition and microstructures of MM systems. (A) Ternary phase diagram at 1000 K for the Cr-Fe-Ni-Ti-V system, illustrating the composition regions for different phases and the gradient pathways designed for two-powder (red dashed line) and three-powder (blue dotted line) systems. Reprinted with permission from Bobbio *et al.*, Additive Manufacturing **51,** 102649 (2022).[133] Copyright 2022 Elsevier. (B) Comparison of experimental and Potts Monte Carlo simulation results for grain orientation and microstructure across different planes (XY, YZ, XZ). Reprinted with permission from Rodgers *et al.*, Comput. Mater. Sci. **135,** 78–89 (2017).[135] Copyright 2017, licensed under a Creative Commons Attribution (CC BY) license.

that the simulation and experimental results of grain orientation and aspect ratios across different planes (XY, YZ, and XZ) align well. The model accurately captures the variation in grain structure induced by different processing parameters (e.g., solidification rate, scanning speed).

III. MULTI-MATERIAL ADDITIVE MANUFACTURING PROCESSES

This section reviews the working principles of various MMAM techniques, including ink-based and ink-free processes. Ink-based printing includes DIW, IJP, AJP, and binder jetting (BJ), while ink-free techniques include FDM, PBF, DED, and VAT photopolymerization (VPP). Both advantages and drawbacks of applying these printing methods for MMAM were discussed; in the meantime, examples of printed MM devices (with application details in energy storage/conversion) are provided. In the end, we also briefly discuss post-processing methods used for MMAM.

A. Ink-based techniques

Ink-based techniques involve formulating printable inks of energy materials with controlled rheology. Depending on the 3D printing technique, the inks can be Newtonian or non-Newtonian. Newtonian inks are suitable for jetting-based AM methods where low viscosity is required.[142] On the other hand, non-Newtonian or colloidal inks have higher viscosity and are ideal for extrusion-based techniques where shear thinning is necessary.[143,144] Using multiple nozzles or sequential printing, these techniques can be customized for MMAM to fabricate various electrochemical devices for energy storage and conversion. Table III summarizes the applications of different ink-based MMAM techniques.

1. Direct ink writing (DIW)

DIW, or robocasting [Fig. 3(a)], is a popular ink-based deposition system where arbitrary structures are fabricated by extruding inks with controlled rheology.[157] These complex inks are formulated by mixing particles in a suspension and systematically adjusting the ink composition to control the rheology.[158] The flow behavior during the ink deposition process can be explained by the Herschel–Bulkley model:[159]

$$\tau = \tau_y + K\dot{\gamma}^n, \tag{15}$$

where τ_y and τ represent the yield stress and shear stress, respectively, $\dot{\gamma}$ is the shear rate, K is the consistency index, and n is the non-Newtonian exponent. Another critical factor in DIW is the ratio of the nozzle diameter (d) to the particle size (a); typically the ratio of $\frac{d}{2a}$ has to be >100–150 to avoid nozzle clogging.[143] The main advantage of DIW arises from its simplicity and versatility, which allows the extrusion system to be modified by integrating multiple microfluidic printheads that can switch,[14,160] or mix[64,161] different inks for MM devices. Furthermore, DIW can be adjusted or integrated with other processing mechanisms for photopolymerization,[162] droplet generators,[163] or FDM printheads for embedded printing.[164] The customizability of DIW allows the fabrication of batteries or other energy devices with complex form factors that maximize the energy density.[19] Recently, Cardenas *et al.*[165] have demonstrated DIW's potential by fabricating batteries with customizable form factors by printing ion-gel separators onto non-planar cylindrical surfaces. Because of these advantages, DIW is often limited by printing resolution with a linewidth typically >0.1 mm.

2. Inkjet printing (IJP)

IJP [Fig. 3(b)] is a non-contact ink-based printing process that employs a jetting mechanism to deposit, build, and support materials in successive layers.[166] IJP can be classified into continuous inkjet printing (CIJP) and drop-on-demand (DOD) methods.[167] The CIJP method releases a steady stream of ink onto substrates.[168] In contrast to CIJP, the DOD method deposits ink droplets selectively onto predetermined locations, reducing contamination and material waste.[169] Based on the ejection mechanism, the printheads for IJP can be thermal or piezoelectric.[170] Thermal printheads have a thin film heater within the ink chamber that forms vapor bubbles and allows inks to flow through the printhead,[171] while piezoelectric printheads convert electrical stimulation into mechanical vibrations, generating a pressure wave that allows droplet formation.[172] In both processes, droplet

TABLE III. Examples of ink-based MMAM techniques and their applications. Abbreviations: AJP: aerosol jet printing, DIW: direct ink writing, GO: graphene oxide, IJP: inkjet printing, LFP: lithium iron phosphate, LTO: lithium titanium oxide, LLZTO: $Li_{6.4}La_3Zr_{1.4}Ta_{0.6}O_{12}$, PAN: polyacrylonitrile, PDMS: polydimethylsiloxane, PEDOT:PSS: poly(3,4-ethylene dioxythiophene) polystyrene sulfonate, PEO: polyethylene oxide, PPCANT: PPy-PANI coaxis nanotube, PVDF: polyvinylidene fluoride.

Printing methods	Functional materials	Application	Reference
DIW	$CoSe_2$-$Ti_3C_2T_n$/Carbon	Hybrid capacitor	34
DIW	GO/PPCANT	Micro-supercapacitor	145
DIW	LFP/LTO/Carbon	Li-ion battery	146
DIW	NdFeB/PDMS/Ga/In	Electromagnetic energy harvester	147
IJP	Ag/PVDF	Self-powered sensor	148
IJP	NiO/YSZ/LSM	Solid oxide fuel cell	149
IJP	NiO/YSZ/LSM	Solid oxide fuel cell	150
IJP	Ag/P(VDF-TrFE)	Piezoelectric energy harvester	151
AJP	PAN-LLZTO/PEO-LLZTO	Lithium metal battery	152
AJP	PEDOT: PSS/Bi_2Te_3/Sb_2Te_3	Thermoelectric energy harvester	153
AJP	P(VDF-TrFE)-Ag/Al/ITO	Triboelectric energy harvester	154
BJ	NiO/YSZ/LSM	Solid oxide fuel cell	155
Screen printing	P(VDF-TrFE)/Ag/$CoFe_2O_4$	Electromagnetic energy harvester	32
Flexographic printing	Ag/PZT	Piezoelectric energy harvester	156

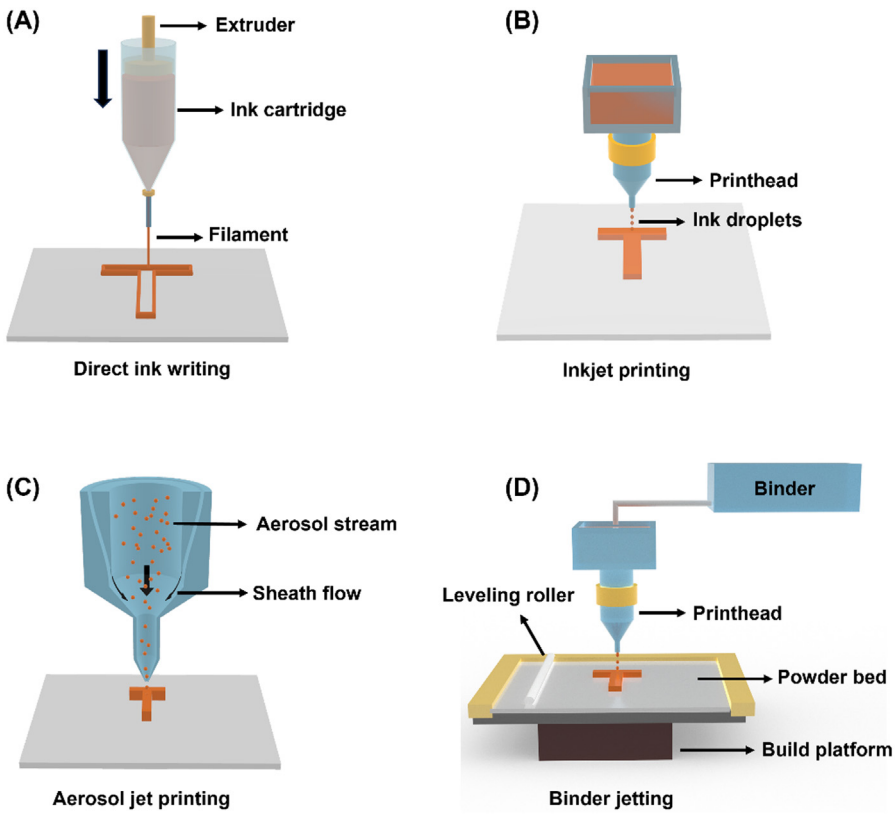

FIG. 3. Schematic diagrams of ink-based MMAM techniques: (a) direct ink writing, (b) inkjet printing, (c) aerosol jet printing, and (d) binder jetting.

ejection is strongly influenced by the ink's physical and rheological properties.[158] To avoid nozzle clogging, the particle size should ideally be less than 2% of the nozzle size.[173] To further enhance resolution, an electrohydrodynamic printing (EHDP) method has been proposed that uses electric fields to eject charged ink droplets with sub-micron level resolution.[174–176] In a recent study, EHDP has been tuned to achieve high throughput by electrohydrodynamic redox printing (EHD-RP), wherein *in situ* mixing of multiple metals and deposition

from a sacrificial anode eliminate any post-treatment steps.[177] The narrow viscosity range of inks (1–50 cP) for conventional IJP systems allows the deposition of only low-viscosity Newtonian fluids.[178] Thus, the ink solvent must be volatile for rapid drying to prevent the spreading or smudging of the printed pattern.[18] The stable jetting of the ink droplets can be correlated by a dimensionless parameter, Z:[167,179,180]

$$Z = \frac{1}{Oh} = \frac{\sqrt{\gamma \rho D}}{\eta}. \quad (16)$$

Here, D is the nozzle diameter, Oh is the dimensionless Ohnesorge number, γ is the surface tension of the ink, ρ is the ink density, and η is the ink viscosity. Stable jetting of ink droplets can only occur when the Z number is between 1 and 14, while lower values prevent droplet ejection and higher values cause satellite droplets.[180] IJP has been widely employed to fabricate MM systems, with precise deposition of various functional materials in complex architectures.[181–184] Moreover, implementing multiple jetting heads can enable parallel material deposition.[185,186] Eggenhuisen *et al.*[184] demonstrated a fully inkjet-printed organic solar cell by depositing six functional layers, including electrodes. IJP's high precision, excellent resolution, and low material consumption have been leveraged to deposit micro and nanomaterials for self-powered wearable thermoelectric devices.[187]

3. Aerosol jet printing (AJP)

Another example of an ink-based jetting process is AJP [Fig. 3(c)], which deposits material in a maskless and non-contact manner.[188–190] This method uses aerosolized ink droplets, aerodynamically focused by a sheath gas and directed onto a substrate.[191–193] The atomization of the ink is done by sonication or flow forces, with droplet sizes typically ranging from 2 to 5 μm.[194] The aerosol is transported through a tube using a carrier gas, typically air or an inert gas. This helps to keep the particles suspended and moving toward the printhead. Once the aerosol reaches the printhead, a sheath gas focuses the aerosol into a fine jet stream (10–100 μm diameter).[195] Aerosolizing and aerodynamic focusing of the ink droplets allows AJP to handle more viscous (1–1000 cP) and particle-laden inks compared to IJP.[158] Moreover, the broader viscosity ranges expand the material types compatible with AJP.[154,196–198] However, ink particles are typically smaller than a few micrometers to prevent clogging of the atomizer nozzle, and their size distribution must be narrowly controlled.[199,200] Another crucial requirement in AJP is to select a suitable solvent that will not evaporate before deposition on the substrate. Like IJP, the AJP process can be modified with multiple aerosol streams and a tunable mixing ratio of inks for MMAM.[198] The on-the-fly mixing of multiple inks can enable localized composition control with high spatial resolution in MM systems.[20,201–203] AJP is widely employed in fabricating energy storage devices due to its ability to create close contact between electrodes and electrolytes while allowing for customizable electrode thickness at the sub-micrometer scale, all without requiring additional masking.[152,204,205] For example, Lopez-Hallman *et al.*[205] utilized AJP to fabricate solid-state batteries by printing a composite cathode and a solvent-free solid polymer electrolyte with a seamless interface between the electrode and electrolyte.

4. Binder jetting (BJ)

BJ [Fig. 3(d)] is a printing technique that selectively deposits compatible polymeric binders through multiple nozzles to connect powder particles layer by layer, forming a solid object at low temperatures.[206] BJ is also one type of ink-based manufacturing in a broad sense, as it utilizes a liquid binding agent. Unlike IJP depositing inks of functional particles, BJ deposits polymeric binders to fuse functional particles in a powder bed. This method stands out because it can produce components from diverse materials, even conventionally unprintable refractory metals. BJ can also have higher build rates and thus can fabricate large devices; for example, a system with 100 nozzles can fabricate parts up to 200 cm^3 min^{-1}.[207] In this process, a layer of powder is spread across the build platform, followed by the precise placement of the binder in specific locations as determined by the digital model.[208] After the initial layer is bonded, a fresh layer of powder is spread over it using a roller, and the binding process is repeated for each subsequent layer until the 3D object is formed. The powder bed is an *in situ* support material, facilitating the manufacturing of complex geometrical structures. In addition to using multiple powder feeds,[209] multiple polymeric binders can be deposited through different nozzles to fabricate heterogeneous MM parts.[210] Furthermore, the local composition of alloys can be controlled by selectively dispensing binders with varying concentrations of alloying elements at specific locations.[211–213] Subsequent debinding and sintering steps are required to remove binder residues and densify the green body.[214] However, lateral wicking of the liquid binder during dispensing can reduce the adhesive forces to keep the structure together.[215] Also, the shrinkage of the printed structure upon post-processing can lower the resolution of the green body.[208] The ability of BJ to create functional gradients has been investigated in the literature to fabricate MM composites for energy storage devices with high conductivity and flexibility.[216] Table IV summarizes the strengths and

TABLE IV. Common strengths and potential weaknesses of various MMAM techniques for manufacturing energy devices.

MMAM techniques	Common strength	Potential weaknesses
DIW	Wide range of materials for customized electrodes[19]	Limited resolution[217]
IJP	Scalable, high resolution, and low material waste[218]	Low active material loading due to rheological constraints[219]
AJP	High resolution enables conformal printing[220]	Variation in ink composition over time[199] higher operational cost[188]
BJ	Suitable for fabricating large components[155]	High cost for mass production[208]
FDM	Low-cost, customizable form factors for batteries[170]	Limited resolution and low surface quality[221]
PBF	High strength, no requirement for support structures[222]	Energy intensive, low surface quality[82]
VPP	Higher spatial resolution suitable for microstructures[223]	Limited range of materials, high costs[224]

TABLE V. Examples of ink-free MMAM techniques and their applications. Abbreviations: DLD: direct laser deposition, DLP: digital light processing, EBM: electron beam melting, FDM: fused deposition modeling, FEP: fluorinated ethylene propylene LENS: laser engineered net shaping, PBF: powder bed fusion, SLM: selective laser melting, SLA: stereolithography, SLS: selective laser sintering, YPSZ: yttria partially stabilized zirconia.

Print methods	Functional materials	Application	Reference
SLS	NdFeB/TPU	Magnetoelectric energy harvester	225
FDM	ABS/FEP/PLA	Hybrid droplet-based electric generator	226
PBF	NiO/YSZ/LSM	Solid oxide fuel cell	227
DLP	PtO_2/WO_3	Catalyst for hydrogenation of alkynes	228
LENS	ZrTiVCrFeNi	H_2 storage	229
DLD	FeAlCuCoCr/YPSZ/SiB_2	Aviation turbine blade	230
SLM	$Al_{0.5}$FeCoCrNi	Turbine blade	231
EBM	Stainless steel	Parts for thermonuclear reactor	232

weaknesses of various ink-based and ink-free MMAM techniques for manufacturing energy storage and conversion devices.

B. Ink-free techniques

Ink-free AM techniques refer to methods that do not rely on drying-induced solidification of liquid- or paste-based inks. Based on the solidification mechanism, these techniques can be further categorized into melting-based (e.g., PBF and DED) and cross-linking-based (e.g., SLA, DLP, and TPP) techniques. Since these processes typically do not rely on ink formulation, the amount of inactive materials can be minimized when fabricating energy devices, thereby enhancing electrical/mechanical performance. Table V summarizes the applications of different ink-free MMAM techniques in energy device fabrication.

1. Fused deposition modeling (FDM)

FDM is a pressure-driven AM process that involves melting thermoplastic filaments through heated extrusion heads and depositing the filaments layer by layer to build the 3D object.[233] The extrusion system can be customized by employing coaxial feeding of different polymers or by using multiple extruders to fabricate MM systems.[234] Introducing static or dynamic mixing inside the extrusion nozzle can enhance the interface strength of the MM composites.[234,235] However, typical nozzle diameters of 200–500 μm can limit the resolution of the final product.[236] In addition, thermal gradients present in the deposited layers may allow defect formation, such as warping or deformation.[236,237] FDM has been widely used to manufacture storage systems with high energy density and minimal material waste.[238,239] Thermoplastic polymers such as PLA, ABS, and polymethyl methacrylate (PMMA) have been used to develop energy storage devices free from the interdiffusion issue between electrodes and electrolytes.[240,241] However, these polymers must be mixed with conductive fillers to make the composite conductive.[242] If the material is still not conductive enough, parts of the insulating polymers need to be removed by sintering or etching.[243,244] Polymer composites such as PLA/graphene,[245] PLA/LTO/carbon,[243] PLA/LFP/carbon,[243] and ABS/Carbon[246] are commonly used to fabricate electrodes for energy storage devices. Palacios-Corella *et al.*[247] fabricated hetero-layered FDM-printed electrodes with alternating layers of CNTs and carbon filaments that have the potential to be used in energy conversion devices like fuel cells.

2. Powder bed fusion (PBF)

PBF [Fig. 4(a)] is a group of AM techniques that typically use a laser or electron beam as the thermal energy source to melt/sinter material powders, layer by layer, to fabricate 3D structures.[248] Various commercially developed printing processes, such as SLS, SLM, or direct metal laser sintering (DMLS), are variations of the PBF process.[249] The energy delivered to the melt pool in the PBF process is controlled by focusing the beam onto a smaller area to minimize the melt pool and increase the energy density.[250] The energy density (E_d) of the melt pool can be estimated as:[251]

$$E_d = \frac{P}{vht} \tag{17}$$

Here, P, v, h, and t are the beam power, scan speed, predefined hatch spacing, and layer thickness, respectively. Over the years, PBF has shown promise in reducing the total number of components with higher production rates for thermal energy conversion devices.[252] However, rapid cooling rates, reaching 10^4–10^8 K/s, can result in surface and sub-surface defects in the final product.[253] Utilizing process sensing during the PBF process can enhance understanding of the complex physical mechanisms occurring in the melt pool and enable the *in situ* detection and control of defect formation.[254] PBF can fabricate MM systems by switching powder feedstocks between layers, where different materials are deposited at specific layers.[255,256] This process can either involve manual changes in the material or innovative techniques like powder layup and removal or a hopper-nozzle system that precisely places and mixes materials within and between layers.[257,258] Thus, metallurgically compatible transitions at interfaces can be introduced to reduce stress concentration between dissimilar materials.[259] Optimizing process parameters is vital for successfully remelting previous layers and enhancing metallurgical adhesion between subsequent layers. Furthermore, smaller particle sizes can enhance the homogeneity of the final component and reduce micro-defects.[260] PBF has been increasingly adopted for manufacturing core components in thermonuclear reactors, offering enhanced radiation tolerance and improved corrosion resistance.[21–23] Additionally, PBF has been

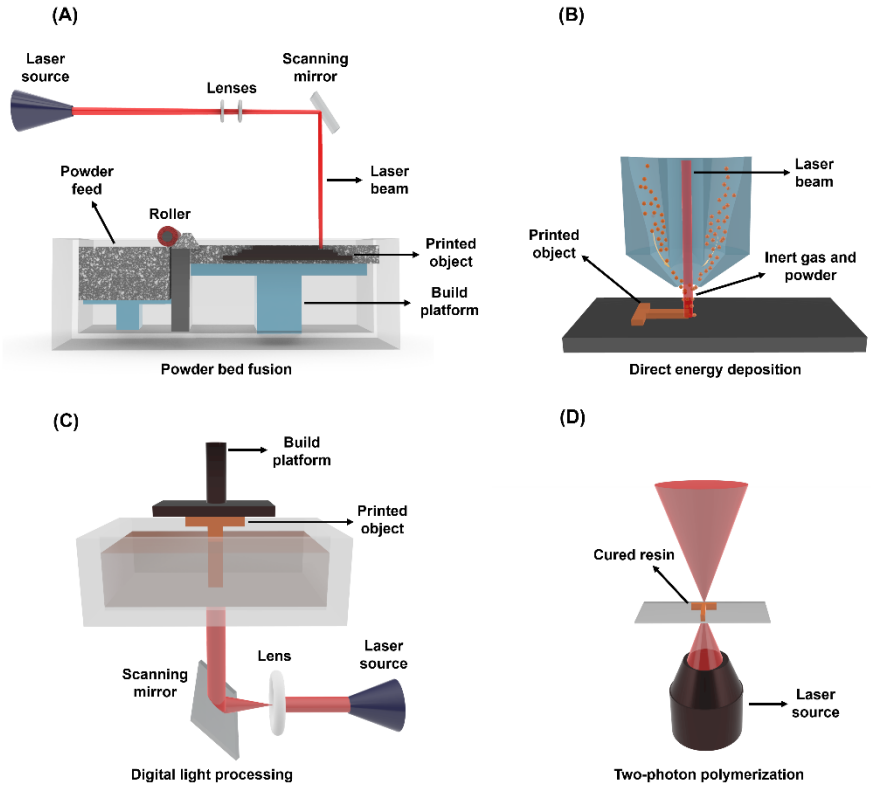

FIG. 4. Schematic diagrams of ink-free MMAM techniques (a) powder bed fusion, (b) direct energy deposition, (c) digital light processing, and (d) two-photon polymerization.

effectively used to produce MM bipolar plates reinforced with CNF for proton exchange membranes in fuel cells.[261]

3. Direct energy deposition (DED)

In DED [Fig. 4(b)], a concentrated thermal energy source, such as a laser, electron beam, or plasma, fuses metals delivered from a powder feedstock by melting them at high temperatures and then rapidly solidifying.[262] Due to the energy source, a melt pool is formed with a dynamic equilibrium.[263] The deposited material solidifies as the heating source moves, forming a continuous metal track. The tracks are arranged to overlap based on predetermined hatch spacing (the distance between consecutive tracks). Once a layer is complete, the deposition nozzle and the powder feedstock elevate by a predefined slice thickness to initiate the deposition of the subsequent layers. DED processes are differentiated depending on the energy sources and material feedstocks used, leading to their classification into several commercial types: Laser Metal Deposition (LMD), Direct Metal Deposition (DMD), Direct Light Fabrication (DLF), Wire and Arc Additive Manufacturing (WAAM), and Laser Engineering Net Shaping (LENS).[264] DED processes are distinguished by their high deposition rates (~0.5 kg/h for LENS,[265] ~10 kg/h for WAAM[265]) but limited by dimensional accuracy. *In situ,* the mixing of multiple powder feeds allows the fabrication of gradient structures and MM layers.[266] DED has been attracting interest in the energy sector, particularly for nuclear applications.[267,268] DED can repair or coat components such as turbine blades, fuel rods, and other components exposed to high radiation and thermal stresses in nuclear energy systems, reducing downtime and extending the lifespan of nuclear reactors.[269] Additionally, the capability of DED to fabricate complex geometries enables the development of efficient cooling systems and heat exchangers by optimizing the component design to enhance heat transfer efficiency in nuclear plants. High-entropy alloy coating of AlCoCrFeNi was successfully applied to a stainless-steel component using a DED process that exhibited enhanced irradiation and corrosion tolerance.[270] DED has also improved the resistance to irradiation-assisted stress corrosion cracking (IASCC) in metal alloy components.[271]

4. Vat photopolymerization

VPP is a light-driven AM technique that selectively cures liquid photopolymer resins with a focused UV light source, with faster build speeds and higher resolution than other mature AM techniques.[272] VPP has many variants based on scanning and curing techniques such as SLA, micro-SLA (μSLA), DLP, and TPP.[223] In these techniques, the submerged platform in the liquid vat is scanned by a laser beam and is cured at specific locations based on a predetermined 3D model. After a layer is cured, the build platform moves in the vertical direction by the layer height, and the cycle is repeated until the 3D object is complete. However, a potential concern for VPP is the possibility of uncured resins and residual photo-initiators, which might be cytotoxic.[273] The resolution in light-driven printers is determined mainly by the curing depth (C_d) of the composite resin. The curing depth can be theoretically modeled according to the Beer-Lambert law,[274]

$$C_d \propto \frac{d}{Q\Phi}\ln\left(\frac{E}{E_c}\right), \tag{18}$$

where d is the average size of the particles, Q is the scattering index of the composite resin, Φ is the volume fraction of the particles, E is the exposure intensity, and E_c is the critical exposure intensity for triggering the polymerization reaction. It is evident from Eq. (18) that the composite resin must be tuned with specific liquid resins compatible with the selected material particles to increase UV absorptivity and reduce scattering for efficient curing and higher resolution. Adding a photo-initiator and light-absorbing monomers/oligomers can trigger the photopolymerization reaction and improve the final printed structure.[275,276] μSLA systems can achieve an x-y resolution of 2 and 30 μm in the z-direction.[277]

Mask-projection vat photopolymerization (MPVP) or DLP (Fig. 4C) varies with SLA only in the curing method. DLP uses liquid crystal displays (LCDs) or digital micromirror devices (DMDs) as projection devices to cure the entire layer of a photopolymer resin simultaneously.[278] Hence, DLP can reach higher fabrication speeds of up to 15 mm/s and resolutions down to 1 μm.[279,280]

TPP, direct laser writing (DLW), or two-photon absorption (TPA) [Fig. 4(d)] utilizes the nonlinear optical process of two-photon absorption. This allows for the polymerization of photosensitive resins at the highest light intensity, generally at the focal point, enabling the creation of high-resolution micro-scale and nano-scale structures.[281] High-energy radiation leads to multiple photon absorption that triggers the cross-linking or decomposition of the photopolymer in a nonlinear manner.[282] While SLA and DLP typically do not achieve nano-scale resolution, TPP can reach resolutions as low as 10 nm, much lower than the theoretical diffraction limit.[283–285]

For fabricating MM systems through VPP, rotating platforms with multiple vats can be employed.[286–288] However, this approach significantly increases production time due to the longer time required to switch the vats. Downtime can be reduced by integrating dynamic fluid control of multiple photopolymers within VAT.[289] Dolinski *et al.*[290] developed a novel solution-based mask liquid lithography (SMaLL) technique with a one-step MM 3D printing method that utilizes tunable visible wavelength photoswitches combined with orthogonal cross-linking reactions. SMaLL can achieve high-resolution, isotropic structures using photobleaching fronts, providing deep curing, fast build rates, and creating complex bioinspired designs such as soft joints and brick-and-mortar architectures. Baek *et al.*[291] used DLP to create complex 2D and 2.5D architectures of multiple inorganic materials with engineered microstructures for a micro-scale thermoelectric energy harvester. Although VPP techniques have not yet been widely adopted for fabricating multi-material energy devices, the higher resolution and printing speeds compared to more established MMAM methods present promising opportunities for future research in this area.

In addition to single deposition techniques, hybrid methods have been developed by combining two or more techniques to fabricate MM systems. Some examples of hybrid MMAM techniques for energy applications are listed in Table VI, while detailed descriptions of hybrid MMAM techniques can be found in other literature reviews.[292,293]

C. Post-processing methods

Post-processing treatments for energy devices are critical for optimizing electrical, electrochemical, and mechanical performance over long-term use. The as-printed devices typically undergo various mechanical, thermal, or chemical treatments to decompose inactive materials, modify composition and surface morphology, and remove contaminants that could otherwise hinder energy output.[299] Ink-based processes (e.g., solutions, dispersions, gels) often require a curing step (i.e., sintering, liquid evaporation, gelation) to remove inactive materials (e.g., solvents, stabilizers, additives), promote structural stability, and enhance the functionality of the final device.[19,300] For energy devices, these curing steps must ensure specific functional properties without degradation of the MM structure. Depending on the material properties, the curing or sintering process can be done by thermal, chemical, light, or laser methods.[158,301,302] Similarly, solution-based inks containing metal precursors must also be sintered to reduce the metal ions to their elemental state.[303,304] Moreover, the performance of some devices might need to be fine-tuned by additional elemental doping during post-processing.[305]

In ink-free MMAM techniques, defects, such as cracks, delamination, porosity, and powder agglomeration, influence the microstructure at the interface.[306–308] Thus, post-processing steps are needed to reduce the micro-defects and residual stresses between the interface.[309] High-temperature annealing techniques such as solution heat treatment (SHT),[310] hot isostatic pressings (HIP),[311] and thermal annealing[312] can release residual stresses. For example, HIP is a thermo-mechanical method that operates under temperatures up to 2000 °C in an inert environment with high pressures reaching 200 MPa.[313] This extreme environment causes the densification of the materials, eliminating

TABLE VI. Examples of hybrid MMAM techniques and their applications. Abbreviations: BTO: barium titanate, FFF: fused filament fabrication, NZF: NiZn ferrite, PP: polypropylene.

Printing methods	Functional materials	Application	Reference
DIW, FDM	Carbon/CNT/$ZnSO_4$/PLA	Hybrid capacitor	294
DIW, FFF	Carbon/Ag/KCl/PP	Capacitor	164
DIW, FFF	Ag/TPU/BTO/PLA	Piezoelectric energy harvester	295
AJP, DIW	Ag/Silicone/Te	Self-powered sensors	296
FDM, SLA, SLM	Nylon/Ti6Al4V/ABS/PLA/MMA	Triboelectric energy harvester	33
FDM, SLM	Ni-MoS_2/stainless steel/Ni-Fe/PLA	Electrolyzer	297
DIW, DLP	NZF/photocurable resin	Inductive force sensor	298
DIW, IJP	LSM-YSZ/YSZ	Solid oxide fuel cell	29

defects and pores.[314] Applying thermal treatments in DED-manufactured parts can significantly reduce the detrimental laves phases and micro-segregation.[315] Furthermore, laser peening can improve the fatigue resistance of metal composites.[316] This process applies plastic compression perpendicular to the surface to induce lateral expansion.[316] Higher strain rates can also trigger continuous dynamic recrystallization to refine the grain boundaries.[317] The surface irregularities in the fabricated components can be reduced by laser polishing, machining, and abrasive finishing.[318,319]

Although post-processing methods for MMAM are similar to conventional single-material AM, it is worth mentioning that MM systems may require additional considerations and optimizations. Different materials in the energy device may require varying sintering temperatures because of dissimilar properties, such as the thermal expansion coefficient. Thus, selective and sequential post-processing methods must be applied based on the compatibility of the different materials. Materials that have higher thermal stability or require harsher sintering conditions must be deposited and treated first, followed by the next material with the lower requirement. Additionally, photonic or laser sintering has the potential for localized heating and could effectively reduce the risk of degradation by selective sintering of each material layer.[320,321] Cutting-edge techniques, such as cold sintering, can be applied to co-sinter ceramic-polymer composites from room temperature to 300 °C.[322] Alternatively, hybrid platforms integrating different post-processing techniques must be developed for fast and efficient curing steps.

IV. DEVICE APPLICATIONS

A. Energy storage

Conventional methods of fabricating energy storage devices, such as capacitors and batteries, often face several challenges due to their multi-step and subtractive nature. These challenges include limited design flexibility, high material waste, and lengthy and complex assembly processes that can lead to increased design-to-product time and environmental concerns.[323] In this context, MMAM can be a game changer by bridging the gap between advanced energy material discovery and their integration into electrochemical energy storage devices (EESDs) in a single step. Table VII provides a detailed comparison of conventional and MMAM techniques for manufacturing energy storage and conversion devices. This section will only focus on electronic energy devices, whereas other energy devices, such as phase-change materials, thermal cells, and wind turbines, can be found in other literature.[324,325]

1. Capacitors

Capacitors are passive electronic devices with a dielectric layer between two conductive electrode layers to store electrical energy. Developing advanced dielectrics, electrolytes, and electrode materials has been a prime focus for manufacturing next-generation capacitors with enhanced energy density, reduced charging times, and extended cycle lives (exceeding 1000 cycles).[336,337] Capacitors can be fabricated through MMAM by printing the bottom electrode layer first on a substrate and then sequentially printing the dielectric and top electrode layer, thereby removing process complexity that generally arises in conventional techniques such as compression molding,[338] electrospinning,[339] and solvent coating.[340] Among the different MMAM techniques, ink-based methods are more frequently used because they allow easy customization of the inks with organic,[341] metallic[342] or ceramic fillers.[143]

Carbon-based materials, for example, have been widely used as nanofillers in ink formulations because they offer high surface area and capacitance.[343] Rocha *et al.*[344] developed scalable thermo-responsive inks for fabricating graphene electrodes for supercapacitors. Chemically modified graphene (CMG) was used as the active electrode material, and copper was used as the current collector. Because graphene can handle high current densities ($\sim 4 \times 10^7\,\mathrm{A\,cm^{-2}}$)[345] and offers a large surface area ($\sim 2360\,\mathrm{m^2\,g^{-1}}$),[345] the MM structure showed low resistance at the electrode-current collector interface and maintained structural stability. The supercapacitors assembled using these electrodes maintained high electrochemical performance and stability over 10 000 cycles. Furthermore, metal oxides and noble metals have also been explored as active materials due to their pseudocapacitive properties. However, these materials are susceptible to dendrite formation, which limits their functional and structural performance.[346] Liu *et al.*[294] developed zinc-ion hybrid capacitors through multistage sequential printing of a porous cathode, a graphene-based metal anode stabilizer, and a quasi-solid gel electrolyte. The graphene-based metal stabilizer allowed homogeneous deposition of the Zn^{2+} ions, inhibiting dendrite formation that allowed 100% capacity retention over 10 000 cycles.

Encapsulating the electrodes in flexible packaging can enhance the stability of the capacitors and prevent potentially hazardous electrolyte leakage.[347] Yuan *et al.*[348] fabricated an all-printed micro-supercapacitor (MSC) by sequentially printing and encapsulating the activated carbon electrode within a gel electrolyte [Fig. 5(a)]. Encapsulating the electrodes shortened the ion transport paths while improving flexibility and stability, maintaining a capacitance retention of 96.84% even under high strain. Similarly, Fieber *et al.*[164] fabricated

TABLE VII. Comparison of conventional manufacturing techniques with MMAM techniques for manufacturing energy devices.

Aspects	Conventional manufacturing techniques	MMAM techniques
Material range	Wide material types[326]	Limited by material compatibility[17]
Design freedom	Limited to standard geometries[327]	Near complete design freedom[328]
Costs	Cost-effective for high-volume production[329]	Cost-efficient for low-volume prototyping[330]
Scalability	Scalable to standard designs[331]	Lower scalability[332]
Properties	Limited scope for customization of properties[333]	Tailorable properties within a single device[31]
Environmental Impact	High material waste[334]	Minimal material waste[335]

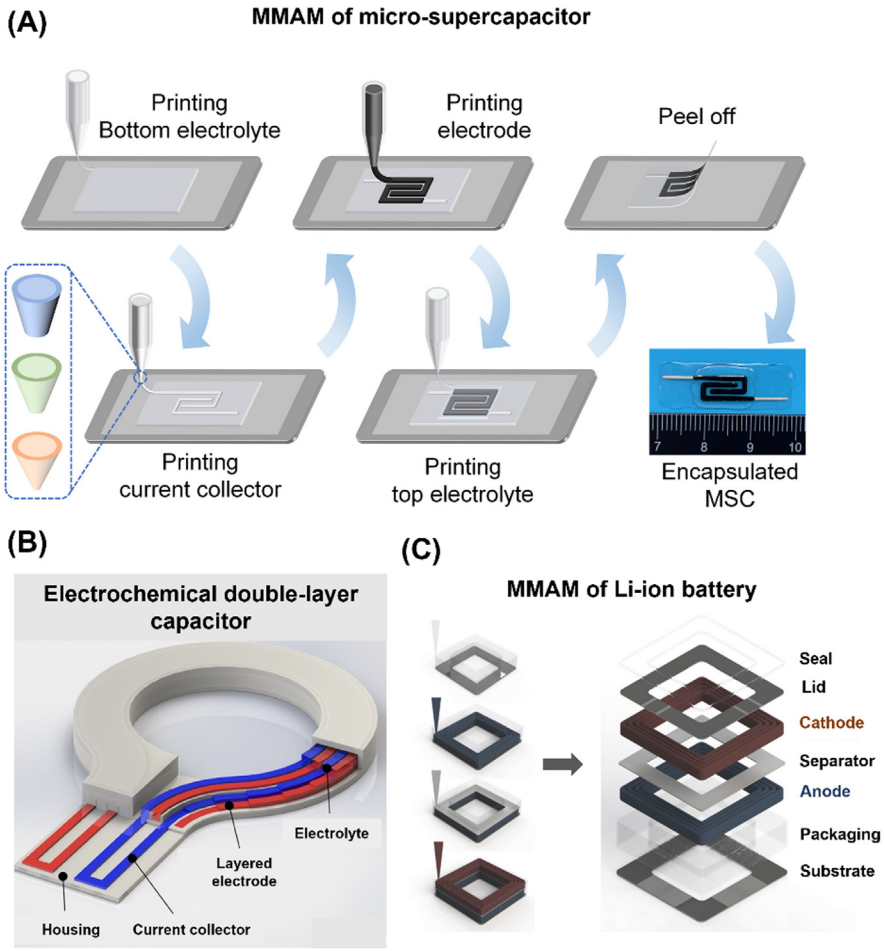

FIG. 5. MMAM of energy storage devices: (A) Schematic of the printing process for an all-printed micro-supercapacitor. Reprinted with permission from Yuan *et al.*, Energy Environ. Mater. **7**, e12657 (2024).[348] Copyright 2024, licensed under a Creative Commons Attribution (CC BY) license. (B) Schematic of an electrochemical double-layer capacitor with a layered electrode within a polypropylene housing. Reprinted with permission from Additive Manufacturing **28,** 344–353 (2019).[164] Copyright 2019 Elsevier. (C) Fabrication process of all-printed lithium-ion batteries. Reprinted with permission from Adv. Mater. **30**, 1703027 (2018).[146] Copyright 2018 WILEY-VCH Verlag GmbH & Co. KGaA, Weinheim.

all the components of an electrochemical double-layer capacitor through a single-operation, hybrid MMAM process [Fig. 5(b)]. This method successfully produced functional ring-shaped capacitors using activated carbon electrodes and a KCl hydrogel electrolyte encapsulated inside a polypropylene housing to prevent leakage. The all-printed capacitor had a columbic efficiency of 99.6 ± 0.4% in its as-printed state while demonstrating gravimetric and areal capacitances of 116.4 ± 0.6 F g^{-1} and 599.2 ± 3.0 mF cm^{-2}, respectively, at a scan rate of 10 mV/s.

Additionally, developing additive-free inks for energy devices has been under focus over the past few years. The post-processing steps required for decomposing the additives often degrade the electrical conductivity and energy density of the overall device.[349,350] Zhang *et al.*[351] have developed additive-free graphene inks for 3D printing customizable MSCs. The exfoliated graphene ink enables large-scale production without cryogenic assistance or post-processing reduction. The integrated MSC pack exhibited a maximum areal cell count density of 16 cells cm^{-2} and an output voltage of 192.5 V, one of the highest reported for 3D-printed MSCs. While additive-free ink formulations can address challenges in scalability by reducing complexity in the MMAM workflow, the development of recyclable capacitors can promote sustainability and a circular economy.[352] Recycling e-waste from end-of-life electronic devices can reduce environmental impact.[353] Sanati *et al.*[354] recently developed an MM-printed supercapacitor using eutectic gallium indium (EGaIn) droplets coated with rGO nanosheets. The enhanced stretchability and reduced electrochemical gauge factor of EGaIn make the capacitor suitable for wearable electronics. A standout feature of this device is its recyclability, achieved through an electrowinning process that enables the recovery of gallium and silver from used supercapacitors. Similarly, Idrees *et al.*[355] highlighted the importance of integrating recycling into developing advanced energy storage systems by fabricating a fully 3D-printed capacitor using activated carbon recovered from packaging waste.

2. Batteries

Batteries are among the most widely used EESDs due to their availability in various forms, high energy density, and long power duration.[356] Typically, three primary components of a battery are the anode, cathode, and electrolyte.[357] Assembly of these layers is done through layer-by-layer stacking and winding techniques, which can restrict the electrode geometries to standard designs (e.g., cylindrical, prismatic, pouch, coin cells), resulting in suboptimal material

utilization and energy density.[358] Moreover, the energy and power density decrease as the ratio of active materials to inactive materials (e.g., current collectors and separators) decreases.[359] MMAM can facilitate the manufacturing of advanced batteries through complex electrode designs and the combination of functional MMs to reduce the amount of inactive materials. Additionally, embedding current collectors in the form of CNF or CNT can keep the ionic paths short.[6,360] Furthermore, the design freedom provided by MMAM enables the fabrication of interdigitated structures for electrodes, providing a higher surface area for ion diffusion with a shorter pathway for electron transfer.[361]

In traditional manufacturing techniques, the electrolyte and the electrodes are fabricated separately. Thus, during assembly, a lack of adhesion between the electrolyte and the electrode might induce shorting or hamper the mechanical integrity during operation.[362] Meng *et al.*[363] developed a multi-nozzle printing method that fabricated current collectors, electrodes, and electrolytes in one step with intercalated Na^+ ions inside $LeFePO_4$ for enhancing ion migration channels. The all-printed battery demonstrated a discharge capacity of 91.3 mAh g^{-1} after 2000 cycles, with a charge/discharge efficiency exceeding 96%. Fu *et al.*[364] fabricated rGO-based electrodes and a solid-state electrolyte for lithium-ion batteries (LIBs) through an MMAM process. The electrode inks included highly concentrated rGO sheets mixed with LFP and LTO for the positive and negative electrodes. The GO sheets' alignment along the extrusion direction enhanced electrical conductivity, while their porous structure allowed higher electroactive material loading. The printed electrodes demonstrated high specific capacities close to theoretical values (LFP: ∼170 mAh g^{-1} and LTO: ∼175 mAh g^{-1}) and stable cycling performance. The high electrical conductivity (LFP/rGO ∼31.6 S cm^{-1}, LTO/rGO ∼6.1 S cm^{-1}) contributed to the excellent electrochemical performance. An alternative approach to enhance the energy density of printed batteries is to create thick electrodes (≫100 μm).[365,366] However, this approach limits the power density as the transport resistance for ions and electrons is increased.[367,368] Wei *et al.*[146] customized LIBs with thick electrodes, achieving significant improvements in areal capacity with comparable power density to thin electrodes [Fig. 5(c)]. They demonstrated the fabrication of all-printed LIBs using semisolid electrode inks, photosensitive packaging ink, and separator inks.

LIBs utilizing liquid organic electrolytes are widely considered to have achieved their maximum theoretical energy density (250 Wh kg^{-1}).[369] However, the emerging energy demand and the safety issues associated with organic electrolytes have prompted research on developing higher energy density (∼400 Wh kg^{-1}) solid-state lithium batteries (SSLB).[370,371] For example, Blake *et al.*[372] introduced a novel method for creating DIW-printed ceramic polymer electrolyte (CPE) for SSLB, utilizing a dry phase inversion technique that mixes N-methyl-2-pyrrolidone and glycerol to form highly porous structures without additional post-processing treatments. The multilayer printing of the electrodes and the electrolyte ensured tight and continuous interfacial contact. However, the energy density of SSLBs is often limited as the solid-state electrolytes face challenges in withstanding both the reduction and oxidation environments in the anode and cathode.[373] Jiang *et al.*[152] developed a combinatorial printing process to fabricate a functionally graded solid-state electrolyte (FGSSE) that simultaneously handles both the reduction and oxidation environments. The smooth transition of oxidation-tolerant PAN and reduction-tolerant PEO in the FGSSE exhibited oxidation stability exceeding 5.5 V and ionic conductivity over seven times higher than traditional heterogeneous multilayered solid-state electrolytes. In addition to SSLBs, other solid-state battery technologies, such as those based on nickel, iron, sodium, and zinc, also present promising alternatives due to their abundant resource availability. Kong *et al.*[35] fabricated Ni-Fe batteries with rGO/CNT-$Ni(OH)_2$ cathode and rGO/CNT-α-Fe_2O_3 anode. Utilizing a 3D-printed rGO/CNT micro-lattice as a scaffold, the batteries exhibited high energy density with an active material loading of 130 mg cm^{-3}. Additionally, the batteries demonstrated long-term cycling durability with high-capacity retention after 10 000 cycles.

In recent years, the demand for smart, flexible, and wearable EESDs has been on the rise, particularly for bio-signal monitors and various other wearable technologies.[374] Wang *et al.*[375] addressed these challenges by utilizing MMAM to develop flexible, all-fiber LIBs. These batteries combine CNTs with LFP or LTO to print fiber electrodes, demonstrating flexibility and high electrochemical performance. Their method involves the co-extrusion of highly viscous polymer inks. This process ensures structural fidelity and mechanical robustness and integrates the electrodes with a gel polymer electrolyte, enhancing the device's flexibility and electrochemical properties. The resulting all-fiber LIBs exhibit a high specific capacity of approximately 110 mAh g^{-1} at a current density of 50 mA g^{-1} while maintaining mechanical flexibility that allows integration into textile fabrics. Li *et al.*[376] developed a highly conductive and mechanically robust CNT/NFC composite microfiber. The homogeneous alignment of CNTs within the microfiber network improved mechanical and electrical properties. The amphiphilic nature of NFCs facilitated the uniform dispersion of CNTs in the aqueous solution. The 3D-printed CNT-NFC microfibers had a tensile strength of 247 ± 5 MPa and an electrical conductivity of 216.7 ± 10 S cm^{-1}. Gallium-based batteries have drawn interest among researchers due to their high stretchability for wearable applications and the ease with which gallium can be recycled from composites.[377] Additionally, the low melting point of gallium (∼29 °C) allows higher diffusion of ions and reduced volume change during charge/discharge cycles.[378] Freitas *et al.*[379] developed an all-printed MM silver-gallium (Ag-Ga) battery with an aerial capacitance of 78.7 mAh cm^{-2} and stretchability of up to 170%. The composite ink used to fabricate the electrode did not require sintering and was printable at room temperature. These batteries can be a promising solution for wearable and flexible electronics and Internet of Things (IoT) devices.

The performance of metal batteries can be reduced by dendrite formation. Dendrites are needle-like formations that develop from uneven lithium-ion deposition on the anode during battery charging.[380] The needlelike structures can pierce the anode and cathode separators as they build up, causing internal short circuits.[380] This reduces the battery's capacity and lifespan by creating unwanted electrical paths and increases the risk of fires or explosions due to thermal runaway conditions.[381] Cao *et al.*[382] demonstrated the effective use of NFCs in preventing dendrite formation in 3D-printed lithium metal batteries (LMBs). Using NFCs as a scaffold for lithium metal decreased the local current density and improved ion accessibility at the anode. This configuration suppressed dendrite growth, a common issue that leads to short circuits and decreased cyclability. Additionally, the LMBs exhibited a capacity retention of 85% after 3000 cycles at a high charge/discharge rate of 10 C.

3D micro-storage devices are increasingly recognized for their critical role in various applications, including micro-electromechanical systems (MEMS), wearable electronics, biomedical devices, and particularly within the IoT ecosystem.[383] Cohen *et al.*[384] developed a novel 3D-printed, high-performance tri-layered lithium metal microbattery using electrophoretic deposition (EPD). They efficiently deposited active material layers (LFP cathode, $LiAlO_2$-PEO, and LTO anode) directly onto 3D-printed polymer substrates with a high aspect ratio. This method achieved a uniform coating of active materials, which is generally difficult for cathodes with complex geometry. Sun *et al.*[385] developed a facile approach to 3D printing interdigitated lithium-ion micro-battery architectures on a sub-millimeter scale. The interdigitated structure created shorter paths for the ions to travel between the electrodes during cyclic operation. The all-printed 3D micro-batteries showed impressive results. Specific capacities for the 8-layer structures were recorded at 160 mAh g^{-1} for LTO and 131 mAh g^{-1} for LFP at 1 C rate, closely aligning with theoretical values. Additionally, these structures maintained their performance even at higher rates.

B. Energy conversion

Energy conversion devices convert waste mechanical, electromagnetic, or thermal energy to usable electrical energy utilizing atomic scale phenomena such as lattice distortion, charge carrier diffusion, or electrostatic polarization. Therefore, harvesting ambient energies using nano-scale technologies like thermoelectric, piezoelectric, triboelectric, and magnetoelectric nanogenerators presents a viable alternative for a clean energy source. MMAM techniques allow for integrating multifunctional materials with conductive, insulating, and structural properties essential for developing advanced energy harvesting devices.

1. Piezoelectric energy harvesters

Piezoelectric materials can generate electric voltage when subjected to mechanical stress or deformation, and vice versa.[386] These materials, including certain ceramics, crystals, and polymers, are essential in developing self-powered sensors and energy-harvesting devices.[387] Their ability to convert mechanical vibrations, pressure, or movement into electrical signals without external power makes them ideal for structural health monitoring, diagnostics, wearable electronics, and environmental sensing applications. Moreover, piezoelectric materials can capture ambient mechanical energy from human motion, vibrations, or environmental forces, converting it into electrical energy, which has the potential to power low-energy devices or recharge batteries.[386]

A piezoelectric harvester typically comprises a piezoelectric layer sandwiched between conductive electrodes and separated by an insulating layer.[388] The electrodes transport the generated electricity to the piezoelectric layer, and the insulating layer prevents short circuits.[388] This complex structure of different functional layers can be readily fabricated through MMAM techniques. For example, Rafiee *et al.*[295] developed a hybrid printing platform for fabricating a flexible and stretchable piezoelectric energy harvester (PEH) [Fig. 6(a)] by integrating BTO as the active piezoelectric material and silver flakes as the conductive electrode. The functional inks developed for this process are highly stretchable and less toxic than traditional solvent-based inks. Under forced vibration, a straight beam PEH achieved an open-circuit voltage (OCV) of approximately 2.7 V. In comparison, configurations like the variable cross section beam and arc beam produced voltages of 0.72 and 0.80 V, respectively. Additionally, the straight beam configuration generated a maximum peak current of 35 nA, indicating the device's potential for application in harvesting energy from mechanical vibrations/movements. Similarly, Ali *et al.*[156] fabricated a fully printed PEH using flexographic printing. The PEH was fabricated on a 100 μm thick PET substrate with multiple silver and PZT ink layers. The device generated a peak voltage of around 0.4 V when bent manually at 0.5 Hz. By connecting four PEH cells in series, the peak voltage increased to 1.7 V. Additionally, a printed bridge rectifier was developed to convert the alternating current generated by the PEH into direct current. The rectified output voltage from the printed PEH device was approximately 0.41 V after 85 s of charging a 100 μF capacitor, corresponding to a power density of 0.2 μW cm^{-3}.

Recently, there has been ongoing research to improve the energy density and efficiency of PEHs. PVDF polymer has a dominant α phase with poor piezoelectric performance, as certain regions of the crystal have opposite polarities that cancel each other out.[389] However, the piezoelectric effect can be enhanced if the α phase can be converted to the β phase with higher polarity.[390] Yuan *et al.*[391] reported that the energy density of the piezoelectric PVDF-polymer nanocomposite was significantly enhanced through multiple synergistic mechanisms. They prepared the nanocomposite by doping PVDF with polar PZT ceramic particles using high-energy ball milling, creating micro-cavities to hold these polar particles, and incorporating uniformly spaced Ag electrode films through MMAM. This enhancement was attributed to the high β-crystal phase induced by the mechanically directional stress field, the strong electret effect from micro-cavities, and the floating electrode films. Additionally, increasing porosity in 3D structures can result in higher deformation and hydrostatic strain, resulting in higher output voltage.[392,393] Megdich *et al.*[394] utilized the nucleating effect of BTO nanoparticles on the PVDF matrix to induce controlled porosity and a high β phase fraction of 95.72%. Pei *et al.*[395] fabricated lamellar piezoelectric generators by intercalating piezoelectric and conductive layers, with enhanced polarization achieved through interfacial regulation and 3D graphene nanoplatelet networks. Additionally, microwave irradiation selectively heated the nanoplatelets, improving the polymer interface and piezoelectric output. The output current of the lamellar generator was approximately 18 times higher than conventional non-porous devices.

However, challenges remain in the 3D printing of PEHs, particularly due to the limited options of materials and the need for high-energy poling processes. Ceramic particles are challenging to print directly due to their high melting points and brittleness.[396] In contrast, piezoelectric polymers like PVDF are easier to print because of their lower processing temperatures, but they typically offer reduced performance and resolution.[397–399] Moreover, the high-temperature and energy-poling process complicates the printing process and degrades the piezoelectric performance of the device.[400] Du *et al.*[296] addressed these challenges by developing a hybrid printing method, enabling the fabrication of stretchable piezoelectric devices without the need for post-processing steps. The lack of point symmetry in Te NWs allowed intrinsic piezoelectric properties without needing a high-energy polling process,[401] while the Ag NWs served as highly conductive and stretchable electrodes. The self-powered sensor was tested for its ability to detect hand gestures and heartbeat when attached to the human body, showcasing its potential for wearable applications. Furthermore, the

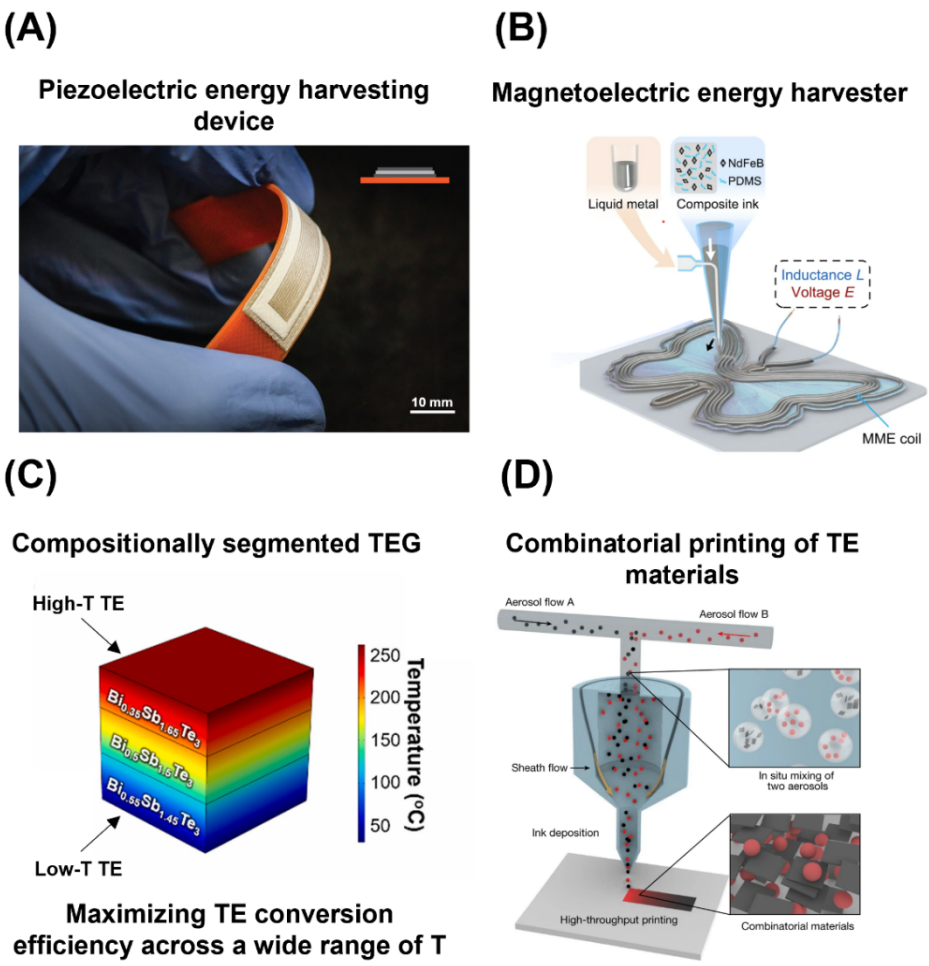

FIG. 6. MMAM of energy conversion devices: (A) All-printed flexible piezoelectric energy harvesting device under bending strain. Reprinted with permission from Rafiee *et al.*, Advanced Engineering Materials **24**, 2200294 (2022).[295] Copyright 2022 Wiley-VCH GmbH. (B) Coaxial printing of a magneto-mechano-electric structure for harvesting energy by coupling magnetoactive and electrically conductive inks. Reprinted with permission from Zhang *et al.*, Nat. Comm. **14**, 4428 (2023).[147] Copyright 2023, licensed under a Creative Commons Attribution (CC BY) license. (C) A compositionally segmented thermoelectric generator designed to operate efficiently across a wide range of temperatures in a gradient. Reprinted with permission from Yang *et al.*, Nano Energy **81** (2021).[31] Copyright 2021 Elsevier. (D) Combinatorial printing of thermoelectric materials. Reprinted with permission from Zeng *et al.*, Nature 617, 7960 (2023).[20] Copyright 2023, licensed under a Creative Commons Attribution (CC BY) license.

device demonstrated excellent durability, maintaining performance over 1000 stretching-releasing cycles.

2. Triboelectric energy harvesters

In addition to PEHs, triboelectric nanogenerators (TENGs) can convert mechanical energy into electrical energy. This conversion process occurs through the interaction of materials that generate electric charges when subjected to repeated mechanical actions, such as friction and periodic contact-separation, between two triboelectric materials with different abilities to gain or lose electrical charges that lead to electrostatic induction.[402–404] The harvested energy from TENGs can power IoT sensors, wearable devices, and diagnostic devices.[405–407]

Seol *et al.*[33] developed a fully printed, free-standing TENG with an electrode layer (EL) and a triboelectric layer (TL) for autonomous energy harvesting. Their device demonstrated an OCV of 231 V, a short circuit current of 18.9 μA, and a maximum root mean square power of 2.13 mW, sufficient for powering small electronic devices. They suggested that the device's performance improves with an increased number of gratings despite the higher areal loss factor. The design freedom provided by MMAM allows for finer gratings, enhancing performance. Additionally, they found that material combinations such as nylon (TL) and Al (EL) were effective, achieving a triboelectric charge density of 31.2 μC/m^2. Moreover, hybrid systems can optimize the energy output of TENGs by utilizing additional mechanisms, such as droplet impacts. Scattered water droplets, such as raindrops and condensation, are abundant in nature but typically overlooked as energy sources. For example, Kam *et al.*[226] fabricated an FDM-printed MM hybrid droplet-based electric generator (HDEG) that combines a droplet-based electric generator (DEG) and a solid–solid triboelectric nanogenerator (S–S TENG). The HDEGs showed a 30% improvement in energy output over a single DEG and a 25% better energy supply performance. The authors hypothesized that the enhanced performance was due to the simultaneous activation of the DEG and S–S TENG by a single droplet impact, which allowed the conversion of dissipated kinetic energy into elastic energy, thereby optimizing the energy output. The HDEG achieved a peak voltage of 96 V from the DEG and 36.8 V from the S–S TENG, with a combined energy generation efficiency of 0.258%, compared to 0.195% for a single DEG. This hybrid system can power small electronic devices.

Over the years, converting waste to energy has been a focus for organizations such as the U.S. Energy Information Administration and

Environmental Protection Agency (EPA).[408,409] Utilizing electronic and plastic waste from laboratories for energy harvesting can promote the circular economy of sustainable energy. MMAM can be used to remanufacture TENGs from different waste sources. In this regard, Sahu *et al.*[410] developed a TENG from recycled laboratory waste, such as plastic Petri dishes, for energy harvesting applications. Using a plastic-glass combination, the device operated in a vertical contact-separation mode and achieved a maximum output voltage of 185 V, a current of 1.25 μA, and a power density of 8.1 μW cm^{-2}.

3. Electromagnetic energy harvesters

Electromagnetic energy harvesters (EMEHs) can convert low-frequency magnetic fields generated by current-carrying wires into usable electrical energy based on Faraday's law.[411,412] When an external magnetic field is applied to the device, it induces a magnetostrictive strain in the magnetic phase of the composite.[413] This strain is transmitted to the piezoelectric phase, which converts the mechanical strain into usable electrical energy. Since the performance of EMEHs relies on strong interfacial bonding between piezoelectric and magnetostrictive materials, MMAM is an effective tool for meeting these complex structural requirements.

For example, Wu *et al.*[225] reported the development of an MM magnetoelectric architecture. Utilizing SLS, the researchers fabricated the devices using TPU powder and magnetic NdFeB/TPU composite powders. The output voltage of these devices is highly dependent on structural parameters. Additionally, the thickness of the magnetic layer significantly impacted the voltage output, with a thickness of 8 mm, yielding a voltage of 21.7 mV. It was hypothesized that the increase in thickness resulted in higher active material that strengthened the magnetic intensity and flux. Numerical simulations showed that higher strain results in greater magnetic flux changes, thus generating higher voltages. Furthermore, the developed architecture was utilized in real-world applications by an MM-printed sneaker capable of generating an output voltage of approximately 2 V, sufficient to power an LED lamp during walking or running. However, EMEHs are often limited by stress concentrations or delamination at the interface.[414,415] Additionally, there is a trade-off between electromagnetic properties and flexibility when higher concentrations of conductive fillers or magnetic particles are used.[416–419] Zhang *et al.*[147] addressed these challenges by developing a hybrid magnetic-mechanical-electrical (MME) core-sheath fiber fabricated using a coaxial DIW method [Fig. 6(b)]. The liquid metal core provided high electrical conductivity, and the soft magnetoactive sheath enabled programmable magnetic response with flexible mechanical properties. The conversion of energy was carried out by either an electromagnetic generator (EMG), radio frequency (RF), or triboelectric nanogenerator (TENG). In the EMG mode, the device demonstrated a significant increase in output capacity with a maximum energy output of 2660 mJ m^{-2} within 1 second under varying magnetic field strengths and frequencies. For the RF mode, power generation was primarily influenced by the working distance, with a peak power density of 163 mW m^{-2} at an external load resistance of 19 Ω when the distance was 28 mm. The TENG mode, actuated by magnetic fields, produced an OCV of 18 V, a short-circuit peak current of 1.2 μA, and a peak power density of 13.8 mW m^{-2} at an actuation magnetic field strength of 180 mT. The authors hypothesized that the observed performance variations across different modes are due to the distinct interaction mechanisms between the magnetic fields and the structural elements of the device.

Furthermore, the performance of EMEHs can be enhanced by strain-mediated coupling between magnetostrictive and piezoelectric materials.[420,421] Brito-Pereira *et al.*[32] developed a multifunctional harvester with magnetic field sensing capabilities using MMAM. $CoFe_2O_4$ nanoparticles/wax composite was used as the magnetoactive material, and P(VDF-TrFE) as the piezoelectric material. The harvester exhibited an output power of approximately 160 μW, which increased to around 350 μW with mechanical stimulation. The device demonstrated a maximum output power density of 9.7 mW cm^{-3} and magnetic field sensing capabilities with a 30 V T^{-1} sensitivity. The authors hypothesized that the high magnetic force acting on the magnetic layer increased mechanical stimulation on the piezoelectric layer, thus enhancing voltage generation. Additionally, increasing the thickness of the magnetoactive layer initially raised the output voltage due to increased magnetic force. However, it led to a plateau or decrease due to greater mechanical stiffness. Optimal performance was observed when the magnetic layer had a composition gradient present, which induced varying mechanical stimuli along the piezoelectric layer, resulting in higher output voltages.

4. Thermoelectric (TE) energy harvesters

TE materials are narrow bandgap semiconductors that convert thermal energy into electricity directly through the Seebeck effect and vice versa using the Peltier effect.[302] The working principle of thermoelectric generators (TEGs) involves creating a temperature gradient across a TE material, which causes charge carriers (electrons or holes) to migrate, generating a voltage difference.[422] The efficiency of TEGs is characterized by a dimensionless number $zT = \frac{S^2\sigma T}{\kappa}$, where S represents the Seebeck coefficient, σ denotes the electrical conductivity, κ is the thermal conductivity, and T is the absolute temperature.[423,424] Examples of TE materials include bismuth telluride (Bi_2Te_3), antimony telluride (Sb_2Te_3), lead telluride (PbTe), silicon-germanium (SiGe) alloys,[425–427] and other systems. The power factor ($PF = S^2\sigma$) is an alternative metric for assessing TE materials.[424]

A critical challenge for homogeneous single-phase TEGs is attaining high conversion efficiency across a broad temperature range while maintaining peak zT.[428,429] Segmented TEGs can address this issue by combining different TE materials optimized for specific temperature ranges.[430–432] Each segment operates at an optimal temperature gradient, enhancing the overall efficiency by maximizing the total voltage output. For example, Yang *et al.*[31] reported on the fabrication and performance of a composition-segmented BiSbTe TEG using MMAM. The segmented TEG demonstrated a record-high conversion of 8.7% under a temperature gradient of 236 °C. The TEG was constructed using compositionally segmented thermoelectric legs of $Bi_xSb_{2-x}Te_3$, which allowed the peak zTs of the material to shift from room temperature to 250 °C [Fig. 6(c)]. This segmentation enabled the TEG to maintain a high average zT of 0.94 over a wide temperature range, achieving optimal compatibility between the thermoelectric segments and minimizing electrical and thermal losses at the junctions. This high value of zT can be attributed to the MM printing technique that allowed for precise geometric control of the segmented TE legs, minimizing junction losses. Also, using all-inorganic viscoelastic TE inks facilitated the formation of smooth, well-fused interfaces, reducing electrical and thermal resistance. Current research on continuous

compositionally graded thermoelectric composites (CG-TECs) remains at the prototype stage, and there is still uncertainty about whether the grading in these materials can be effectively controlled during mass production. To optimize composition and doping, MMAM can provide a fast material optimization and discovery platform through fast prototyping. Zeng *et al.*[20] developed a high-throughput combinatorial printing method capable of generating gradients in composition using *in situ* aerosol mixing [Fig. 6(d)]. This method allows control of the mixing ratio of various materials on the fly, creating microscale spatial resolution in the printed structures. This technique achieved a spatial resolution of around 20 μm in the x–y plane and ultrathin films of approximately 100 nm. This combinatorial approach rapidly optimized sulfur doping concentrations in printed $Bi_2Te_{2.7}Se_{0.3}$ materials. It was observed that increasing sulfur doping significantly increased the Seebeck coefficient of the film from -130 to $-200\,\mu V\,K^{-1}$, eventually reaching a plateau at around $-213\,\mu V\,K^{-1}$. Other advanced methods, such as material co-sputtering, pulsed laser deposition, and wire-fed droplet alloying, have also been reported for the high-throughput fabrication of graded TE materials.[433–435]

While traditional inorganic TE materials offer high performance, organic TE materials are gaining attention for applications requiring lightweight and customizable designs.[423] Certain semiconducting polymers like poly(4-ethyleneoxythiophene) (PEDOT), polyacetylenes (PA), PANI, etc., have suitable Seebeck coefficients and PF for organic-inorganic hybrid TEGs.[423] Ou *et al.*[153] used PEDOT:PSS as the polymer matrix and developed a CG-TEC by tuning the composition of Bi_2Te_3 nanoparticles and Sb_2Te_3 nanoflakes using an AJP technique. The smooth transitions between different material segments reduced interface-related issues, such as cracks and thermal mismatches. The optimized CG-TECs exhibited significantly improved thermoelectric performance, with a peak power output of approximately 13 nW for waste heat harvesting. Gel-based ionic-conducting TE materials hold great promise for next-generation TEGs. Ionic TE materials have 2–3 orders of magnitude higher Seebeck coefficients than conventional inorganic chalcogenides due to the Soret effect that arises from the difference in cationic and anionic diffusivities in the gel matrix.[436,437] Although there have been no reported instances of ionic TEGs being fabricated through MMAM (as of the date of this review), future research in this area holds the potential to develop green and pollution-free giant thermoelectric generators for wearable applications ($\sim mV\,K^{-1}$).[438–440]

5. Fuel cells

Fuel cells represent another green and high-efficiency energy conversion system that can convert chemical energy stored in molecules to electrical energy. Fuel cells produce electricity through an electrochemical redox reaction. At the anode, hydrogen atoms are split into protons and electrons, while at the cathode, oxygen reacts, enabling the electrons to flow through an external circuit, generating electrical power.[441] MMAM is a promising technology for fabricating hierarchical structures for fuel cells that can reduce various polarization losses while providing a higher surface area for improved reaction kinetics and mass transfer.[442]

In solid oxide fuel cells (SOFCs), ceramic materials, especially YSZ, are commonly used as electrolytes with mixed ionic-electronic conducting electrodes.[443,444] YSZ is a stable and fast ionic conductor even under harsh operating conditions (e.g., high temperature, reducing environment).[443,444] Anelli *et al.*[29] demonstrated a novel hybrid printing process for fabricating symmetrical SOFCs utilizing a combination of robocasting and IJP. This method successfully produced thick, porous electrode layers via robocasting and thin, dense electrolytes via IJP, both essential for forming the triple-phase boundary.[443,445] The ink and slurry formulations were optimized to ensure co-sintering compatibility, achieving an electrolyte shrinkage of approximately 26% and a thin 2.8 μm dense electrolyte layer. The SOFC showed superior electrochemical performance with an area-specific resistance of roughly 2.1 $\Omega\,cm^2$ at 750 °C. Similarly, in another study, Esposito *et al.*[149] demonstrated the fabrication of a 1.2 μm thick, dense YSZ electrolyte for SOFCs using highly diluted colloidal inks. The results showed that multiple printings were necessary to achieve gas-tight layers, with a five-layer electrolyte exhibiting a high degree of gas tightness compared to a two-layer electrolyte. SOFCs with a five-layer electrolyte achieved OCV between 1.07 and 1.15 V in dry hydrogen and a peak power density of 1.5 W/cm^2 at 800 °C. The optimal dispersion and stability of the YSZ particles in the ink, the effectiveness of multiple printing passes to cover defects, and the high sintering temperature (1300 °C) ensured densified grain growth of the electrolyte layer.

However, the requirement of post-heat treatment for ceramics increases cost and complexity, particularly for large-sized MM components with dissimilar thermal properties. Consequently, Bai *et al.*[227] used PBF to create MM and multi-layered structures for SOFCs. They fabricated a three-layered cell comprising a Ni–YSZ anode, YSZ electrolyte, and LSM cathode. This method eliminates the need for binders and post-treatment, allowing for precise control over density and porosity through laser power, scan speed, and pattern adjustments. Results showed that high-density Ni–YSZ layers were achievable, with uniform YSZ layers providing strong interface adhesion and minimal defects. However, higher resistance was noted compared to conventional methods due to non-uniformity in the YSZ layer.

V. CHALLENGES IN MMAM FOR ENERGY DEVICES

Despite significant advances in printed energy devices, challenges still exist. Industrial scalability is one of the primary limitations for the commercial implementation of MMAM techniques.[12] Scaling MMAM for large-scale production of energy devices requires modifications in the process.[446] As most energy devices require a combination of diverse material systems such as conductive, insulating, and structural materials, mechanical and chemical compatibility at the microscale becomes an important consideration.[447,448] For example, volumetric changes due to the metal intercalation process in metal ion batteries or mismatches in thermal expansion coefficients can lead to delamination and interface cracking and gradually cause performance reduction in electrochemical systems.[449] Moreover, MMAM techniques are often restricted in the types and viscosities of materials they can handle, impacting the geometric accuracy and functional capabilities of complex device architectures. As a result, many energy devices requiring fine features are constrained by the limited resolution of existing MMAM technologies.[450] Additionally, ensuring repeatable and reproducible outputs requires precise monitoring of process conditions; otherwise, defects can compromise structural stability and functional reliability.[451] Ensuring the functional reliability of energy devices heavily depends on various characterization techniques to confirm their electrical and thermal outputs. These techniques often delay

TABLE VIII. Characterization techniques for energy devices manufactured through MMAM techniques.

Character type	Technique	Measured property	Testing time
Electrical	Cyclic voltammetry	Redox reaction kinetics	Minutes to hours[454]
	Electrochemical impedance spectroscopy	Cell resistance	Minutes to hours (depending on frequency)[455]
	Galvanostatic charge/discharge	Energy density, cycle life, capacitance	Hours to days (depending on the current rate)[456]
	Four-point probe	Electrical conductivity	Seconds to minutes[457]
	Van Der Pauw's method	Electrical conductivity	Seconds to minutes[458]
Thermal	Thermal gravimetric analysis	Thermal stability	Minutes to hours[459]
	Accelerated rate calorimetry	Thermal stability	Minutes to hours[460]
	Differential scanning calorimetry	Phase transitions, heat capacity	Minutes to hours[461]
	Laser flash method	Thermal conductivity	Minutes to hours[462]
	3ω method	Thermal conductivity	Minutes to hours[463]
	Harman method	Thermoelectric figure of merit	Minutes to hours[464]

iterative optimization and increase workflow complexity by requiring specialized equipment, calibration protocols, and extensive data acquisition time, while new characterization efforts are proposed to improve throughput and efficiency.[452] Table VIII summarizes the various electrical and thermal characterization techniques for characterizing energy devices with their corresponding measured properties and required run time. Although MMAM systems for energy devices are still primarily at the lab scale, establishing clear guidelines for standardization in terms of cost, time efficiency, reliability, and functionality is essential for successful commercial implementation.[453]

VI. CONCLUDING REMARKS

The emergence of MMAM has been revolutionary for its design freedom and fast prototyping, both of which are critical for designing micro- and macrostructures for energy devices. Recent implementations of MMAM have shown promise in real-world applications for energy device production. Sakuu's Kavian platform is already on its way to commercial production of solid-state batteries with enhanced safety and energy density and possible adaptation to electric vehicles.[465,466] Panasonic and Nanyang Technological University (NTU) in Singapore have collaborated to develop an MMAM-based 3D printer that targets flexible, wearable energy devices.[467] However, various process- and material-based challenges still need to be addressed before this technology can be used to its maximum potential.

Material options for MMAM remain limited, particularly for ink-based approaches that require stable and high loading of active materials in the inks. Challenges include engineering-compatible inks for device manufacturing that have high functional properties even after post-processing steps. Optimizing MMAM for energy devices necessitates novel additive-free inks, which enhance conductivity and carrier mobility without high-temperature sintering steps that often cause decomposition or unwanted phase transition.[468] Quantitative models and dimensionless parameters need to be developed to assess the ink's printability and predict the functional reliability of the energy device. Furthermore, engineering the ink composition to fabricate compositionally gradient electrodes can add another degree of freedom for designing advanced energy storage and conversion systems with site-specific electrical, electrochemical, and thermal properties.[469–471]

Understanding the printed microstructure is particularly crucial for MMAM systems in energy devices to optimize material properties, enhance efficiency, and ensure the durability required for advanced energy applications. Various techniques have been used to evaluate structural, mechanical, chemical, and functional properties of fabricated parts, including microscopy (SEM and TEM), x-ray methods (XRD), tensile and compression testing, spectroscopy (FTIR, Raman, and XPS), thermal analysis (DSC and TGA), and surface analysis (AFM, contact angle measurement). While these methods are effective, increasing the throughput through lab-automated characterization and testing is necessary for the complex interface and phase distribution in MM components. Techniques like small-angle X-ray scattering (SAXS), small-angle neutron scattering (SANS), and X-ray correlation spectroscopy (XPCS) can be utilized for detecting internal stresses, voids, and other defects that can arise during the complex thermal and mechanical interactions during the post-processing.[472–474] Characterization techniques that use X-rays can provide real-time information about the rapidly transitioning melt pool in laser-based MMAM processes and generate quantitative data on the fractions of different phases present in the system.[475,476] Neutrons can penetrate deep into materials, including metals and thick samples, without significant attenuation. This allows for the study of bulk properties and internal structures. In particular, SANS can be used to understand polymer chain conformation or nano-defects in MM composites, providing crucial knowledge to correlate molecular-level microstructures to the material properties.[477–481] Moreover, X-ray computed tomography and SAXS can be used to probe the fiber orientation in composites at a microscopic level.[482,483]

Recently, the rise of AI has revolutionized material design by enabling the rapid discovery of advanced materials through predictive machine-learning models and high-throughput simulations.[484] These machine learning models have been used to assist the optimization of materials design,[485–487] manufacturing,[488] processing,[489,490] and characterizations.[491] In addition, AI-driven algorithms can be integrated with the process workflow for early defect detection, optimizing printing parameters for defect-free manufacturing and creating material libraries that can be easily screened for specific properties.

Energy storage and conversion predominantly take place at the nanoscale. TPP is currently the only mature MMAM technology capable of nanoscale fabrication, but it is limited by material options. Thus, the current resolution of the available MMAM printers needs to be improved for nanoscale fabrication with the capability of engineering the MM interface for higher energy density, faster charge transport, and improved durability. Additionally, post-processing steps like annealing or sintering must be carefully optimized considering the dissimilar material properties to avoid adverse effects on the printed interface. Independent post-processing technologies for different material systems must be developed without compromising the overall manufacturing time and the device's performance.[492] Future research should focus on "one-shot" fabrication without requiring additional post-processing steps to reduce costs, streamline the workflow, and enable scalable, sustainable manufacturing of high-performance energy devices. Finally, standardized stability testing of the energy devices in full-cell configuration should be benchmarked to validate their performance against conventional systems and ensure long-term functionality.

Although challenges exist in MMAM for energy devices, it also offers unique opportunities for collaborative research across various disciplines. This collaboration should involve materials science and engineering, machine design experts, and end-users whose practical needs can guide technical development. The focus should not only be on enhancing printing precision and fabrication speeds but also on developing reliable and user-friendly systems for high-performance device fabrication, promoting sustainable and green energy infrastructures for societal impacts.

ACKNOWLEDGMENTS

M. Z. acknowledges the support from the NSF (Grant Nos. CMMI-2400169 and DMR-2418915). The authors also thank Dr. Changwoo Do from Oak Ridge National Laboratory for insightful discussions on various scattering techniques.

AUTHOR DECLARATIONS

Conflict of Interest

The authors have no conflicts to disclose.

Author Contributions

Naimul Arefin: Data curation (lead); Formal analysis (lead); Project administration (equal); Validation (equal); Writing – original draft (lead); Writing – review & editing (lead). **Hur-E-Jannat Moni:** Resources (supporting); Writing – review & editing (supporting). **David Espinosa:** Writing – original draft (supporting); Writing – review & editing (supporting). **Weilong Cong:** Writing – review & editing (supporting). **Minxiang Zeng:** Conceptualization (lead); Data curation (lead); Funding acquisition (lead); Investigation (lead); Project administration (lead); Supervision (lead); Writing – review & editing (equal).

DATA AVAILABILITY

Data sharing is not applicable to this article as no new data were created or analyzed in this study.

REFERENCES

[1]A. M. Omer, "Energy, environment and sustainable development," Renewable Sustainable Energy Rev. **12**(9), 2265–2300 (2008).
[2]U.S. Energy Information Administration, "EIA projects that increased electrification, higher equipment efficiencies, and more zero-carbon power sources will reduce U.S. energy-related carbon dioxide emissions through 2050," 2023. See https://www.eia.gov/pressroom/releases/press529.php (last accessed June 25, 2024).
[3]J. A. Rogers, R. Ghaffari, and D.-H. Kim, *Stretchable Bioelectronics for Medical Devices and Systems* (Springer, 2016).
[4]S. Cohen, W. Eimicke, and A. Miller, *Sustainability Policy: Hastening the Transition to a Cleaner Economy* (Wiley Online Library, 2015).
[5]C. Xie, H. Shan, X. Song, L. Chen, J. Wang, J.-W. Shi, J. Hu, J. Zhang, and X. Li, "Flexible S@ C-CNTs cathodes with robust mechanical strength via blade-coating for lithium-sulfur batteries," J. Colloid Interface Sci. **592**, 448–454 (2021).
[6]L. Hu, H. Wu, F. La Mantia, Y. Yang, and Y. Cui, "Thin, flexible secondary Li-ion paper batteries," ACS Nano **4**(10), 5843–5848 (2010).
[7]Y.-H. Chang, S.-R. Tseng, C.-Y. Chen, H.-F. Meng, E.-C. Chen, S.-F. Horng, and C.-S. Hsu, "Polymer solar cell by blade coating," Org. Electron. **10**(5), 741–746 (2009).
[8]J.-S. Park, W.-H. Chung, H.-S. Kim, and Y.-B. Kim, "Rapid fabrication of chemical-solution-deposited $La_{0.6}Sr_{0.4}CoO_{3-\delta}$ thin films via flashlight sintering," J. Alloys Compd. **696**, 102–108 (2017).
[9]K. Nagata and T. Nanno, "All solid battery with phosphate compounds made through sintering process," J. Power Sources **174**(2), 832–837 (2007).
[10]J. Madan, M. Mani, and K. W. Lyons, "Characterizing energy consumption of the injection molding process," In *International Manufacturing Science and Engineering Conference* (American Society of Mechanical Engineers, 2013), Vol. 55461, p. V002T004A015.
[11]V. M. Werner, R. Krumpholz, C. Rehekampff, T. Scherzer, and M. Eblenkamp, "Thermoplastic encapsulations of a sensor platform by high-temperature injection molding up to 360 °C," Polym. Eng. Sci. **59**(7), 1315–1331 (2019).
[12]C. Zhu, T. Liu, F. Qian, W. Chen, S. Chandrasekaran, B. Yao, Y. Song, E. B. Duoss, J. D. Kuntz, and C. M. Spadaccini, "3D printed functional nanomaterials for electrochemical energy storage," Nano Today **15**, 107–120 (2017).
[13]X. Kuang, J. Wu, K. Chen, Z. Zhao, Z. Ding, F. Hu, D. Fang, and H. J. Qi, "Grayscale digital light processing 3D printing for highly functionally graded materials," Sci. Adv. **5**(5), eaav5790 (2019).
[14]M. A. Skylar-Scott, J. Mueller, C. W. Visser, and J. A. Lewis, "Voxelated soft matter via multimaterial multinozzle 3D printing," Nature **575**(7782), 330–335 (2019).
[15]H. Wang, J. Chen, H. Luo, D. Wang, C. Song, X. Yao, P. Chen, and M. Yan, "Bimetal printing of high entropy alloy/metallic glass by laser powder bed fusion additive manufacturing," Intermetallics **141**, 107430 (2022).
[16]J. S. Pelz, N. Ku, W. T. Shoulders, M. A. Meyers, and L. R. Vargas-Gonzalez, "Multi-material additive manufacturing of functionally graded carbide ceramics via active, in-line mixing," Addit. Manuf. **37**, 101647 (2021).
[17]X. Zheng, C. Williams, C. M. Spadaccini, and K. Shea, "Perspectives on multi-material additive manufacturing," J. Mater. Res. **36**, 3549–3557 (2021).
[18]R. Šakalys, B. S. Mohammadlou, and R. Raghavendra, "Fabrication of multi-material electronic components applying non-contact printing technologies: A review," Results Eng. **15**, 100578 (2022).
[19]S. Tagliaferri, A. Panagiotopoulos, and C. Mattevi, "Direct ink writing of energy materials," Mater. Adv. **2**(2), 540–563 (2021).
[20]M. Zeng, Y. Du, Q. Jiang, N. Kempf, C. Wei, M. V. Bimrose, A. Tanvir, H. Xu, J. Chen, and D. J. Kirsch, "High-throughput printing of combinatorial materials from aerosols," Nature **617**(7960), 292–298 (2023).
[21]X. Lou, M. Song, P. W. Emigh, M. A. Othon, and P. L. Andresen, "On the stress corrosion crack growth behaviour in high temperature water of 316L stainless steel made by laser powder bed fusion additive manufacturing," Corros. Sci. **128**, 140–153 (2017).
[22]M. Song, M. Wang, X. Lou, R. B. Rebak, and G. S. Was, "Radiation damage and irradiation-assisted stress corrosion cracking of additively manufactured 316L stainless steels," J. Nucl. Mater. **513**, 33–44 (2019).
[23]S. Z. Uddin, L. E. Murr, C. A. Terrazas, P. Morton, D. A. Roberson, and R. B. Wicker, "Processing and characterization of crack-free aluminum 6061 using

high-temperature heating in laser powder bed fusion additive manufacturing," Addit. Manuf. **22**, 405–415 (2018).
[24]M. Aliqué, C. D. Simão, G. Murillo, and A. Moya, "Fully-printed piezoelectric devices for flexible electronics applications," Adv. Mater. Technol. **6**(3), 2001020 (2021).
[25]H. M. Ali, T.-U. Rehman, M. Arıcı, Z. Said, B. Duraković, H. I. Mohammed, R. Kumar, M. K. Rathod, O. Buyukdagli, and M. Teggar, "Advances in thermal energy storage: Fundamentals and applications," Prog. Energy Combust. Sci. **100**, 101109 (2024).
[26]J. Lee, B. Jeong, and J. D. Ocon, "Oxygen electrocatalysis in chemical energy conversion and storage technologies," Curr. Appl. Phys. **13**(2), 309–321 (2013).
[27]Z.-R. Li, N. Hu, and L.-W. Fan, "Nanocomposite phase change materials for high-performance thermal energy storage: A critical review," Energy Storage Mater. **55**, 727–753 (2023).
[28]B. Tyagi, H. B. Lee, N. Kumar, W.-Y. Jin, K.-J. Ko, M. M. Ovhal, R. Sahani, H.-J. Chung, J. Seo, and J.-W. Kang, "High-performance, large-area semi-transparent and tandem perovskite solar cells featuring highly scalable a-ITO/Ag mesh 3D top electrodes," Nano Energy **95**, 106978 (2022).
[29]S. Anelli, M. Rosa, F. Baiutti, M. Torrell, V. Esposito, and A. Tarancón, "Hybrid-3D printing of symmetric solid oxide cells by inkjet printing and robocasting," Addit. Manuf. **51**, 102636 (2022).
[30]R. Tao, J. Shi, F. Granier, M. Moeini, A. Akbarzadeh, and D. Therriault, "Multi-material fused filament fabrication of flexible 3D piezoelectric nanocomposite lattices for pressure sensing and energy harvesting applications," Appl. Mater. Today **29**, 101596 (2022).
[31]S. E. Yang, F. Kim, F. Ejaz, G. S. Lee, H. Ju, S. Choo, J. Lee, G. Kim, S. Jung, and S.-h. Ahn, "Composition-segmented BiSbTe thermoelectric generator fabricated by multimaterial 3D printing," Nano Energy **81**, 105638 (2021).
[32]R. Brito-Pereira, C. Ribeiro, N. Pereira, S. Lanceros-Mendez, and P. Martins, "Printed multifunctional magnetically activated energy harvester with sensing capabilities," Nano Energy **94**, 106885 (2022).
[33]M.-L. Seol, R. Ivaškevičiūtė, M. A. Ciappesoni, F. V. Thompson, D.-I. Moon, S. J. Kim, S. J. Kim, J.-W. Han, and M. Meyyappan, "All 3D printed energy harvester for autonomous and sustainable resource utilization," Nano Energy **52**, 271–278 (2018).
[34]W. Liu, Y. Yi, Z. He, T. Han, J. Sun, J. Zhou, and Y-y Li, "Customizing $CoSe_2$/Ti_3C_2Tn MXene hybrid inks toward high-energy-density 3D-printed K-ion hybrid capacitors," Chem. Eng. J. **474**, 145326 (2023).
[35]D. Kong, Y. Wang, S. Huang, B. Zhang, Y. V. Lim, G. J. Sim, P. Valdivia y Alvarado, Q. Ge, and H. Y. Yang, "3D printed compressible quasi-solid-state nickel–iron battery," ACS Nano **14**(8), 9675–9686 (2020).
[36]Y. Jiang, Q. Lv, C. Bao, B. Wang, P. Ren, H. Zhong, Y. Yang, X. Liu, Y. Dong, and F. Jin, "Seamless alloying stabilizes solid-electrolyte interphase for highly reversible lithium metal anode," Cell Rep. Phys. Sci. **3**(3), 100785 (2022).
[37]S. Jung, D. Mandal, W. K. Min, J. Y. Jeong, I. S. Lee, J. Chung, B. S. Singu, H. Kim, and H. J. Kim, "All-printed 3-dimensional micro-supercapacitors with homogeneous Ag interface: Achieving precision on curved surfaces through Electrohydrodynamic jet printing," Chem. Eng. J. **497**, 154152 (2024).
[38]A. Bhattacharya, S. Sarkar, A. Halder, N. Biswas, and N. K. Manna, "Mixing performance of T-shaped wavy-walled micromixers with embedded obstacles," Phys. Fluids **36**(3), 033609 (2024).
[39]W. Guo, Z. Jiang, H. Zhong, R. Hou, and J. Xu, "Impact of online mixing via KSM on the accuracy of ingredient deposition in manufacturing FGMs," Int. J. Mech. Sci. **241**, 107971 (2023).
[40]D. Vinay, R. Keshavamurthy, and V. Tambrallimath, "Enhanced mechanical properties of metal filled 3D printed polymer composites," J. Inst. Eng. India. Ser. D **104**(1), 181–195 (2023).
[41]P. Agnihotri, "Analysis of interfacial mixing zone and mixing index in microfluidic channels," Microfluid. Nanofluid. **27**(2), 12 (2023).
[42]T. Dehghani, F. S. Moghanlou, M. Vajdi, M. S. Asl, M. Shokouhimehr, and M. Mohammadi, "Mixing enhancement through a micromixer using topology optimization," Chem. Eng. Res. Des. **161**, 187–196 (2020).
[43]A. Hashmi and J. Xu, "On the quantification of mixing in microfluidics," SLAS Technol. **19**(5), 488–491 (2014).
[44]B. Mondal, S. K. Mehta, P. K. Patowari, and S. Pati, "Numerical study of mixing in wavy micromixers: Comparison between raccoon and serpentine mixer," Chem. Eng. Process.-Process Intensification **136**, 44–61 (2019).
[45]P. R. de Souza Mendes, "Dimensionless non-Newtonian fluid mechanics," J. Non-Newtonian Fluid Mech. **147**(1-2), 109–116 (2007).
[46]V. Hessel, H. Löwe, and F. Schönfeld, "Micromixers—A review on passive and active mixing principles," Chem. Eng. Sci. **60**(8-9), 2479–2501 (2005).
[47]C.-Y. Lee, W.-T. Wang, C.-C. Liu, and L.-M. Fu, "Passive mixers in microfluidic systems: A review," Chem. Eng. J. **288**, 146–160 (2016).
[48]D. J. Beebe, G. A. Mensing, and G. M. Walker, "Physics and applications of microfluidics in biology," Annu. Rev. Biomed. Eng. **4**(1), 261–286 (2002).
[49]D. Gobby, P. Angeli, and A. Gavriilidis, "Mixing characteristics of T-type microfluidic mixers," J. Micromech. Microeng. **11**(2), 126 (2001).
[50]S. R. Bazaz, A. Sayyah, A. H. Hazeri, R. Salomon, A. A. Mehrizi, and M. E. Warkiani, "Micromixer research trend of active and passive designs," Chem. Eng. Sci. **293**, 120028 (2024).
[51]J. Green, A. Holdø, and A. Khan, "A review of passive and active mixing systems in microfluidic devices," Int. J. Multiphys. **1**(1), 1–32 (2007).
[52]N.-T. Nguyen, "Mixing in microscale," Microfluidic Technol. Miniaturized Anal. Syst. **194**, 117–155 (2007).
[53]M. S. Cheri, H. Latifi, M. S. Moghaddam, and H. Shahraki, "Simulation and experimental investigation of planar micromixers with short-mixing-length," Chem. Eng. J. **234**, 247–255 (2013).
[54]M. Yang, L. Yang, J. Zheng, N. Hondow, R. A. Bourne, T. Bailey, G. Irons, E. Sutherland, D. Lavric, and K.-J. Wu, "Mixing performance and continuous production of nanomaterials in an advanced-flow reactor," Chem. Eng. J. **412**, 128565 (2021).
[55]S. Kakaç, L. Vasiliev, Y. Bayazitoglu, and Y. Yener, "Microscale heat transfer-fundamentals and applications," in *Proceedings of the NATO Advanced Study Institute on Microscale Heat Transfer-Fundamentals and Applications in Biological and Microelectromechanical Systems*, Cesme-Izmir, Turkey, 18–30 July, 2004 (Springer Science & Business Media, 2006).
[56]M. Bayareh, "Artificial diffusion in the simulation of micromixers: A review," Proc. Inst. Mech. Eng., Part C: J. Mech. Eng. Sci. **235**(21), 5288–5296 (2021).
[57]J. J. Chen, C. H. Chen, and S. R. Shie, "Optimal designs of staggered dean vortex micromixers," Int. J. Mol. Sci. **12**(6), 3500–3524 (2011).
[58]N. Nivedita, P. Ligrani, and I. Papautsky, "Dean flow dynamics in low-aspect ratio spiral microchannels," Sci. Rep. **7**(1), 44072 (2017).
[59]A. P. Sudarsan and V. M. Ugaz, "Fluid mixing in planar spiral microchannels," Lab Chip **6**(1), 74–82 (2006).
[60]K. Cheng, R.-C. Lin, and J.-W. Ou, "Fully developed laminar flow in curved rectangular channels," J. Fluids Eng. **98**(1), 41–48 (1976).
[61]K. Ghia and J. Sokhey, "Laminar incompressible viscous flow in curved ducts of regular cross-sections," J. Fluids Eng. **99**(4), 640–648 (1977).
[62]F. Jiang, K. S. Drese, S. Hardt, M. Küpper, and F. Schönfeld, "Helical flows and chaotic mixing in curved micro channels," AlChE. J. **50**(9), 2297–2305 (2004).
[63]X. Feng, Y. Ren, and H. Jiang, "Effect of the crossing-structure sequence on mixing performance within three-dimensional micromixers," Biomicrofluidics **8**(3), 034106 (2014).
[64]T. J. Ober, D. Foresti, and J. A. Lewis, "Active mixing of complex fluids at the microscale," Proc. Natl. Acad. Sci. U. S. A. **112**(40), 12293–12298 (2015).
[65]C. F. Ceballos-González, E. J. Bolívar-Monsalve, D. A. Quevedo-Moreno, C. Chávez-Madero, S. Velásquez-Marín, L. L. Lam-Aguilar, Ó. E. Solís-Pérez, A. Cantoral-Sánchez, M. Neher, and E. Yzar-García, "Plug-and-play multimaterial chaotic printing/bioprinting to produce radial and axial micropatterns in hydrogel filaments," Adv. Mater. Technol. **8**(17), 2202208 (2023).
[66]M. Wang, W. Li, L. S. Mille, T. Ching, Z. Luo, G. Tang, C. E. Garciamendez, A. Lesha, M. Hashimoto, and Y. S. Zhang, "Digital light processing based bioprinting with composable gradients," Adv. Mater. **34**(1), 2107038 (2022).
[67]S. T. Chang, E. Beaumont, D. N. Petsev, and O. D. Velev, "Remotely powered distributed microfluidic pumps and mixers based on miniature diodes," Lab Chip **8**(1), 117–124 (2008).
[68]L. Lopes, A. Silva, and O. Carneiro, "Multi-material 3D printing: The relevance of materials affinity on the boundary interface performance," Addit. Manuf. **23**, 45–52 (2018).
[69]M. Ribeiro, O. S. Carneiro, and A. Ferreira da Silva, "Interface geometries in 3D multi-material prints by fused filament fabrication," RPJ. **25**(1), 38–46 (2019).
[70]M.-A. de Pastre, Y. Quinsat, and C. Lartigue, "Effects of additive manufacturing processes on part defects and properties: A classification review," Int. J. Interact. Des. Manuf. **16**(4), 1471–1496 (2022).

[71]H. Taheri, M. R. B. M. Shoaib, L. W. Koester, T. A. Bigelow, P. C. Collins, and L. J. Bond, "Powder-based additive manufacturing-a review of types of defects, generation mechanisms, detection, property evaluation and metrology," IJASMM. **1**(2), 172–209 (2017).
[72]M. Li, S. Huang, E. Willems, J. Soete, M. Inokoshi, B. Van Meerbeek, J. Vleugels, and F. Zhang, "UV-curing assisted direct ink writing of dense, crack-free, and high-performance zirconia-based composites with aligned alumina platelets," Adv. Mater. **36**(5), 2306764 (2024).
[73]D. Zhang, C. Chu, S. Ma, Y. Wang, C. Duan, J. Guo, X. Shi, G. Xu, Y. Cheng, and A. Sun, "A novel method to avoid the sintering shrinkage of Al_2O_3-Cr cermets formed by direct ink writing," J. Alloys Compd. **931**, 167632 (2023).
[74]T. Wang, W. Yang, Z. Wang, B. Wang, M. Li, L. Shi, and S. Rao, "Taming the coffee-ring effect on solid surface by localized heating upon the suspension droplet," Int. J. Heat Mass Transfer **219**, 124920 (2024).
[75]R. Sliz, J. Czajkowski, and T. Fabritius, "Taming the coffee ring effect: Enhanced thermal control as a method for thin-film nanopatterning," Langmuir **36**(32), 9562–9570 (2020).
[76]K. M. Rahman, A. Wei, H. Miyanaji, and C. B. Williams, "Impact of binder on part densification: Enhancing binder jetting part properties through the fabrication of shelled geometries," Addit. Manuf. **62**, 103377 (2023).
[77]C. B. Sweeney, B. A. Lackey, M. J. Pospisil, T. C. Achee, V. K. Hicks, A. G. Moran, B. R. Teipel, M. A. Saed, and M. J. Green, "Welding of 3D-printed carbon nanotube–polymer composites by locally induced microwave heating," Sci. Adv. **3**(6), e1700262 (2017).
[78]X. Nie, H. Zhang, H. Zhu, Z. Hu, L. Ke, and X. Zeng, "Effect of Zr content on formability, microstructure and mechanical properties of selective laser melted Zr modified Al-4.24 Cu-1.97 Mg-0.56 Mn alloys," J. Alloys Compd. **764**, 977–986 (2018).
[79]L. Zhao, Z. Zhao, L. Ma, Z. Men, Y. Ma, and L. Wu, "Limiting defect in vat photopolymerization via visual-guided in-situ repair," Addit. Manuf. **79**, 103947 (2024).
[80]J. Mc Bain and D. Hopkins, *Second Report of the Adhesives Research Committee* (HMSO, London, UK, 1926).
[81]J. McBain and D. Hopkins, "On adhesives and adhesive action," J. Phys. Chem. **29**(2), 188–204 (1925).
[82]D. Gu, X. Shi, R. Poprawe, D. L. Bourell, R. Setchi, and J. Zhu, "Material-structure-performance integrated laser-metal additive manufacturing," Science **372**(6545), eabg1487 (2021).
[83]G. Fourche, "An overview of the basic aspects of polymer adhesion. Part I: Fundamentals," Polym. Eng. Sci. **35**(12), 957–967 (1995).
[84]S. Ebnesajjad, "Theories of adhesion," in *Surface Treatment Materials Adhesive Bonding*, 2nd ed. (2014), pp. 77–91.
[85]S. Voyutskiĭ, "The diffusion theory of adhesion," Rubber Chem. Technol. **33**(3), 748–756 (1960).
[86]T. J. Coogan and D. O. Kazmer, "Prediction of interlayer strength in material extrusion additive manufacturing," Addit. Manuf. **35**, 101368 (2020).
[87]R. Wool and K. O'Connor, "Time dependence of crack healing," J. Polym. Sci. B Polym. Lett. Ed. **20**(1), 7–16 (1982).
[88]R. Wool and K. O'connor, "A theory crack healing in polymers," J. Appl. Phys. **52**(10), 5953–5963 (1981).
[89]C. Wei, B. Jin, Q. Zhang, X. Zhan, and F. Chen, "Anti-icing performance of super-wetting surfaces from icing-resistance to ice-phobic aspects: Robust hydrophobic or slippery surfaces," J. Alloys Compd. **765**, 721–730 (2018).
[90]Y.-H. Yu, Y.-P. Chen, M. Zeng, and Z. Cheng, "Microwave-assisted rapid synthesis of hexagonal α-zirconium phosphate nanodisks as a Pickering emulsion stabilizer," Mater. Lett. **163**, 158–161 (2016).
[91]M. Zeng, S. A. Shah, D. Huang, D. Parviz, Y.-H. Yu, X. Wang, M. J. Green, and Z. Cheng, "Aqueous exfoliation of graphite into graphene assisted by sulfonyl graphene quantum dots for photonic crystal applications," ACS Appl. Mater. Interfaces **9**(36), 30797–30804 (2017).
[92]J. Luo, M. Zeng, B. Peng, Y. Tang, L. Zhang, P. Wang, L. He, D. Huang, L. Wang, X. Wang *et al.*, "Electrostatic-driven dynamic jamming of 2D nanoparticles at interfaces for controlled molecular diffusion," Angew. Chem. Int. Ed. **57**(36), 11752–11757 (2018).
[93]R. Ma, M. Zeng, D. Huang, and Q. Wang, "Zwitterionic graphene quantum dots to stabilize pickering emulsions for controlled-release applications," ACS Appl. Mater. Interfaces **14**(5), 7486–7492 (2022).
[94]L. Zhang, Q. Lei, J. Luo, M. Zeng, L. Wang, D. Huang, X. Wang, S. Mannan, B. Peng, and Z. Cheng, "Natural halloysites-based janus platelet surfactants for the formation of pickering emulsion and enhanced oil recovery," Sci. Rep. **9**(1), 163 (2019).
[95]M. Zeng, I. Echols, P. Wang, S. Lei, J. Luo, B. Peng, L. He, L. Zhang, D. Huang, C. Mejia *et al.*, "Highly biocompatible, underwater superhydrophilic and multifunctional biopolymer membrane for efficient oil–water separation and aqueous pollutant removal," ACS Sustainable Chem. Eng. **6**(3), 3879–3887 (2018).
[96]M. Zeng, P. Wang, J. Luo, B. Peng, B. Ding, L. Zhang, L. Wang, D. Huang, I. Echols, E. Abo Deeb *et al.*, "Hierarchical, self-healing and superhydrophobic zirconium phosphate hybrid membrane based on the interfacial crystal growth of lyotropic two-dimensional nanoplatelets," ACS Appl. Mater. Interfaces **10**(26), 22793–22800 (2018).
[97]L. Sharpe and H. Schonhorn, "Theory gives direction to adhesion work," Chem. Eng. News **41**(15), 67–68 (1963).
[98]A. Marmur, "Equilibrium and spreading of liquids on solid surfaces," Adv. Colloid Interface Sci. **19**(1-2), 75–102 (1983).
[99]R. N. Wenzel, "Resistance of solid surfaces to wetting by water," Ind. Eng. Chem. **28**(8), 988–994 (1936).
[100]A. Cassie and S. Baxter, "Wettability of porous surfaces," Trans. Faraday Soc. **40**, 546–551 (1944).
[101]H. Park, J. J. Park, P. D. Bui, H. Yoon, C. P. Grigoropoulos, D. Lee, and S. H. Ko, "Laser-based selective material processing for next-generation additive manufacturing," Adv. Mater. **36**, 2307586 (2024).
[102]M. Noeske, J. Degenhardt, S. Strudthoff, and U. Lommatzsch, "Plasma jet treatment of five polymers at atmospheric pressure: Surface modifications and the relevance for adhesion," Int. J. Adhes. Adhes. **24**(2), 171–177 (2004).
[103]Y.-L. Shen, "Thermal expansion of metal–ceramic composites: A three-dimensional analysis," Mater. Sci. Eng, A **252**(2), 269–275 (1998).
[104]T. Christman, A. Needleman, and S. Suresh, "An experimental and numerical study of deformation in metal-ceramic composites," Acta Metall. **37**(11), 3029–3050 (1989).
[105]Z. Ma, W. Liu, W. Li, H. Liu, J. Song, Y. Liu, Y. Huang, Y. Xia, Z. Wang, and B. Liu, "Additive manufacturing of functional gradient materials: A review of research progress and challenges," J. Alloys Compd. **971**, 172642 (2024).
[106]A. Neubrand and J. Rödel, "Gradient materials: An overview of a novel concept," Int. J. Mater. Res. **88**(5), 358–371 (2021).
[107]M. Dao, P. Gu, A. Maewal, and R. Asaro, "A micromechanical study of residual stresses in functionally graded materials," Acta Mater. **45**(8), 3265–3276 (1997).
[108]S. K. Soni, B. Thomas, and V. R. Kar, "A comprehensive review on CNTs and CNT-reinforced composites: Syntheses, characteristics and applications," Mater. Today Commun. **25**, 101546 (2020).
[109]J. Li and R. A. Laghari, "A review on machining and optimization of particle-reinforced metal matrix composites," Int. J. Adv. Manuf. Technol. **100**, 2929–2943 (2019).
[110]D. K. Rajak, D. D. Pagar, R. Kumar, and C. I. Pruncu, "Recent progress of reinforcement materials: A comprehensive overview of composite materials," J. Mater. Res. Technol. **8**(6), 6354–6374 (2019).
[111]N. Arefin, G. Podolak, J. Lewis-Sandy, and M. Zeng, "Printing and patterning of clay-based nanocomposites for healthcare and sustainable applications," MRS Commun. **13**(6), 980–993 (2023).
[112]Ö. Balcı, K. G. Prashanth, S. Scudino, M. Somer, and J. Eckert, "Powder metallurgy of Al-based composites reinforced with Fe-based glassy particles: Effect of microstructural modification," Part. Sci. Technol. **37**(3), 286–291 (2019).
[113]P. Wan, X. Wen, C. Sun, B. K. Chandran, H. Zhang, X. Sun, and X. Chen, "Flexible transparent films based on nanocomposite networks of polyaniline and carbon nanotubes for high-performance gas sensing," Small **11**(40), 5409–5415 (2015).
[114]N. Arefin, R. Shanmugam, and M. Zeng, "Natural 2D material polymer composites: Processing, properties, and applications," in *Sustainable Structural Materials*, 1st ed. (CRC Press, 2025) p. 19.
[115]I. Ahmad, M. Unwin, H. Cao, H. Chen, H. Zhao, A. Kennedy, and Y. Zhu, "Multi-walled carbon nanotubes reinforced Al_2O_3 nanocomposites: Mechanical properties and interfacial investigations," Compos. Sci. Technol. **70**(8), 1199–1206 (2010).

[116]M. Estili, A. Kawasaki, Y. Pittini-Yamada, I. Utke, and J. Michler, "In situ characterization of tensile-bending load bearing ability of multi-walled carbon nanotubes in alumina-based nanocomposites," J. Mater. Chem. **21**(12), 4272–4278 (2011).
[117]R. Latif, S. Wakeel, N. Zaman Khan, A. Noor Siddiquee, S. Lal Verma, and Z. Akhtar Khan, "Surface treatments of plant fibers and their effects on mechanical properties of fiber-reinforced composites: A review," J. Reinf. Plast. Compos. **38**(1), 15–30 (2019).
[118]A. Reichardt, A. A. Shapiro, R. Otis, R. P. Dillon, J. P. Borgonia, B. W. McEnerney, P. Hosemann, and A. M. Beese, "Advances in additive manufacturing of metal-based functionally graded materials," Int. Mater. Rev. **66**(1), 1–29 (2021).
[119]B. Li, J. Fu, J. Feng, C. Shang, and Z. Lin, "Review of heterogeneous material objects modeling in additive manufacturing," Vis. Comput. Ind. Biomed. Art **3**, 1–18 (2020).
[120]Y. Song, Z. Yang, Y. Liu, and J. Deng, "Function representation based slicer for 3D printing," Comput. Aided Geom. Des. **62**, 276–293 (2018).
[121]D. W. Rosen, "Computer-aided design for additive manufacturing of cellular structures," Comput-Aided. Des. Applic. **4**(5), 585–594 (2007).
[122]G. H. Loh, E. Pei, D. Harrison, and M. D. Monzón, "An overview of functionally graded additive manufacturing," Addit. Manuf. **23**, 34–44 (2018).
[123]Y. Li, Z. Feng, L. Hao, L. Huang, C. Xin, Y. Wang, E. Bilotti, K. Essa, H. Zhang, and Z. Li, "A review on functionally graded materials and structures via additive manufacturing: From multi-scale design to versatile functional properties," Adv. Mater. Technol. **5**(6), 1900981 (2020).
[124]M. P. Bendsøe and N. Kikuchi, "Generating optimal topologies in structural design using a homogenization method," Comput. Methods Appl. Mech. Eng. **71**(2), 197–224 (1988).
[125]K. Ghabraie, "An improved soft-kill BESO algorithm for optimal distribution of single or multiple material phases," Struct. Multidiscip. Optim. **52**, 773–790 (2015).
[126]T. Liu, S. Guessasma, J. Zhu, W. Zhang, and S. Belhabib, "Functionally graded materials from topology optimisation and stereolithography," Eur. Polym. J. **108**, 199–211 (2018).
[127]V. Gupta and P. Tandon, "Heterogeneous object modeling with material convolution surfaces," Comput-Aided. Des. **62**, 236–247 (2015).
[128]J. Chen, Y. Yang, C. Song, M. Zhang, S. Wu, and D. Wang, "Interfacial microstructure and mechanical properties of 316L/CuSn10 multi-material bimetallic structure fabricated by selective laser melting," Mater. Sci. Eng, A **752**, 75–85 (2019).
[129]M. A. Groeber and M. A. Jackson, "DREAM. 3D: A digital representation environment for the analysis of microstructure in 3D," Integr. Mater. Manuf. Innov. **3**(1), 56–72 (2014).
[130]L. D. Bobbio, R. A. Otis, J. P. Borgonia, R. P. Dillon, A. A. Shapiro, Z.-K. Liu, and A. M. Beese, "Additive manufacturing of a functionally graded material from Ti-6Al-4V to Invar: Experimental characterization and thermodynamic calculations," Acta Mater. **127**, 133–142 (2017).
[131]H. Sahasrabudhe, R. Harrison, C. Carpenter, and A. Bandyopadhyay, "Stainless steel to titanium bimetallic structure using LENS™," Addit. Manuf. **5**, 1–8 (2015).
[132]Y. Kok, X. P. Tan, P. Wang, M. Nai, N. H. Loh, E. Liu, and S. B. Tor, "Anisotropy and heterogeneity of microstructure and mechanical properties in metal additive manufacturing: A critical review," Mater. Des. **139**, 565–586 (2018).
[133]L. D. Bobbio, B. Bocklund, E. Simsek, R. T. Ott, M. J. Kramer, Z.-K. Liu, and A. M. Beese, "Design of an additively manufactured functionally graded material of 316 stainless steel and Ti-6Al-4V with Ni-20Cr, Cr, and V intermediate compositions," Addit. Manuf. **51**, 102649 (2022).
[134]A. R. Moustafa, A. Durga, G. Lindwall, and Z. C. Cordero, "Scheil ternary projection (STeP) diagrams for designing additively manufactured functionally graded metals," Addit. Manuf. **32**, 101008 (2020).
[135]T. M. Rodgers, J. D. Madison, and V. Tikare, "Simulation of metal additive manufacturing microstructures using kinetic Monte Carlo," Comput. Mater. Sci. **135**, 78–89 (2017).
[136]M. Lißner, B. Erice, E. Alabort, D. Thomson, H. Cui, C. Kaboglu, B. Blackman, M. Gude, and N. Petrinic, "Multi-material adhesively bonded structures: Characterisation and modelling of their rate-dependent performance," Composites Part B **195**, 108077 (2020).
[137]R. B. Tipton, D. Hou, Z. Shi, T. M. Weller, and V. R. Bhethanabotla, "Optical interconnects on a flexible substrate by multi-material hybrid additive and subtractive manufacturing," Addit. Manuf. **48**, 102409 (2021).
[138]Y. Wang and X. Li, "4D-printed bi-material composite laminate for manufacturing reversible shape-change structures," Composites Part B **219**, 108918 (2021).
[139]Z. Sun, Y.-H. Chueh, and L. Li, "Multiphase mesoscopic simulation of multiple and functionally gradient materials laser powder bed fusion additive manufacturing processes," Addit. Manuf. **35**, 101448 (2020).
[140]M. He, X. Zhang, L. dos Santos Fernandez, A. Molter, L. Xia, and T. Shi, "Multi-material topology optimization of piezoelectric composite structures for energy harvesting," Compos. Struct. **265**, 113783 (2021).
[141]J. Y. Kim, D. Garcia, Y. Zhu, D. M. Higdon, and Z. Y. Hang, "A Bayesian learning framework for fast prediction and uncertainty quantification of additively manufactured multi-material components," J. Mater. Process. Technol. **303**, 117528 (2022).
[142]S. Mora, N. M. Pugno, and D. Misseroni, "3D printed architected lattice structures by material jetting," Mater. Today **59**, 107–132 (2022).
[143]J. A. Lewis and G. M. Gratson, "Direct writing in three dimensions," Mater. Today **7**(7-8), 32–39 (2004).
[144]J. A. Lewis, J. E. Smay, J. Stuecker, and J. Cesarano, "Direct ink writing of three-dimensional ceramic structures," J. Am. Ceram. Soc. **89**(12), 3599–3609 (2006).
[145]Y. Zhang, T. Ji, S. Hou, L. Zhang, Y. Shi, J. Zhao, and X. Xu, "All-printed solid-state substrate-versatile and high-performance micro-supercapacitors for in situ fabricated transferable and wearable energy storage via multi-material 3D printing," J. Power Sources **403**, 109–117 (2018).
[146]T. S. Wei, B. Y. Ahn, J. Grotto, and J. A. Lewis, "3D printing of customized Li-ion batteries with thick electrodes," Adv. Mater. **30**(16), 1703027 (2018).
[147]Y. Zhang, C. Pan, P. Liu, L. Peng, Z. Liu, Y. Li, Q. Wang, T. Wu, Z. Li, and C. Majidi, "Coaxially printed magnetic mechanical electrical hybrid structures with actuation and sensing functionalities," Nat. Commun. **14**(1), 4428 (2023).
[148]M. Xie, M. Zhu, Z. Yang, S. Okada, and S. Kawamura, "Flexible self-powered multifunctional sensor for stiffness-tunable soft robotic gripper by multimaterial 3D printing," Nano Energy **79**, 105438 (2021).
[149]V. Esposito, C. Gadea, J. Hjelm, D. Marani, Q. Hu, K. Agersted, S. Ramousse, and S. H. Jensen, "Fabrication of thin yttria-stabilized-zirconia dense electrolyte layers by inkjet printing for high performing solid oxide fuel cells," J. Power Sources **273**, 89–95 (2015).
[150]N. Farandos, L. Kleiminger, T. Li, A. Hankin, and G. Kelsall, "Three-dimensional inkjet printed solid oxide electrochemical reactors. I. Yttria-stabilized zirconia electrolyte," Electrochim. Acta **213**, 324–331 (2016).
[151]D. Thuau, K. Kallitsis, F. D. Dos Santos, and G. Hadziioannou, "All inkjet-printed piezoelectric electronic devices: Energy generators, sensors and actuators," J. Mater. Chem. C **5**(38), 9963–9966 (2017).
[152]Q. Jiang, S. Atampugre, Y. Du, L. Yang, J. L. Schaefer, and Y. Zhang, "Combinatorial printing of functionally graded solid-state electrolyte for high-voltage lithium metal batteries," ACS Mater. Lett. **6**(6), 2205–2212 (2024).
[153]C. Ou, L. Zhang, Q. Jing, V. Narayan, and S. Kar-Narayan, "Compositionally graded organic–inorganic nanocomposites for enhanced thermoelectric performance," Adv. Elect. Mater. **6**(1), 1900720 (2020).
[154]H. Hwang, S. Park, M. Smith, S. T. Bose, A. R. Peringath, J. Zhang, J.-T. Kim, Q. Jing, S. Kar-Narayan, and Y. Choi, "Highly dispersed nanomaterials in polymer matrix via aerosol-jet-based multi-material 3D printing," Nano Energy **128**, 109803 (2024).
[155]G. Manogharan, M. Kioko, and C. Linkous, "Binder jetting: A novel solid oxide fuel-cell fabrication process and evaluation," JOM **67**, 660–667 (2015).
[156]M. Ali, D. Prakash, T. Zillger, P. K. Singh, and A. C. Hübler, "Printed piezoelectric energy harvesting device," Adv. Energy Mater **4**(2) (2014).
[157]M. Saadi, A. Maguire, N. T. Pottackal, M. S. H. Thakur, M. M. Ikram, A. J. Hart, P. M. Ajayan, and M. M. Rahman, "Direct ink writing: A 3D printing technology for diverse materials," Adv. Mater. **34**(28), 2108855 (2022).
[158]M. Zeng and Y. Zhang, "Colloidal nanoparticle inks for printing functional devices: Emerging trends and future prospects," J. Mater. ChemA. **7**(41), 23301–23336 (2019).

[159]W. H. Herschel and R. Bulkley, "Konsistenzmessungen von gummi-benzollösungen," Kolloid-Z. **39**, 291–300 (1926).
[160]J. O. Hardin, T. J. Ober, A. D. Valentine, and J. A. Lewis, "Microfluidic printheads for multimaterial 3D printing of viscoelastic inks," Adv. Mater. **27**(21), 3279–3284 (2015).
[161]J. M. Ortega, M. Golobic, J. D. Sain, J. M. Lenhardt, A. S. Wu, S. E. Fisher, L. X. Perez Perez, A. W. Jaycox, J. E. Smay, and E. B. Duoss, "Active mixing of disparate inks for multimaterial 3D printing," Adv. Mater. Technol. **4**(7), 1800717 (2019).
[162]K. Chen, X. Kuang, V. Li, G. Kang, and H. J. Qi, "Fabrication of tough epoxy with shape memory effects by UV-assisted direct-ink write printing," Soft Matter **14**(10), 1879–1886 (2018).
[163]X. Li, J. M. Zhang, X. Yi, Z. Huang, P. Lv, and H. Duan, "Multimaterial microfluidic 3D printing of textured composites with liquid inclusions," Adv. Sci. **6**(3), 1800730 (2019).
[164]L. Fieber, J. D. Evans, C. Huang, and P. S. Grant, "Single-operation, multiphase additive manufacture of electro-chemical double layer capacitor devices," Addit. Manuf. **28**, 344–353 (2019).
[165]J. A. Cardenas, J. P. Bullivant, B. R. Wygant, A. S. Lapp, N. S. Bell, T. N. Lambert, L. C. Merrill, A. A. Talin, A. W. Cook, E. Allcorn, and K. L. Harrison, "Custom-form iron trifluoride Li-batteries using material extrusion and electrolyte exchanged ionogels," Addit. Manuf. **84**, 104102 (2024).
[166]B. J. De Gans, P. C. Duineveld, and U. S. Schubert, "Inkjet printing of polymers: State of the art and future developments," Adv. Mater. **16**(3), 203–213 (2004).
[167]M. A. Shah, D. G. Lee, B. Y. Lee, and S. Hur, "Classifications and applications of inkjet printing technology: A review," IEEE Access. **9**, 140079–140102 (2021).
[168]J. Mei, M. R. Lovell, and M. H. Mickle, "Formulation and processing of novel conductive solution inks in continuous inkjet printing of 3-D electric circuits," IEEE Trans. Electron. Packag. Manuf. **28**(3), 265–273 (2005).
[169]R. Bernasconi, S. Brovelli, P. Viviani, M. Soldo, D. Giusti, and L. Magagnin, "Piezoelectric drop-on-demand inkjet printing of high-viscosity inks," Adv. Eng. Mater. **24**(1), 2100733 (2022).
[170]Y. Pang, Y. Cao, Y. Chu, M. Liu, K. Snyder, D. MacKenzie, and C. Cao, "Additive manufacturing of batteries," Adv. Funct. Mater. **30**(1), 1906244 (2020).
[171]J.-D. Lee, J.-B. Yoon, J.-K. Kim, H.-J. Chung, C.-S. Lee, H.-D. Lee, H.-J. Lee, C.-K. Kim, and C.-H. Han, "A thermal inkjet printhead with a monolithically fabricated nozzle plate and self-aligned ink feed hole," J. Microelectromech. Syst. **8**(3), 229–236 (1999).
[172]B.-H. Kim, H.-S. Lee, S.-W. Kim, P. Kang, and Y.-S. Park, "Hydrodynamic responses of a piezoelectric driven MEMS inkjet print-head," Sens. Actuators, A **210**, 131–140 (2014).
[173]F. Torrisi, T. Hasan, W. Wu, Z. Sun, A. Lombardo, T. S. Kulmala, G.-W. Hsieh, S. Jung, F. Bonaccorso, and P. J. Paul, "Inkjet-printed graphene electronics," ACS Nano **6**(4), 2992–3006 (2012).
[174]K.-H. Lee, S.-S. Lee, D. B. Ahn, J. Lee, D. Byun, and S.-Y. Lee, "Ultrahigh areal number density solid-state on-chip microsupercapacitors via electrohydrodynamic jet printing," Sci. Adv. **6**(10), eaaz1692 (2020).
[175]H. Liu, X. Yin, C. Chi, T. Feng, P. Wang, W. Wang, and H. Tian, "Direct printing of flexible multilayer composite electrodes based on electrohydrodynamic printing," ACS Appl. Electron. Mater. **6**(2), 724–736 (2024).
[176]S. Wang, G. Zeng, Q. Sun, Y. Feng, X. Wang, X. Ma, J. Li, H. Zhang, J. Wen, and J. Feng, "Flexible electronic systems via electrohydrodynamic jet printing: A MnSe@ rGO cathode for aqueous zinc-ion batteries," ACS Nano **17**(14), 13256–13268 (2023).
[177]A. Reiser, M. Lindén, P. Rohner, A. Marchand, H. Galinski, A. S. Sologubenko, J. M. Wheeler, R. Zenobi, D. Poulikakos, and R. Spolenak, "Multi-metal electrohydrodynamic redox 3D printing at the submicron scale," Nat. Commun. **10**(1), 1853 (2019).
[178]B. Derby, "Inkjet printing of functional and structural materials: Fluid property requirements, feature stability, and resolution," Annu. Rev. Mater. Res. **40**(1), 395–414 (2010).
[179]J. Fromm, "Numerical calculation of the fluid dynamics of drop-on-demand jets," IBM J. Res. Dev. **28**(3), 322–333 (1984).
[180]G. Hu, J. Kang, L. W. Ng, X. Zhu, R. C. Howe, C. G. Jones, M. C. Hersam, and T. Hasan, "Functional inks and printing of two-dimensional materials," Chem. Soc. Rev. **47**(9), 3265–3300 (2018).
[181]T.-T. Huang and W. Wu, "Scalable nanomanufacturing of inkjet-printed wearable energy storage devices," J. Mater. Chem A. **7**(41), 23280–23300 (2019).
[182]S. Lawes, Q. Sun, A. Lushington, B. Xiao, Y. Liu, and X. Sun, "Inkjet-printed silicon as high performance anodes for Li-ion batteries," Nano Energy **36**, 313–321 (2017).
[183]W. Zhou, X. Li, H. Duan, and P. Lv, "Multi-material integrated three-dimensional printing of cylindrical Li-Ion battery," J. Manuf. Sci. Eng. **144**(6), 064501 (2022).
[184]T. Eggenhuisen, Y. Galagan, A. Biezemans, T. Slaats, W. Voorthuijzen, S. Kommeren, S. Shanmugam, J. Teunissen, A. Hadipour, and W. Verhees, "High efficiency, fully inkjet printed organic solar cells with freedom of design," J. Mater. Chem A. **3**(14), 7255–7262 (2015).
[185]I. F. Ituarte, N. Boddeti, V. Hassani, M. L. Dunn, and D. W. Rosen, "Design and additive manufacture of functionally graded structures based on digital materials," Addit. Manuf. **30**, 100839 (2019).
[186]E. Salcedo, D. Baek, A. Berndt, and J. E. Ryu, "Simulation and validation of three dimension functionally graded materials by material jetting," Addit. Manuf. **22**, 351–359 (2018).
[187]Y. Liu, Q. Zhang, A. Huang, K. Zhang, S. Wan, H. Chen, Y. Fu, W. Zuo, Y. Wang, and X. Cao, "Fully inkjet-printed Ag_2Se flexible thermoelectric devices for sustainable power generation," Nat. Commun. **15**(1), 2141 (2024).
[188]L. J. Deiner and T. L. Reitz, "Inkjet and aerosol jet printing of electrochemical devices for energy conversion and storage," Adv. Eng. Mater. **19**(7), 1600878 (2017).
[189]M. Saeidi-Javash, Y. Du, M. Zeng, B. C. Wyatt, B. Zhang, N. Kempf, B. Anasori, and Y. Zhang, "All-printed MXene–graphene nanosheet-based bimodal sensors for simultaneous strain and temperature sensing," ACS Appl. Electron. Mater. **3**(5), 2341–2348 (2021).
[190]M. Zeng, W. Kuang, I. Khan, D. Huang, Y. Du, M. Saeidi-Javash, L. Zhang, Z. Cheng, A. J. Hoffman, and Y. Zhang, "Colloidal nanosurfactants for 3D conformal printing of 2D van der Waals materials," Adv. Mater. **32**(39), 2003081 (2020).
[191]J. A. Paulsen, M. Renn, K. Christenson, and R. Plourde, "Printing conformal electronics on 3D structures with Aerosol Jet technology," in *Future of Instrumentation International Workshop (FIIW) Proceedings* (IEEE, 2012), pp. 1–4.
[192]N. Turan, M. Saeidi-Javash, J. Chen, M. Zeng, Y. Zhang, and D. B. Go, "Atmospheric pressure and ambient temperature plasma jet sintering of aerosol jet printed silver nanoparticles," ACS Appl. Mater. Interfaces **13**(39), 47244–47251 (2021).
[193]M. Zeng, H. Xie, M. Saeidi-Javash, A. Tanvir, Y. Du, J. Chen, M. G. Kanatzidis, and Y. Zhang, "Scalable nanomanufacturing of chalcogenide inks: A case study on thermoelectric V–VI nanoplates," J. Mater. Chem. A. **9**(39), 22555–22562 (2021).
[194]Q. Huang and Y. Zhu, "Printing conductive nanomaterials for flexible and stretchable electronics: A review of materials, processes, and applications," Adv. Mater. Technol. **4**(5), 1800546 (2019).
[195]N. Wilkinson, M. Smith, R. Kay, and R. Harris, "A review of aerosol jet printing—A non-traditional hybrid process for micro-manufacturing," Int. J. Adv. Manuf. Technol. **105**, 4599–4619 (2019).
[196]C. Cao, J. B. Andrews, and A. D. Franklin, "Completely printed, flexible, stable, and hysteresis-free carbon nanotube thin-film transistors via aerosol jet printing," Adv. Elect. Mater. **3**(5), 1700057 (2017).
[197]L. Gamba, J. A. Lajoie, T. R. Sippel, and E. B. Secor, "Multi-material aerosol jet printing of Al/Cuo nanothermites for versatile fabrication of energetic antennas," Adv. Funct. Mater. **33**(49), 2304060 (2023).
[198]S. Taccola, H. Bakhshi, M. Sanchez Sifuentes, P. Lloyd, L. J. Tinsley, J. Macdonald, A. Bacchetti, O. Cespedes, J. H. Chandler, and P. Valdastri, "Dual-material aerosol jet printing of magneto-responsive polymers with in-process tailorable composition for small-scale soft robotics," Adv. Mater. Technol. **9**, 2400463 (2024).
[199]E. B. Secor, "Principles of aerosol jet printing," Flex. Print. Electron. **3**(3), 035002 (2018).

[200]A. Sukeshini, T. Jenkins, P. Gardner, R. Miller, and T. Reitz, "Investigation of aerosol jet deposition parameters for printing SOFC layers," In ASME 2010 8th International Conference on Fuel Cell Science, Engineering and Technology, June 14–16, Brooklyn, New York, USA (2010), Vol. 44045, pp 325–332.
[201]L. Gamba, M. E. A. Razzaq, S. Diaz-Arauzo, M. C. Hersam, X. Bai, and E. B. Secor, "Tailoring electrical properties in carbon nanomaterial patterns with multimaterial aerosol jet printing," ACS Appl. Mater. Interfaces **15**(49), 57525–57532 (2023).
[202]Q. Jing, Y. S. Choi, M. Smith, C. Ou, T. Busolo, and S. Kar-Narayan, "Freestanding functional structures by aerosol-jet printing for stretchable electronics and sensing applications," Adv. Mater. Technol. **4**(7), 1900048 (2019).
[203]J. Chen, M. Saeidi-Javash, M. Palei, M. Zeng, Y. Du, K. Mondal, M. D. McMurtrey, A. J. Hoffman, and Y. Zhang, "Printing noble metal alloy films with compositional gradient," Appl. Mater. Today **27**, 101405 (2022).
[204]L. J. Deiner, T. Jenkins, T. Howell, and M. Rottmayer, "Aerosol jet printed polymer composite electrolytes for solid-state li-ion batteries," Adv. Eng. Mater. **21**(12), 1900952 (2019).
[205]R. Lopez-Hallman, R. Rodriguez, Y.-T. Lai, Q. Zhang, B.-H. Tsao, J. Deiner, J. P. Fellner, and Y. Zhu, "All-solid-state battery fabricated by 3D aerosol jet printing," Adv. Eng. Mater. **26**(4), 2300953 (2024).
[206]A. S. K. Kiran, J. B. Veluru, S. Merum, A. Radhamani, M. Doble, T. S. Kumar, and S. Ramakrishna, "Additive manufacturing technologies: An overview of challenges and perspective of using electrospraying," Nanocomposites **4**(4), 190–214 (2018).
[207]Y. Bai and C. B. Williams, "An exploration of binder jetting of copper," Rapid Prototyping J. **21**(2), 177–185 (2015).
[208]M. Ziaee and N. B. Crane, "Binder jetting: A review of process, materials, and methods," Addit. Manuf. **28**, 781–801 (2019).
[209]A. Nazir, O. Gokcekaya, K. M. M. Billah, O. Ertugrul, J. Jiang, J. Sun, and S. Hussain, "Multi-material additive manufacturing: A systematic review of design, properties, applications, challenges, and 3D printing of materials and cellular metamaterials," Mater. Des. **226**, 111661 (2023).
[210]P.-J. Chiang, K. P. Davidson, J. M. Wheeler, A. Ong, K. Erickson, and M. Seita, "Site-specific alloying through binder jet 3D printing," Mater. Des. **235**, 112384 (2023).
[211]D. Godlinski and S. Morvan, "Steel parts with tailored material gradients by 3D-printing using nano-particulate ink," MSF **492**, 679–684 (2005).
[212]M. Lehmann, C. G. Kolb, F. Klinger, and M. F. Zaeh, "Preparation, characterization, and monitoring of an aqueous graphite ink for use in binder jetting," Mater. Des. **207**, 109871 (2021).
[213]M. Lehmann and M. Zaeh, "Process integrated production of wc-co tools with local cobalt gradient fabricated by binder jetting," in Solid Freeform Fabrication 2019: Proceedings of the 30th Annual International Solid Freeform Fabrication Symposium—An Additive Manufacturing Conference, Preprint (2021).
[214]M. Li, W. Du, A. Elwany, Z. Pei, and C. Ma, "Metal binder jetting additive manufacturing: A literature review," J. Manuf. Sci. Eng. **142**(9), 090801 (2020).
[215]N. B. Crane, "Impact of part thickness and drying conditions on saturation limits in binder jet additive manufacturing," Addit. Manuf. **33**, 101127 (2020).
[216]X. Shen, M. Chu, F. Hariri, G. Vedula, and H. E. Naguib, "Binder jetting fabrication of highly flexible and electrically conductive graphene/PVOH composites," Addit. Manuf. **36**, 101565 (2020).
[217]G. M. Gratson, M. Xu, and J. A. Lewis, "Direct writing of three-dimensional webs," nature **428**(6981), 386–386 (2004).
[218]C. Li, F. Bu, Q. Wang, and X. Liu, "Recent developments of inkjet-printed flexible energy storage devices," Adv. Mater. Inter. **9**(34), 2201051 (2022).
[219]P. Yang and H. J. Fan, "Inkjet and extrusion printing for electrochemical energy storage: A minireview," Adv. Mater. Technol. **5**(10), 2000217 (2020).
[220]H. Shi, J. Cao, Z. Sun, Z. A. Ghazi, X. Zhu, S. Han, D. Ren, G. Lu, H. Lan, and F. Li, "3D printing enables customizable batteries," Batteries Supercaps **6**(7), e202300161 (2023).
[221]P. Parandoush and D. Lin, "A review on additive manufacturing of polymer-fiber composites," Compos. Struct. **182**, 36–53 (2017).
[222]R. Nandhakumar and K. Venkatesan, "A process parameters review on selective laser melting-based additive manufacturing of single and multi-material: Microstructure, physical properties, tribological, and surface roughness," Mater. Today Commun. **35**, 105538 (2023).
[223]F. Zhang, L. Zhu, Z. Li, S. Wang, J. Shi, W. Tang, N. Li, and J. Yang, "The recent development of vat photopolymerization: A review," Addit. Manuf. **48**, 102423 (2021).
[224]J. Persad and S. Rocke, "A survey of 3D printing technologies as applied to printed electronics," IEEE Access **10**, 27289–27319 (2022).
[225]H. Wu, Q. Wang, Z. Wu, M. Wang, L. Yang, Z. Liu, S. Wu, B. Su, C. Yan, and Y. Shi, "Multi-material additively manufactured magnetoelectric architectures with a structure-dependent mechanical-to-electrical conversion capability," Small Methods **6**(12), 2201127 (2022).
[226]D. Kam, G. Gwon, S. Jang, D. Yoo, S. J. Park, M. La, and D. Choi, "Advancing energy harvesting efficiency from a single droplet: A mechanically guided 4D printed elastic hybrid droplet-based electricity generator," Adv. Mater. **35**(48), 2303681 (2023).
[227]S. Bai and J. Liu, "Femtosecond laser additive manufacturing of multi-material layered structures," Appl. Sci. **10**(3), 979 (2020).
[228]X. Wang, W. Guo, R. Abu-Reziq, and S. Magdassi, "High-complexity WO3-based catalyst with multi-catalytic species via 3D printing," Catalysts **10**(8), 840 (2020).
[229]I. Kunce, M. Polanski, and J. Bystrzycki, "Structure and hydrogen storage properties of a high entropy ZrTiVCrFeNi alloy synthesized using Laser Engineered Net Shaping (LENS)," Int. J. Hydrogen Energy **38**(27), 12180–12189 (2013).
[230]J. Li, W. Craeghs, C. Jing, S. Gong, and F. Shan, "Microstructure and physical performance of laser-induction nanocrystals modified high-entropy alloy composites on titanium alloy," Mater. Des. **117**, 363–370 (2017).
[231]P. Zhou, D. Xiao, Z. Wu, and X. Ou, "$Al_{0.5}$FeCoCrNi high entropy alloy prepared by selective laser melting with gas-atomized pre-alloy powders," Mater. Sci. Eng, A **739**, 86–89 (2019).
[232]Y. Zhong, L.-E. Rännar, S. Wikman, A. Koptyug, L. Liu, D. Cui, and Z. Shen, "Additive manufacturing of ITER first wall panel parts by two approaches: Selective laser melting and electron beam melting," Fusion Eng. Des. **116**, 24–33 (2017).
[233]K. Rajan, M. Samykano, K. Kadirgama, W. S. W. Harun, and M. M. Rahman, "Fused deposition modeling: Process, materials, parameters, properties, and applications," Int. J. Adv. Manuf. Technol. **120**(3), 1531–1570 (2022).
[234]M. A. H. Khondoker, A. Asad, and D. Sameoto, "Printing with mechanically interlocked extrudates using a custom bi-extruder for fused deposition modelling," RPJ. **24**(6), 921–934 (2018).
[235]Z. C. Kennedy and J. F. Christ, "Printing polymer blends through in situ active mixing during fused filament fabrication," Addit. Manuf. **36**, 101233 (2020).
[236]B. N. Turner, R. Strong, and S. A. Gold, "A review of melt extrusion additive manufacturing processes: I. Process design and modeling," Rapid Prototyping J. **20**(3), 192–204 (2014).
[237]T.-M. Wang, J.-T. Xi, and Y. Jin, "A model research for prototype warp deformation in the FDM process," Int. J. Adv. Manuf. Technol. **33**, 1087–1096 (2007).
[238]A. Asghar, K. Khan, M. S. Rashid, M. Hamza, Z. Liu, C. Liu, and Z. Chen, "Extrusion-based additive manufacturing of carbonaceous and non-carbonaceous electrode materials for electrochemical energy storage devices," Adv. Mater. Technol. **10**(3), 2400136 (2024).
[239]A. Maurel, S. Grugeon, B. Fleutot, M. Courty, K. Prashantha, H. Tortajada, M. Armand, S. Panier, and L. Dupont, "Three-dimensional printing of a $LiFePO_4$/graphite battery cell via fused deposition modeling," Sci. Rep. **9**(1), 18031 (2019).
[240]A. Mehta, R. Singh, B. Pabla, and V. Kumar, "On 3D printed polyvinylidene fluoride-based smart energy storage devices," J. Thermoplast. Compos. Mater. **37**(6), 1921–1937 (2024).
[241]R. Singh, S. Prakash, V. Kumar, and B. S. Pabla, "3D printed flame retardant, ABS-$C_4H_8N_6O$ composite as energy storage device," Arab. J. Sci. Eng. **48**(3), 2995–3007 (2023).
[242]E. Vaněčková, M. Bouša, ŠN. Lachmanová, J. Rathouský, M. Gal, T. Sebechlebská, and V. Kolivoška, "3D printed polylactic acid/carbon black electrodes with nearly ideal electrochemical behaviour," J. Electroanal. Chem. **857**, 113745 (2020).

[243]C. Reyes, R. Somogyi, S. Niu, M. A. Cruz, F. Yang, M. J. Catenacci, C. P. Rhodes, and B. J. Wiley, "Three-dimensional printing of a complete lithium ion battery with fused filament fabrication," ACS Appl. Energy Mater. **1**(10), 5268–5279 (2018).
[244]D. Zhang, B. Chi, B. Li, Z. Gao, Y. Du, J. Guo, and J. Wei, "Fabrication of highly conductive graphene flexible circuits by 3D printing," Synth. Met. **217**, 79–86 (2016).
[245]C. W. Foster, M. P. Down, Y. Zhang, X. Ji, S. J. Rowley-Neale, G. C. Smith, P. J. Kelly, and C. E. Banks, "3D printed graphene based energy storage devices," Sci. Rep. **7**(1), 42233 (2017).
[246]M. H. Omar, K. A. Razak, M. N. Ab Wahab, and H. H. Hamzah, "Recent progress of conductive 3D-printed electrodes based upon polymers/carbon nanomaterials using a fused deposition modelling (FDM) method as emerging electrochemical sensing devices," RSC Adv. **11**(27), 16557–16571 (2021).
[247]M. Palacios-Corella, M. Sanna, J. Muñoz, K. Ghosh, S. Wert, and M. Pumera, "Heterolayered carbon allotrope architectonics via multi-material 3D printing for advanced electrochemical devices," Virtual Phys. Prototyping **18**(1), e2276260 (2023).
[248]S. Sun, M. Brandt, and M. Easton, "2-Powder bed fusion processes: An overview," in *Laser Additive Manufacturing* edited by B. Milan (Woodhead Publishing, 2017), pp. 55–77.
[249]A. K. Kushwaha, M. H. Rahman, E. Slater, R. Patel, C. Evangelista, E. Austin, E. Tompkins, A. McCarroll, D. K. Rajak, and P. L. Menezes, "Powder bed fusion–based additive manufacturing: SLS, SLM, SHS, and DMLS," in *Tribology of Additively Manufactured Materials* (Elsevier, 2022), pp. 1–37.
[250]J. Yang, J. Han, H. Yu, J. Yin, M. Gao, Z. Wang, and X. Zeng, "Role of molten pool mode on formability, microstructure and mechanical properties of selective laser melted Ti-6Al-4V alloy," Mater. Des. **110**, 558–570 (2016).
[251]G. de Leon Nope, L. Perez-Andrade, J. Corona-Castuera, D. Espinosa-Arbelaez, J. Muñoz-Saldaña, and J. Alvarado-Orozco, "Study of volumetric energy density limitations on the IN718 mesostructure and microstructure in laser powder bed fusion process," J. Manuf. Processes **64**, 1261–1272 (2021).
[252]K. K. Wong, J. Y. Ho, K. C. Leong, and T. N. Wong, "Fabrication of heat sinks by selective laser melting for convective heat transfer applications," Virtual Phys. Prototyping **11**(3), 159–165 (2016).
[253]W. Abd-Elaziem, S. Elkatatny, A.-E. Abd-Elaziem, M. Khedr, M. A. Abd El-baky, M. A. Hassan, M. Abu-Okail, M. Mohammed, A. Järvenpää, and T. Allam, "On the current research progress of metallic materials fabricated by laser powder bed fusion process: A review," J. Mater. Res. Technol. **20**, 681–707 (2022).
[254]R. McCann, M. A. Obeidi, C. Hughes, É. McCarthy, D. S. Egan, R. K. Vijayaraghavan, A. M. Joshi, V. A. Garzon, D. P. Dowling, P. J. McNally, and D. Brabazon, "In-situ sensing, process monitoring and machine control in laser powder bed fusion: A review," Addit. Manuf. **45**, 102058 (2021).
[255]H. Exner, P. Regenfuss, L. Hartwig, S. Kloetzer, and R. Ebert, "Selective laser micro sintering with a novel process," in *Fourth International Symposium on Laser Precision Microfabrication* (SPIE, 2003), Vol. 5063, pp. 145–151.
[256]X. Mei, X. Wang, Y. Peng, H. Gu, G. Zhong, and S. Yang, "Interfacial characterization and mechanical properties of 316L stainless steel/Inconel 718 manufactured by selective laser melting," Mater. Sci. Eng, A **758**, 185–191 (2019).
[257]C. Anstaett, C. Seidel, and G. Reinhart, "Fabrication of 3D multi-material parts using laser-based powder bed fusion," in Solid Freeform Fabrication 2017: Proceedings of the 28th Annual International Solid Freeform Fabrication Symposium – An Additive Manufacturing Conference, Austin, Texas, USA (2017).
[258]C. Wei, L. Li, X. Zhang, and Y.-H. Chueh, "3D printing of multiple metallic materials via modified selective laser melting," CIRP Ann. **67**(1), 245–248 (2018).
[259]J. Zhang, X. Wang, J. Gao, L. Zhang, B. Song, L. Zhang, Y. Yao, J. Lu, and Y. Shi, "Additive manufacturing of Ti–6Al–4V/Al–Cu–Mg multi-material structures with a Cu interlayer," Int. J. Mech. Sci. **256**, 108477 (2023).
[260]I. Raffeis, F. Adjei-Kyeremeh, U. Vroomen, P. Suwanpinij, S. Ewald, and A. Bührig-Polazcek, "Investigation of the lithium-containing aluminum copper alloy (AA2099) for the laser powder bed fusion process [L-PBF]: Effects of process parameters on cracks, porosity, and microhardness," JOM **71**, 1543–1553 (2019).
[261]D. L. Bourell, M.-C. Leu, K. Chakravarthy, N. Guo, and K. Alayavalli, "Graphite-based indirect laser sintered fuel cell bipolar plates containing carbon fiber additions," CIRP Ann. **60**(1), 275–278 (2011).
[262]A. Singh, S. Kapil, and M. Das, "A comprehensive review of the methods and mechanisms for powder feedstock handling in directed energy deposition," Addit. Manuf. **35**, 101388 (2020).
[263]S. M. Thompson, L. Bian, N. Shamsaei, and A. Yadollahi, "An overview of direct laser deposition for additive manufacturing; Part I: Transport phenomena, modeling and diagnostics," Addit. Manuf. **8**, 36–62 (2015).
[264]D. Svetlizky, M. Das, B. Zheng, A. L. Vyatskikh, S. Bose, A. Bandyopadhyay, J. M. Schoenung, E. J. Lavernia, and N. Eliaz, "Directed energy deposition (DED) additive manufacturing: Physical characteristics, defects, challenges and applications," Mater. Today **49**, 271–295 (2021).
[265]S. W. Williams, F. Martina, A. C. Addison, J. Ding, G. Pardal, and P. Colegrove, "Wire+ arc additive manufacturing," Mater. Sci. Technol. **32**(7), 641–647 (2016).
[266]D. D. Singh, S. Arjula, and A. R. Reddy, "Functionally graded materials manufactured by direct energy deposition: A review," Mater. Today: Proc. **47**, 2450–2456 (2021).
[267]B. M. Arkhurst, J.-J. Park, C.-H. Lee, and J. H. Kim, "Direct laser deposition of 14Cr oxide dispersion strengthened steel powders using Y_2O_3 and HfO_2 dispersoids," Korean J. Met. Mater. **55**(8), 550–558 (2017).
[268]R. Wang, K. Zhang, C. Davies, and X. Wu, "Evolution of microstructure, mechanical and corrosion properties of AlCoCrFeNi high-entropy alloy prepared by direct laser fabrication," J. Alloys Compd. **694**, 971–981 (2017).
[269]A. Saboori, A. Aversa, G. Marchese, S. Biamino, M. Lombardi, and P. Fino, "Application of directed energy deposition-based additive manufacturing in repair," Appl. Sci. **9**(16), 3316 (2019).
[270]Q. Chao, T. Guo, T. Jarvis, X. Wu, P. Hodgson, and D. Fabijanic, "Direct laser deposition cladding of AlxCoCrFeNi high entropy alloys on a high-temperature stainless steel," Surf. Coat. Technol. **332**, 440–451 (2017).
[271]M. D. McMurtrey, R. C. O'Brien, C. Sun, C.-H. Shiau, and F. Teng, *Irradiation Damage and IASCC of Printed 316L for Use as Fuel Cladding* (Idaho National Lab., Idaho Falls, ID, USA, 2019).
[272]D. Ahn, L. M. Stevens, K. Zhou, and Z. A. Page, "Rapid high-resolution visible light 3D printing," ACS Cent. Sci. **6**(9), 1555–1563 (2020).
[273]X. Wang, M. Jiang, Z. Zhou, J. Gou, and D. Hui, "3D printing of polymer matrix composites: A review and prospective," Composites Part B **110**, 442–458 (2017).
[274]M. L. Griffith and J. W. Halloran, "Freeform fabrication of ceramics via stereolithography," J. Am. Ceram. Soc. **79**(10), 2601–2608 (1996).
[275]R. M. Hensleigh, H. Cui, J. S. Oakdale, C. Y. Jianchao, P. G. Campbell, E. B. Duoss, C. M. Spadaccini, X. Zheng, and M. A. Worsley, "Additive manufacturing of complex micro-architected graphene aerogels," Mater. Horiz. **5**(6), 1035–1041 (2018).
[276]X. Song, Z. Chen, L. Lei, K. Shung, Q. Zhou, and Y. Chen, "Piezoelectric component fabrication using projection-based stereolithography of barium titanate ceramic suspensions," RPJ. **23**(1), 44–53 (2017).
[277]J.-W. Choi, E. MacDonald, and R. Wicker, "Multi-material microstereolithography," Int. J. Adv. Manuf. Technol. **49**, 543–551 (2010).
[278]E. M. Maines, M. K. Porwal, C. J. Ellison, and T. M. Reineke, "Sustainable advances in SLA/DLP 3D printing materials and processes," Green Chem. **23**(18), 6863–6897 (2021).
[279]H. H. Hwang, W. Zhu, G. Victorine, N. Lawrence, and S. Chen, "3D-Printing of functional biomedical microdevices via light-and extrusion-based approaches," Small Methods **2**(2), 1700277 (2018).
[280]B. Zhang, X. Gui, P. Song, X. Xu, L. Guo, Y. Han, L. Wang, C. Zhou, Y. Fan, and X. Zhang, "Three-dimensional printing of large-scale, high-resolution bioceramics with micronano inner porosity and customized surface characterization design for bone regeneration," ACS Appl. Mater. Interfaces **14**(7), 8804–8815 (2022).
[281]K. S. Lee, D. Y. Yang, S. H. Park, and R. H. Kim, "Recent developments in the use of two-photon polymerization in precise 2D and 3D microfabrications," Polym. Adv. Technol. **17**(2), 72–82 (2006).
[282]S. You, J. Li, W. Zhu, C. Yu, D. Mei, and S. Chen, "Nanoscale 3D printing of hydrogels for cellular tissue engineering," J. Mater. Chem. B **6**(15), 2187–2197 (2018).

[283]Z. Gan, Y. Cao, R. A. Evans, and M. Gu, "Three-dimensional deep sub-diffraction optical beam lithography with 9 nm feature size," Nat. Commun. **4**(1), 2061 (2013).
[284]X. He, T. Li, J. Zhang, and Z. Wang, "STED direct laser writing of 45 nm width nanowire," Micromachines **10**(11), 726 (2019).
[285]S. Juodkazis, V. Mizeikis, K. K. Seet, M. Miwa, and H. Misawa, "Two-photon lithography of nanorods in SU-8 photoresist," Nanotechnology **16**(6), 846 (2005).
[286]Q. Wang, J. A. Jackson, Q. Ge, J. B. Hopkins, C. M. Spadaccini, and N. X. Fang, "Lightweight mechanical metamaterials with tunable negative thermal expansion," Phys. Rev. Lett. **117**(17), 175901 (2016).
[287]C. Zhou, Y. Chen, Z. Yang, and B. Khoshnevis, Development of a multi-material mask-image-projection-based stereolithography for the fabrication of digital materials," in *22nd Annual International Solid Freeform Fabrication Symposium—An Additive Manufacturing Conference* (SFF, 2011), pp. 65–80.
[288]C. Zhou, Y. Chen, Z. Yang, and B. Khoshnevis, "Digital material fabrication using mask-image-projection-based stereolithography," Rapid Prototyping J. **19**(3), 153–165 (2013).
[289]D. Han, C. Yang, N. X. Fang, and H. Lee, "Rapid multi-material 3D printing with projection micro-stereolithography using dynamic fluidic control," Addit. Manuf. **27**, 606–615 (2019).
[290]N. D. Dolinski, Z. A. Page, E. B. Callaway, F. Eisenreich, R. V. Garcia, R. Chavez, D. P. Bothman, S. Hecht, F. W. Zok, and C. J. Hawker, "Solution mask liquid lithography (SMaLL) for one-step, multimaterial 3D printing," Adv. Mater. **30**(31), 1800364 (2018).
[291]S. Baek, H. W. Ban, S. Jeong, S. H. Heo, D. H. Gu, W. Choi, S. Choo, Y. E. Park, J. Yoo, and M. K. Choi, "Generalised optical printing of photocurable metal chalcogenides," Nat. Commun. **13**(1), 5262 (2022).
[292]J. Pragana, R. F. Sampaio, I. Bragança, C. Silva, and P. Martins, "Hybrid metal additive manufacturing: A state–of–the-art review," Adv. Ind. Manuf. Eng. **2**, 100032 (2021).
[293]D. J. Roach, C. M. Hamel, C. K. Dunn, M. V. Johnson, X. Kuang, and H. J. Qi, "The m^4 3D printer: A multi-material multi-method additive manufacturing platform for future 3D printed structures," Addit. Manuf. **29**, 100819 (2019).
[294]Y. Liu, S. Zheng, J. Ma, X. Wang, L. Zhang, P. Das, K. Wang, and Z. S. Wu, "All 3D printing shape-conformable zinc ion hybrid capacitors with ultrahigh areal capacitance and improved cycle life," Adv. Energy Mater. **12**(27), 2200341 (2022).
[295]M. Rafiee, F. Granier, R. Tao, A. Bhérer-Constant, G. Chenier, and D. Therriault, "Multi-material, multi-process, planar, and nonplanar additive manufacturing of piezoelectric devices," Adv. Eng. Mater. **24**(10), 2200294 (2022).
[296]Y. Du, R. Wang, M. Zeng, S. Xu, M. Saeidi-Javash, W. Wu, and Y. Zhang, "Hybrid printing of wearable piezoelectric sensors," Nano Energy **90**, 106522 (2021).
[297]A. Ambrosi and M. Pumera, "Multimaterial 3D-printed water electrolyzer with earth-abundant electrodeposited catalysts," ACS Sustainable Chem. Eng. **6**(12), 16968–16975 (2018).
[298]T. An, S. Yoon, and J. Kim, "Additive manufacturing of inductive force sensor with NiZn-ferrite magnetic core for robotic gripper," Addit. Manuf. **71**, 103600 (2023).
[299]R. Fantin, E. Trevisanello, R. Ruess, A. Pokle, G. Conforto, F. H. Richter, K. Volz, and J. R. Janek, "Synthesis and postprocessing of single-crystalline $LiNi_{0.8}Co_{0.15}Al_{0.05}O_2$ for solid-state lithium-ion batteries with high capacity and long cycling stability," Chem. Mater. **33**(7), 2624–2634 (2021).
[300]X. Xu, J. Yang, W. Jonhson, Y. Wang, A. Suwardi, J. Ding, C. Guan, and D. Zhang, "Additive manufacturing solidification methodologies for ink formulation," Addit. Manuf. **56**, 102939 (2022).
[301]G. Podolak, N. Arefin, H.-E.-J. Moni, and M. Zeng, "Alternative sintering processes and their influence on the electrical resistance of printed Ag nanoparticle conductive networks," ACS Appl. Electron. Mater. **6**, 8590 (2024).
[302]M. Zeng, D. Zavanelli, J. Chen, M. Saeidi-Javash, Y. Du, S. LeBlanc, G. J. Snyder, and Y. Zhang, "Printing thermoelectric inks toward next-generation energy and thermal devices," Chem. Soc. Rev. **51**(2), 485–512 (2022).
[303]Y. Choi, K. d Seong, and Y. Piao, "Metal-organic decomposition ink for printed electronics," Adv. Mater. Inter. **6**(20), 1901002 (2019).
[304]S. Tao, J. Ramirez, H. M. Shewan, M. Lyu, I. Gentle, L. Wang, and R. Knibbe, "Ink to power: An organic-based polymer electrolyte for ambient printing of flexible zinc batteries," Adv. Funct. Mater. **34**, 2402050 (2024).
[305]L. Yu, Z. Fan, Y. Shao, Z. Tian, J. Sun, and Z. Liu, "Versatile N-doped MXene ink for printed electrochemical energy storage application," Adv. Energy Mater. **9**(34), 1901839 (2019).
[306]A. Gisario, M. Kazarian, F. Martina, and M. Mehrpouya, "Metal additive manufacturing in the commercial aviation industry: A review," J. Manuf. Syst. **53**, 124–149 (2019).
[307]C. L. A. Leung, S. Marussi, M. Towrie, R. C. Atwood, P. J. Withers, and P. D. Lee, "The effect of powder oxidation on defect formation in laser additive manufacturing," Acta Mater. **166**, 294–305 (2019).
[308]B. N. Turner and S. A. Gold, "A review of melt extrusion additive manufacturing processes: II. Materials, dimensional accuracy, and surface roughness," Rapid Prototyping J. **21**(3), 250–261 (2015).
[309]M. Schneck, M. Horn, M. Schmitt, C. Seidel, G. Schlick, and G. Reinhart, "Review on additive hybrid-and multi-material-manufacturing of metals by powder bed fusion: State of technology and development potential," Prog. Addit. Manuf. **6**, 881–814 (2021).
[310]Y. Bai, D. Wang, Y. Yang, and H. Wang, "Effect of heat treatment on the microstructure and mechanical properties of maraging steel by selective laser melting," Mater. Sci. Eng, A **760**, 105–117 (2019).
[311]M. Bermingham, L. Nicastro, D. Kent, Y. Chen, and M. Dargusch, "Optimising the mechanical properties of Ti-6Al-4V components produced by wire+ arc additive manufacturing with post-process heat treatments," J. Alloys Compd. **753**, 247–255 (2018).
[312]A. H. Maamoun, M. Elbestawi, G. K. Dosbaeva, and S. C. Veldhuis, "Thermal post-processing of AlSi10Mg parts produced by Selective Laser Melting using recycled powder," Addit. Manuf. **21**, 234–247 (2018).
[313]M. Bocanegra-Bernal, "Hot isostatic pressing (HIP) technology and its applications to metals and ceramics," J. Mater. Sci. **39**(21), 6399–6420 (2004).
[314]W. Tillmann, C. Schaak, J. Nellesen, M. Schaper, M. E. Aydinöz, and K.-P. Hoyer, "Hot isostatic pressing of IN718 components manufactured by selective laser melting," Addit. Manuf. **13**, 93–102 (2017).
[315]X. Yu, X. Lin, F. Liu, L. Wang, Y. Tang, J. Li, S. Zhang, and W. Huang, "Influence of post-heat-treatment on the microstructure and fracture toughness properties of Inconel 718 fabricated with laser directed energy deposition additive manufacturing," Mater. Sci. Eng., A **798**, 140092 (2020).
[316]L. Hackel, J. R. Rankin, A. Rubenchik, W. E. King, and M. Matthews, "Laser peening: A tool for additive manufacturing post-processing," Addit. Manuf. **24**, 67–75 (2018).
[317]J. Zhou, S. Huang, J. Sheng, J. Lu, C. Wang, K. Chen, H. Ruan, and H. Chen, "Effect of repeated impacts on mechanical properties and fatigue fracture morphologies of 6061-T6 aluminum subject to laser peening," Mater. Sci. Eng, A **539**, 360–368 (2012).
[318]C. Ni, L. Zhu, Z. Zheng, J. Zhang, Y. Yang, J. Yang, Y. Bai, C. Weng, W. F. Lu, and H. Wang, "Effect of material anisotropy on ultra-precision machining of Ti-6Al-4V alloy fabricated by selective laser melting," J. Alloys Compd. **848**, 156457 (2020).
[319]Q. Wang, J. D. Morrow, C. Ma, N. A. Duffie, and F. E. Pfefferkorn, "Surface prediction model for thermocapillary regime pulsed laser micro polishing of metals," J. Manuf. Processes **20**, 340–348 (2015).
[320]Y. Oh, I. S. Yoon, C. Lee, S. H. Kim, B.-K. Ju, and J.-M. Hong, "Selective photonic sintering of Ag flakes embedded in silicone elastomers to fabricate stretchable conductors," J. Mater. Chem. C **5**(45), 11733–11740 (2017).
[321]Y. Kwon, J. Kim, H. Kim, T. W. Kang, S. S. Jang *et al.*, "Printed nanomaterials for all-in-one integrated flexible wearables and bioelectronics," ACS Appl. Mater. Interfaces **16**(49), 68016–68026 (2024).
[322]J. Guo, X. Zhao, T. Herisson De Beauvoir, J. H. Seo, S. S. Berbano, A. L. Baker, C. Azina, and C. A. Randall, "Recent progress in applications of the cold sintering process for ceramic–polymer composites," Adv. Funct. Mater. **28**(39), 1801724 (2018).
[323]M. Srivastava, S. Rathee, V. Patel, A. Kumar, and P. G. Koppad, "A review of various materials for additive manufacturing: Recent trends and processing issues," J. Mater. Res. Technol. **21**, 2612–2641 (2022).
[324]T. B. Freeman, K. E. Foster, C. J. Troxler, C. W. Irvin, A. Aday, S. K. Boetcher, A. Mahvi, M. K. Smith, and A. Odukomaiya, "Advanced materials and

additive manufacturing for phase change thermal energy storage and management: A review," Adv. Energy Mater. **13**(24), 2204208 (2023).
[325]C. Sun, Y. Wang, M. D. McMurtrey, N. D. Jerred, F. Liou, and J. Li, "Additive manufacturing for energy: A review," Appl. Energy **282**, 116041 (2021).
[326]M. Beltrão, F. M. Duarte, J. C. Viana, and V. Paulo, "A review on in-mold electronics technology," Polym. Eng. Sci. **62**(4), 967–990 (2022).
[327]R. Abbel, Y. Galagan, and P. Groen, "Roll-to-roll fabrication of solution processed electronics," Adv. Eng. Mater. **20**(8), 1701190 (2018).
[328]L. Teawdeswan and G. Dong, "Inverse design of multi-material gyroid structures made by additive manufacturing," Int. J. Mech. Sci. **262**, 108734 (2024).
[329]C. Weller, R. Kleer, and F. T. Piller, "Economic implications of 3D printing: Market structure models in light of additive manufacturing revisited," Int. J. Prod. Econ. **164**, 43–56 (2015).
[330]B. Berman, "3-D printing: The new industrial revolution," Bus. Horizons **55**(2), 155–162 (2012).
[331]H. Yang and P. Jiang, "Large-scale colloidal self-assembly by doctor blade coating," Langmuir **26**(16), 13173–13182 (2010).
[332]G. Liu, X. Zhang, X. Chen, Y. He, L. Cheng, M. Huo, J. Yin, F. Hao, S. Chen, and P. Wang, "Additive manufacturing of structural materials," Mater. Sci. Eng.: R: Rep. **145**, 100596 (2021).
[333]P. Kumar, S. K. Sharma, and R. K. R. Singh, "Recent trends and future outlooks in manufacturing methods and applications of FGM: A comprehensive review," Mater. Manuf. Processes **38**(9), 1033–1067 (2023).
[334]H. Ichou, N. Arrousse, E. Berdimurodov, and N. Aliev, "Exploring the advancements in physical vapor deposition coating: A review," J. Bio. Tribo. Corrosion **10**(1), 3 (2024).
[335]S. Graziosi, J. Faludi, T. Stanković, Y. Borgianni, N. Meisel, S. I. Hallstedt, and D. W. Rosen, "A vision for sustainable additive manufacturing," Nat. Sustainable **7**, 698–698 (2024).
[336]A. Ambrosi and M. Pumera, "3D-printing technologies for electrochemical applications," Chem. Soc. Rev. **45**(10), 2740–2755 (2016).
[337]T. D. Huan, S. Boggs, G. Teyssedre, C. Laurent, M. Cakmak, S. Kumar, and R. Ramprasad, "Advanced polymeric dielectrics for high energy density applications," Prog. Mater. Sci. **83**, 236–269 (2016).
[338]N. Meng, X. Ren, G. Santagiuliana, L. Ventura, H. Zhang, J. Wu, H. Yan, M. J. Reece, and E. Bilotti, "Ultrahigh β-phase content poly (vinylidene fluoride) with relaxor-like ferroelectricity for high energy density capacitors," Nat. Commun. **10**(1), 4535 (2019).
[339]Y. Cui, Y. Feng, T. Zhang, C. Zhang, Q. Chi, Y. Zhang, X. Wang, Q. Chen, and Q. Lei, "Excellent energy storage performance of ferroconcrete-like all-organic linear/ferroelectric polymer films utilizing interface engineering," ACS Appl. Mater. Interfaces **12**(50), 56424–56434 (2020).
[340]Y. Wang, Z. Li, C. Wu, and Y. Cao, "High-temperature dielectric polymer nanocomposites with interposed montmorillonite nanosheets," Chem. Eng. J. **401**, 126093 (2020).
[341]C. N. Hoth, S. A. Choulis, P. Schilinsky, and C. J. Brabec, "High photovoltaic performance of inkjet printed polymer: Fullerene blends," Adv. Mater. **19**(22), 3973–3978 (2007).
[342]T. Duda and L. V. Raghavan, "3D metal printing technology," IFAC-PapersOnLine **49**(29), 103–110 (2016).
[343]L. Liu, Y. Feng, and W. Wu, "Recent progress in printed flexible solid-state supercapacitors for portable and wearable energy storage," J. Power Sources **410-411**, 69–77 (2019).
[344]V. G. Rocha, E. Garcia-Tunon, C. Botas, F. Markoulidis, E. Feilden, E. D'Elia, N. Ni, M. Shaffer, and E. Saiz, "Multimaterial 3D printing of graphene-based electrodes for electrochemical energy storage using thermoresponsive inks," ACS Appl. Mater. Interfaces **9**(42), 37136–37145 (2017).
[345]A. Zhakeyev, P. Wang, L. Zhang, W. Shu, H. Wang, and J. Xuan, "Additive manufacturing: Unlocking the evolution of energy materials," Adv. Sci. **4**(10), 1700187 (2017).
[346]K. Guo, D. Xu, L. Xu, Y. Li, and Y. Tang, "Noble metal nanodendrites: Growth mechanisms, synthesis strategies and applications," Mater. Horiz. **10**(4), 1234–1263 (2023).
[347]A. N. Jansen, K. Amine, A. E. Newman, D. R. Vissers, and G. L. Henriksen, "Low-cost, flexible battery packaging materials," JOM **54**, 29–32 (2002).
[348]Y. Yuan, W. Yuan, Y. Wu, X. Wu, X. Zhang, S. Jiang, B. Zhao, Y. Chen, C. Yang, and L. Ding, "High-performance all-printed flexible micro-supercapacitors with hierarchical encapsulation," Energy Environ. Mater. **7**, e12657 (2024).
[349]A. E. Jakus, E. B. Secor, A. L. Rutz, S. W. Jordan, M. C. Hersam, and R. N. Shah, "Three-dimensional printing of high-content graphene scaffolds for electronic and biomedical applications," ACS Nano **9**(4), 4636–4648 (2015).
[350]M. Wajahat, S. Lee, J. H. Kim, J. Ahn, H. H. Sim, J. H. Kim, J. Bae, S. H. Kim, J. Pyo, and S. K. Seol, "Three-dimensional printing of silver nanoparticle-decorated graphene microarchitectures," Addit. Manuf. **60**, 103249 (2022).
[351]L. Zhang, J. Qin, P. Das, S. Wang, T. Bai, F. Zhou, M. Wu, and Z. S. Wu, "Electrochemically exfoliated graphene additive-free inks for 3D printing customizable monolithic integrated micro-supercapacitors on a large scale," Adv. Mater. **36**(19), 2313930 (2024).
[352]I. Sultana, Y. Chen, S. Huang, and M. M. Rahman, "Recycled value-added circular energy materials for new battery application: Recycling strategies, challenges, and sustainability-a comprehensive review," J. Environ. Chem. Eng. **10**(6), 108728 (2022).
[353]H.-Y. Kang and J. M. Schoenung, "Electronic waste recycling: A review of US infrastructure and technology options," Resour. Conserv. Recycl. **45**(4), 368–400 (2005).
[354]A. L. Sanati, P. A. Lopes, A. Chambel, A. F. Silva, D. M. Oliveira, C. Majidi, A. T. de Almeida, and M. Tavakoli, "Recyclable liquid metal–graphene supercapacitor," Chem. Eng. J. **479**, 147894 (2024).
[355]M. Idrees, S. Ahmed, Z. Mohammed, N. S. Korivi, and V. Rangari, "3D printed supercapacitor using porous carbon derived from packaging waste," Addit. Manuf. **36**, 101525 (2020).
[356]X.-B. Cheng, R. Zhang, C.-Z. Zhao, and Q. Zhang, "Toward safe lithium metal anode in rechargeable batteries: A review," Chem. Rev. **117**(15), 10403–10473 (2017).
[357]D. Di Lecce, R. Verrelli, and J. Hassoun, "Lithium-ion batteries for sustainable energy storage: Recent advances towards new cell configurations," Green Chem. **19**(15), 3442–3467 (2017).
[358]Y. Liu, R. Zhang, J. Wang, and Y. Wang, "Current and future lithium-ion battery manufacturing," IScience **24**(4), 102332 (2021).
[359]N. Fonseca, S. V. Thummalapalli, S. Jambhulkar, D. Ravichandran, Y. Zhu, D. Patil, V. Thippanna, A. Ramanathan, W. Xu, and S. Guo, "3D printing-enabled design and manufacturing strategies for batteries: A review," Small **19**(50), 2302718 (2023).
[360]R. R. Kohlmeyer, A. J. Blake, J. O. Hardin, E. A. Carmona, J. Carpena-Núñez, B. Maruyama, J. D. Berrigan, H. Huang, and M. F. Durstock, "Composite batteries: A simple yet universal approach to 3D printable lithium-ion battery electrodes," J. Mater. Chem A. **4**(43), 16856–16864 (2016).
[361]S. H. Park, M. Kaur, D. Yun, and W. S. Kim, "Hierarchically designed electron paths in 3D printed energy storage devices," Langmuir **34**(37), 10897–10904 (2018).
[362]A. Vlad, N. Singh, C. Galande, and P. M. Ajayan, "Design considerations for unconventional electrochemical energy storage architectures," Adv. Energy Mater. **5**(19), 1402115 (2015).
[363]F. Meng, M. Zhang, J. Huang, W. F. Lu, J. M. Xue, and H. Wang, "Additive manufacturing of stable energy storage devices using a multinozzle printing system," Adv. Funct. Mater. **31**(9), 2008280 (2021).
[364]K. Fu, Y. Wang, C. Yan, Y. Yao, Y. Chen, J. Dai, S. Lacey, Y. Wang, J. Wan, and T. Li, "Graphene oxide-based electrode inks for 3D-printed lithium-ion batteries," Adv. Mater. **28**(13), 2587–2594 (2016).
[365]W. Lai, C. K. Erdonmez, T. F. Marinis, C. K. Bjune, N. J. Dudney, F. Xu, R. Wartena, and Y. M. Chiang, "Ultrahigh-energy-density microbatteries enabled by new electrode architecture and micropackaging design," Adv. Mater. **22**(20), E139–E144 (2010).
[366]G.-F. Yang, K.-Y. Song, and S.-K. Joo, "Ultra-thick Li-ion battery electrodes using different cell size of metal foam current collectors," RSC Adv. **5**(22), 16702–16706 (2015).
[367]R. Zhao, J. Liu, and J. Gu, "The effects of electrode thickness on the electrochemical and thermal characteristics of lithium ion battery," Appl. Energy **139**, 220–229 (2015).
[368]H. Zheng, J. Li, X. Song, G. Liu, and V. S. Battaglia, "A comprehensive understanding of electrode thickness effects on the electrochemical performances of Li-ion battery cathodes," Electrochim. Acta **71**, 258–265 (2012).

[369]Y. S. Meng, *Lithium Metal Anode–Advanced Characterization, Slides from the Web Seminar by Dr. Y. Shirley Meng* (UC San Diego, 2020).
[370]X. Feng, M. Ouyang, X. Liu, L. Lu, Y. Xia, and X. He, "Thermal runaway mechanism of lithium ion battery for electric vehicles: A review," Energy Storage Mater. **10**, 246–267 (2018).
[371]Q. Wang, P. Ping, X. Zhao, G. Chu, J. Sun, and C. Chen, "Thermal runaway caused fire and explosion of lithium ion battery," J. Power Sources **208**, 210–224 (2012).
[372]A. J. Blake, R. R. Kohlmeyer, J. O. Hardin, E. A. Carmona, B. Maruyama, J. D. Berrigan, H. Huang, and M. F. Durstock, "3D printable ceramic–polymer electrolytes for flexible high-performance Li-ion batteries with enhanced thermal stability," Adv. Energy Mater. **7**(14), 1602920 (2017).
[373]Q. Zhao, S. Stalin, C.-Z. Zhao, and L. A. Archer, "Designing solid-state electrolytes for safe, energy-dense batteries," Nat. Rev. Mater. **5**(3), 229–252 (2020).
[374]W. Liu, M. S. Song, B. Kong, and Y. Cui, "Flexible and stretchable energy storage: Recent advances and future perspectives," Adv. Mater. **29**(1), 1603436 (2017).
[375]Y. Wang, C. Chen, H. Xie, T. Gao, Y. Yao, G. Pastel, X. Han, Y. Li, J. Zhao, and K. Fu, "3D-printed all-fiber li-ion battery toward wearable energy storage," Adv. Funct. Mater. **27**(43), 1703140 (2017).
[376]Y. Li, H. Zhu, Y. Wang, U. Ray, S. Zhu, J. Dai, C. Chen, K. Fu, S. H. Jang, and D. Henderson, "Cellulose-nanofiber-enabled 3D printing of a carbon-nanotube microfiber network," Small Methods **1**(10), 1700222 (2017).
[377]W. U. Rehman, R. Z. A. Manj, Y. Ma, and J. Yang, "The promising potential of gallium based liquid metals for energy storage," ChemPlusChem **89**, e202300767 (2024).
[378]E. Parvini, A. Hajalilou, J. o P. Gonc¸alves Vilarinho, P. Alhais Lopes, M. Maranha, and M. Tavakoli, "Gallium–carbon: A universal composite for sustainable 3D printing of integrated sensor–heater–battery systems in wearable and recyclable electronics," ACS Appl. Mater. Interfaces **16**, 32812 (2024).
[379]M. C. Freitas, A. L. Sanati, P. A. Lopes, A. F. Silva, and M. Tavakoli, "3D printed gallium battery with outstanding energy storage: Toward fully printed battery-on-the-board soft electronics," Small **20**, 2304716 (2024).
[380]P. Hundekar, R. Jain, A. S. Lakhnot, and N. Koratkar, "Recent advances in the mitigation of dendrites in lithium-metal batteries," J. Appl. Phys. **128**(1), 010903 (2020).
[381]M. K. Aslam, Y. Niu, T. Hussain, H. Tabassum, W. Tang, M. Xu, and R. Ahuja, "How to avoid dendrite formation in metal batteries: Innovative strategies for dendrite suppression," Nano Energy **86**, 106142 (2021).
[382]D. Cao, Y. Xing, K. Tantratian, X. Wang, Y. Ma, A. Mukhopadhyay, Z. Cheng, Q. Zhang, Y. Jiao, and L. Chen, "3D printed high-performance lithium metal microbatteries enabled by nanocellulose," Adv. Mater. **31**(14), 1807313 (2019).
[383]H. Liu, G. Zhang, X. Zheng, F. Chen, and H. Duan, "Emerging miniaturized energy storage devices for microsystem applications: From design to integration," Int. J. Extrem. Manuf. **2**(4), 042001 (2020).
[384]E. Cohen, S. Menkin, M. Lifshits, Y. Kamir, A. Gladkich, G. Kosa, and D. Golodnitsky, "Novel rechargeable 3D-microbatteries on 3D-printed-polymer substrates: Feasibility study," Electrochim. Acta **265**, 690–701 (2018).
[385]K. Sun, T. S. Wei, B. Y. Ahn, J. Y. Seo, S. J. Dillon, and J. A. Lewis, "3D printing of interdigitated Li-Ion microbattery architectures," Adv. Mater. **25**(33), 4539–4543 (2013).
[386]A. Erturk and D. J. Inman, *Piezoelectric Energy Harvesting* (John Wiley & Sons, 2011).
[387]P. Dineva, D. Gross, R. Müller, T. Rangelov, P. Dineva, D. Gross, R. Müller, and T. Rangelov, *Piezoelectric Materials* (Springer, 2014).
[388]N. Sezer and M. Koç, "A comprehensive review on the state-of-the-art of piezoelectric energy harvesting," Nano Energy **80**, 105567 (2021).
[389]R. Gregorio Jr, "Determination of the α, β, and γ crystalline phases of poly (vinylidene fluoride) films prepared at different conditions," J. Appl. Polym. Sci. **100**(4), 3272–3279 (2006).
[390]B. B. Tian, X. F. Bai, Y. Liu, P. Gemeiner, X. L. Zhao, B. L. Liu, Y. H. Zou, X. D. Wang, H. Huang, J. L. Wang, Sh. Sun, J. L. Sun, B. Dkhil, X. J. Meng, and J. H. Chu, "β phase instability in poly (vinylidene fluoride/trifluoroethylene) thin films near β relaxation temperature," Appl. Phys. Lett. **106**(9), 092902 (2015).
[391]X. Yuan, Z. Mai, H. Li, X. Gao, A. Yan, D. Jiang, X. Wei, H. Jiang, and S. Dong, "Enhanced energy density in piezoelectric PVDF-polymer nanocomposite via multiple mechanism synergetic action," Nano Energy **127**, 109734 (2024).
[392]R. W. Lewis, A. C. Dent, R. Stevens, and C. R. Bowen, "Microstructural modelling of the polarization and properties of porous ferroelectrics," Smart Mater. Struct. **20**(8), 085002 (2011).
[393]S. Song, Y. Han, Y. Li, and Q. Wang, "3D printed piezoelectric porous structure with enhanced output performance and stress-electricity response for road energy harvesting," Addit. Manuf. **72**, 103625 (2023).
[394]A. Megdich, M. Habibi, L. Laperrière, Z. Li, and Y. Abdin, "Advanced 3D-printed PVDF/BT piezoelectric energy harvester with a bio-inspired 3D structure for a self-powered smart mouse," Nano Energy **128**, 109876 (2024).
[395]H. Pei, Y. Chen, Q. Lv, Z. Peng, X. Wang, N. Chen, and H. Zhang, "A novel microwave assisted multi-material 3D printing strategy to architect lamellar piezoelectric generators for intelligent sensing," Composites Part B **280**, 111529 (2024).
[396]B. García-Farrera and L. F. Velásquez-García, "Ultrathin ceramic piezoelectric films via room-temperature electrospray deposition of ZnO nanoparticles for printed GHz devices," ACS Appl. Mater. Interfaces **11**(32), 29167–29176 (2019).
[397]A. Closson, H. Richards, Z. Xu, C. Jin, L. Dong, and J. X. Zhang, "Method for Inkjet-printing PEDOT: PSS polymer electrode arrays on piezoelectric PVDF-TrFE fibers," IEEE Sens. J. **21**(23), 26277–26285 (2021).
[398]J. Kim, S. Byun, S. Lee, J. Ryu, S. Cho, C. Oh, H. Kim, K. No, S. Ryu, and Y. M. Lee, "Cost-effective and strongly integrated fabric-based wearable piezoelectric energy harvester," Nano Energy **75**, 104992 (2020).
[399]J. Ryu, J. Kim, J. Oh, S. Lim, J. Y. Sim, J. S. Jeon, K. No, S. Park, and S. Hong, "Intrinsically stretchable multi-functional fiber with energy harvesting and strain sensing capability," Nano Energy **55**, 348–353 (2019).
[400]S. Bodkhe and P. Ermanni, "Challenges in 3D printing of piezoelectric materials," Multifunct. Mater. **2**(2), 022001 (2019).
[401]Z. He, Y. Yang, J.-W. Liu, and S.-H. Yu, "Emerging tellurium nanostructures: Controllable synthesis and their applications," Chem. Soc. Rev. **46**(10), 2732–2753 (2017).
[402]M. Kanik, M. G. Say, B. Daglar, A. F. Yavuz, M. H. Dolas, M. M. El-Ashry, and M. Bayindir, "A motion-and sound-activated, 3D-printed, chalcogenide-based triboelectric nanogenerator," Adv. Mater. **27**(14), 2367–2376 (2015).
[403]Z. L. Wang, "Triboelectric nanogenerators as new energy technology and self-powered sensors–principles, problems and perspectives," Faraday Discuss. **176**, 447–458 (2014).
[404]B. Zhang, L. Zhang, W. Deng, L. Jin, F. Chun, H. Pan, B. Gu, H. Zhang, Z. Lv, and W. Yang, "Self-powered acceleration sensor based on liquid metal triboelectric nanogenerator for vibration monitoring," ACS Nano **11**(7), 7440–7446 (2017).
[405]Z. Che, S. O'Donovan, X. Xiao, X. Wan, G. Chen, X. Zhao, Y. Zhou, J. Yin, and J. Chen, "Implantable triboelectric nanogenerators for self-powered cardiovascular healthcare," Small **19**(51), 2207600 (2023).
[406]M. Salauddin, S. S. Rana, M. T. Rahman, M. Sharifuzzaman, P. Maharjan, T. Bhatta, H. Cho, S. H. Lee, C. Park, and K. Shrestha, "Fabric-assisted MXene/silicone nanocomposite-based triboelectric nanogenerators for self-powered sensors and wearable electronics," Adv. Funct. Mater. **32**(5), 2107143 (2022).
[407]Q. Shi, Z. Sun, Z. Zhang, and C. Lee, "Triboelectric nanogenerators and hybridized systems for enabling next-generation IoT applications," Research **2021**, 6849171 (2021).
[408]L. Lebreton and A. Andrady, "Future scenarios of global plastic waste generation and disposal," Palgrave Commun. **5**(1), 1–11 (2019).
[409]L. C. Lebreton, J. Van Der Zwet, J.-W. Damsteeg, B. Slat, A. Andrady, and J. Reisser, "River plastic emissions to the world's oceans," Nat. Commun. **8**(1), 15611 (2017).
[410]M. Sahu, S. Hajra, H.-G. Kim, H.-G. Rubahn, Y. K. Mishra, and H. J. Kim, "Additive manufacturing-based recycling of laboratory waste into energy harvesting device for self-powered applications," Nano Energy **88**, 106255 (2021).
[411]A. Kurs, A. Karalis, R. Moffatt, J. D. Joannopoulos, P. Fisher, and M. Soljacic, "Wireless power transfer via strongly coupled magnetic resonances," science **317**(5834), 83–86 (2007).
[412]X. Wei, Z. Wang, and H. Dai, "A critical review of wireless power transfer via strongly coupled magnetic resonances," Energies **7**(7), 4316–4341 (2014).

[413]M. Bichurin, R. Petrov, O. Sokolov, V. Leontiev, V. Kuts, D. Kiselev, and Y. Wang, "Magnetoelectric magnetic field sensors: A review," Sensors **21**(18), 6232 (2021).
[414]W. Hu, G. Z. Lum, M. Mastrangeli, and M. Sitti, "Small-scale soft-bodied robot with multimodal locomotion," Nature **554**(7690), 81–85 (2018).
[415]Y. Kim, H. Yuk, R. Zhao, S. A. Chester, and X. Zhao, "Printing ferromagnetic domains for untethered fast-transforming soft materials," Nature **558**(7709), 274–279 (2018).
[416]S. Ding, M. Wang, H. Yang, F. Hu, Z. Dai, M. Lei, Q. Zhou, D. Zhao, Y. Gao, and J. Zhong, "Sweeping-responsive interface using the intrinsic polarity of magnetized micropillars for self-powered and high-capacity human-machine interaction," Nano Energy **102**, 107671 (2022).
[417]H. Wu, X. Zhang, Z. Ma, C. Zhang, J. Ai, P. Chen, C. Yan, B. Su, and Y. Shi, "A material combination concept to realize 4D printed products with newly emerging property/functionality," Adv. Sci. **7**(9), 1903208 (2020).
[418]S. Wu, J. Eichenberger, J. Dai, Y. Chang, N. Ghalichechian, and R. R. Zhao, "Magnetically actuated reconfigurable metamaterials as conformal electromagnetic filters," Adv. Intelligent Syst. **4**(9), 2200106 (2022).
[419]G. Yun, S.-Y. Tang, S. Sun, D. Yuan, Q. Zhao, L. Deng, S. Yan, H. Du, M. D. Dickey, and W. Li, "Liquid metal-filled magnetorheological elastomer with positive piezoconductivity," Nat. Commun. **10**(1), 1300 (2019).
[420]V. Annapureddy, M. Kim, H. Palneedi, H. Y. Lee, S. Y. Choi, W. H. Yoon, D. S. Park, J. J. Choi, B. D. Hahn, and C. W. Ahn, "Low-loss piezoelectric single-crystal fibers for enhanced magnetic energy harvesting with magnetoelectric composite," Adv. Energy Mater. **6**(24), 1601244 (2016).
[421]J. Ryu, J.-E. Kang, Y. Zhou, S.-Y. Choi, W.-H. Yoon, D.-S. Park, J.-J. Choi, B.-D. Hahn, C.-W. Ahn, and J.-W. Kim, "Ubiquitous magneto-mechano-electric generator," Energy Environ. Sci. **8**(8), 2402–2408 (2015).
[422]D. Champier, "Thermoelectric generators: A review of applications," Energy Convers. Manage. **140**, 167–181 (2017).
[423]B. Russ, A. Glaudell, J. J. Urban, M. L. Chabinyc, and R. A. Segalman, "Organic thermoelectric materials for energy harvesting and temperature control," Nat. Rev. Mater. **1**(10), 1–14 (2016).
[424]T. M. Tritt and M. Subramanian, "Thermoelectric materials, phenomena, and applications: A bird's eye view," MRS Bull. **31**(3), 188–198 (2006).
[425]M. S. Dresselhaus, G. Chen, M. Y. Tang, R. Yang, H. Lee, D. Wang, Z. Ren, J. P. Fleurial, and P. Gogna, "New directions for low-dimensional thermoelectric materials," Adv. Mater. **19**(8), 1043–1053 (2007).
[426]E. Mueller, Č. Drašar, J. Schilz, and W. Kaysser, "Functionally graded materials for sensor and energy applications," Mater. Sci. Eng, A **362**(1-2), 17–39 (2003).
[427]I. Shiota and Y. Miyamoto, *Functionally Graded Materials 1996* (Elsevier, 1997).
[428]P. H. Ngan, D. V. Christensen, G. J. Snyder, L. T. Hung, S. Linderoth, N. V. Nong, and N. Pryds, "Towards high efficiency segmented thermoelectric unicouples," Phys. Status Solidi A **211**(1), 9–17 (2014).
[429]Q. Zhang, J. Liao, Y. Tang, M. Gu, C. Ming, P. Qiu, S. Bai, X. Shi, C. Uher, and L. Chen, "Realizing a thermoelectric conversion efficiency of 12% in bismuth telluride/skutterudite segmented modules through full-parameter optimization and energy-loss minimized integration," Energy Environ. Sci. **10**(4), 956–963 (2017).
[430]J. Schilz, L. Helmers, W. Müller, and M. Niino, "A local selection criterion for the composition of graded thermoelectric generators," J. Appl. Phys. **83**(2), 1150–1152 (1998).
[431]G. J. Snyder and E. S. Toberer, "Complex thermoelectric materials," Nat. Mater. **7**(2), 105–114 (2008).
[432]T. Wallace, Z.-H. Jin, and J. Su, "Efficiency of a sandwiched thermoelectric material with a graded interlayer and temperature-dependent properties," J. Electron. Mater. **45**, 2142–2149 (2016).
[433]R. D. Snyder, E. L. Thomas, and A. A. Voevodin, "Material optimization via combinatorial deposition and analysis for thermoelectric thin films," Thin Solid Films **596**, 233–241 (2015).
[434]G. Han, W. Zhu, S. Guo, J. Zhou, Y. Liu, and Y. Deng, "Combinatorial screening via high-throughput preparation: Thermoelectric performance optimization for n-type Bi–Te–Se film with high average zT>1," J. Mater. Sci. Technol. **160**, 18–27 (2023).
[435]M. Goto, M. Sasaki, Y. Xu, T. Zhan, Y. Isoda, and Y. Shinohara, "Control of p-type and n-type thermoelectric properties of bismuth telluride thin films by combinatorial sputter coating technology," Appl. Surf. Sci. **407**, 405–411 (2017).
[436]H. Cheng, Q. Le, Z. Liu, Q. Qian, Y. Zhao, and J. Ouyang, "Ionic thermoelectrics: Principles, materials and applications," J. Mater. Chem. C **10**(2), 433–450 (2022).
[437]S. Sun, M. Li, X. L. Shi, and Z. G. Chen, "Advances in ionic thermoelectrics: From materials to devices," Adv. Energy Mater. **13**(9), 2203692 (2023).
[438]C. Chi, G. Liu, M. An, Y. Zhang, D. Song, X. Qi, C. Zhao, Z. Wang, Y. Du, and Z. Lin, "Reversible bipolar thermopower of ionic thermoelectric polymer composite for cyclic energy generation," Nat. Commun. **14**(1), 306 (2023).
[439]C.-Y. Lee, Y.-T. Lin, S.-H. Hong, C.-H. Wang, U.-S. Jeng, S.-H. Tung, and C.-L. Liu, "Mixed Ionic–electronic conducting hydrogels with carboxylated carbon nanotubes for high performance wearable thermoelectric harvesters," ACS Appl. Mater. Interfaces **15**(48), 56072–56083 (2023).
[440]H. Wang, D. Zhao, Z. U. Khan, S. Puzinas, M. P. Jonsson, M. Berggren, and X. Crispin, "Ionic thermoelectric figure of merit for charging of supercapacitors," Adv. Elect. Mater. **3**(4), 1700013 (2017).
[441]C.-Y. Wang, "Fundamental models for fuel cell engineering," Chem. Rev. **104**(10), 4727–4766 (2004).
[442]X. Tai, A. Zhakeyev, H. Wang, K. Jiao, H. Zhang, and J. Xuan, "Accelerating fuel cell development with additive manufacturing technologies: State of the art, opportunities and challenges," Fuel Cells **19**(6), 636–650 (2019).
[443]N. Mahato, A. Banerjee, A. Gupta, S. Omar, and K. Balani, "Progress in material selection for solid oxide fuel cell technology: A review," Prog. Mater. Sci. **72**, 141–337 (2015).
[444]K. C. Wincewicz and J. S. Cooper, "Taxonomies of SOFC material and manufacturing alternatives," J. Power Sources **140**(2), 280–296 (2005).
[445]P. A. Connor, X. Yue, C. D. Savaniu, R. Price, G. Triantafyllou, M. Cassidy, G. Kerherve, D. J. Payne, R. C. Maher, and L. F. Cohen, "Tailoring SOFC electrode microstructures for improved performance," Adv. Energy Mater. **8**(23), 1800120 (2018).
[446]A. De, B. Ramasubramian, S. Ramakrishna, and V. Chellappan, "Advances in additive manufacturing techniques for electrochemical energy storage," Adv. Mater. Technol. **9**(4), 2301439 (2024).
[447]J. Y. Jung, H. Jeong, Y. J. Kim, S. M. Cho, Y. Jang, and H. Kim, "Hierarchically coated halide layers: enhancing the performance at composite cathode interfaces in solid-state Li–metal batteries," J. Mater. Chem A. **12**(21), 12405–12411 (2024).
[448]C. Roitzheim, Y. J. Sohn, L.-Y. Kuo, G. Häuschen, M. Mann, D. Sebold, M. Finsterbusch, P. Kaghazchi, O. Guillon, and D. Fattakhova-Rohlfing, "All-solid-state Li batteries with NCM–garnet-based composite cathodes: The impact of NCM composition on material compatibility," ACS Appl. Energy Mater. **5**(6), 6913–6926 (2022).
[449]M. Bertrand, S. Rousselot, D. Aymé-Perrot, and M. Dollé, "Compatibility assessment of solid ceramic electrolytes and active materials based on thermal dilatation for the development of solid-state batteries," Mater. Adv. **2**(9), 2989–2999 (2021).
[450]J. Xie, X. Yang, S. Zhou, and D. Wang, "Comparing one-and two-dimensional heteronanostructures as silicon-based lithium ion battery anode materials," ACS Nano **5**(11), 9225–9231 (2011).
[451]I. Meyer, M. Oel, T. Ehlers, and R. Lachmayer, "Additive manufacturing of multi-material parts–Design guidelines for manufacturing of 316L/CuCrZr in laser powder bed fusion," Heliyon **9**(8), e18301 (2023).
[452]Q. Zheng, D. Chalise, M. Jia, Y. Zeng, M. Zeng, M. Saeidi-Javash, A. N. M. Tanvir, G. UahengoJr, S. Kaur, J. E. Garay *et al.*, "Structured illumination with thermal imaging (SI-TI): A dynamically reconfigurable metrology for parallelized thermal transport characterization," Appl. Phys. Rev. **9**(2), 021411 (2022).
[453]M. Vaezi, S. Chianrabutra, B. Mellor, and S. Yang, "Multiple material additive manufacturing–Part 1: A review: This review paper covers a decade of research on multiple material additive manufacturing technologies which can produce complex geometry parts with different materials," Virtual Phys. Prototyping **8**(1), 19–50 (2013).
[454]E. S. Rountree, B. D. McCarthy, T. T. Eisenhart, and J. L. Dempsey, "Evaluation of homogeneous electrocatalysts by cyclic voltammetry," Inorg. Chem. **53**(19), 9983–10002 (2014).

[455]R. Pachimatla, M. Thomas, S. R. OC, and R. Srinivasan, "Analysis of instabilities in electrochemical systems using nonlinear electrochemical impedance spectroscopy," J. Electrochem. Soc. **166**(8), H304 (2019).
[456]Y. Zheng, Z. Lin, W. Chen, B. Liang, H. Du, R. Yang, X. He, Z. Tang, and X. Gui, "Flexible, sandwich-like CNTs/$NiCo_2O_4$ hybrid paper electrodes for all-solid state supercapacitors," J. Mater. Chem A. **5**(12), 5886–5894 (2017).
[457]J. Li, Y. Wang, and D. Ba, "Characterization of semiconductor surface conductivity by using microscopic four-point probe technique," Phys. Procedia **32**, 347–355 (2012).
[458]L. Yao, D. Yang, Q. Tao, Z. Zhang, J. Luo, Y. Yan, and X. Tang, "Accelerated measurement of electrical resistivity and Seebeck coefficient for thin-layer thermoelectric materials," Meas. Sci. Technol. **34**(9), 095908 (2023).
[459]A. Coats and J. Redfern, "Thermogravimetric analysis. A review," Analyst **88**(1053), 906–924 (1963).
[460]Y. Wang, K. Zaghib, A. Guerfi, F. F. Bazito, R. M. Torresi, and J. Dahn, "Accelerating rate calorimetry studies of the reactions between ionic liquids and charged lithium ion battery electrode materials," Electrochim. Acta **52**(22), 6346–6352 (2007).
[461]G. W. H. Höhne, W. Hemminger, and H.-J. Flammersheim, *Differential Scanning Calorimetry* (Springer, 2003).
[462]D. M. Rowe, *CRC Handbook of Thermoelectrics* (CRC Press, 2018).
[463]D. G. Cahill, H. E. Fischer, T. Klitsner, E. Swartz, and R. Pohl, "Thermal conductivity of thin films: Measurements and understanding," J. Vacuum Sci. Technol. A: Vacuum Surf. Films **7**(3), 1259–1266 (1989).
[464]H. Iwasaki, M. Koyano, and H. Hori, "Evaluation of the figure of merit on thermoelectric materials by Harman method," Jpn. J. Appl. Phys. **41**(11R), 6606 (2002).
[465]Hidier, J. "Multimaterial 3D printing enables solid state batteries," Additive Manufacturing, 2022. See https://www.additivemanufacturing.media/articles/multimaterial-3d-printing-enables-solid-state-batteries (last accessed November 01, 2024).
[466]Metal AM, Case study: *The development of a multi-material heat sink by Additive Manufacturing using Aerosint technology* (Metal AM, 2023). See https://www.metal-am.com/articles/case-study-the-development-of-a-multi-material-heat-sink-by-additive-manufacturing-using-aerosint-technology/ (last accessed November 01, 2024).
[467]Jones, A. T. *Panasonic develops new multi-material 3D printer for the production of wearable electronics* (3D Printing Industry, 2023). See https://3dprintingindustry.com/news/panasonic-develops-new-multi-material-3d-printer-for-the-production-of-wearable-electronics-223038/ (last accessed November 01, 2024).
[468]L. Zhang, D. Chao, P. Yang, L. Weber, J. Li, T. Kraus, and H. J. Fan, "Flexible pseudocapacitive electrochromics via inkjet printing of additive-free tungsten oxide nanocrystal ink," Adv. Energy Mater. **10**(17), 2000142 (2020).
[469]J. Wu, Z. Ju, X. Zhang, X. Xu, K. J. Takeuchi, A. C. Marschilok, E. S. Takeuchi, and G. Yu, "Low-tortuosity thick electrodes with active materials gradient design for enhanced energy storage," ACS Nano **16**(3), 4805–4812 (2022).
[470]J. Yang, Y. Li, A. Mijailovic, G. Wang, J. Xiong, K. Mathew, W. Lu, B. W. Sheldon, and Q. Wu, "Gradient porosity electrodes for fast charging lithium-ion batteries," J. Mater. ChemA. **10**(22), 12114–12124 (2022).
[471]X. Zhang, Z. Hui, S. T. King, J. Wu, Z. Ju, K. J. Takeuchi, A. C. Marschilok, A. C. West, E. S. Takeuchi, and L. Wang, "Gradient architecture design in scalable porous battery electrodes," Nano Lett. **22**(6), 2521–2528 (2022).
[472]T. W. Gräwert and D. I. Svergun, "Structural modeling using solution small-angle X-ray scattering (SAXS)," J. Mol. Biol. **432**(9), 3078–3092 (2020).
[473]C. M. Jeffries, J. Ilavsky, A. Martel, S. Hinrichs, A. Meyer, J. S. Pedersen, A. V. Sokolova, and D. I. Svergun, "Small-angle X-ray and neutron scattering," Nat. Rev. Methods Primers **1**(1), 70 (2021).
[474]F. Malamud, E. Polatidis, M. Busi, J. Capek, L. Deillon, M. Bambach, P. Zehnder, A. Losko, and M. Strobl, "Bragg edge imaging characterization of multi-material laser powder-bed fusion specimens," J. Phys.: Conf. Ser. **2605**, 012030 (2023).
[475]N. An, S. Shuai, T. Hu, C. Chen, J. Wang, and Z. Ren, "Application of synchrotron X-ray imaging and diffraction in additive manufacturing: A review," Acta Metall. Sin. (English Lett.) **35**, 1–24 (2022).
[476]P. Spoerk-Erdely, P. Staron, J. Liu, N. Kashaev, A. Stark, K. Hauschildt, E. Maawad, S. Mayer, and H. Clemens, "Exploring structural changes, manufacturing, joining, and repair of intermetallic γ-TiAl-based alloys: Recent progress enabled by in situ synchrotron X-ray techniques," Adv. Eng. Mater. **23**(11), 2000947 (2021).
[477]V. Arrighi and J. Higgins, "Structural investigation of polymers by neutron scattering," Plast., Rubber Composites **33**(8), 313–330 (2004).
[478]W. Hua, K. Mitchell, L. S. Kariyawasam, C. Do, J. Chen, L. Raymond, N. Valentin, R. Coulter, Y. Yang, and Y. Jin, "Three-dimensional printing in stimuli-responsive yield-stress fluid with an interactive dual microstructure," ACS Appl. Mater. Interfaces **14**(34), 39420–39431 (2022).
[479]T. H. Kang, B. G. Compton, W. T. Heller, S. Qian, G. S. Smith, V. S. Urban, C. E. Duty, and C. Do, "Potentials with small-angle neutron scattering technique for understanding structure–property relation of 3D-printed materials," Polym. Eng. Sci. **59**(s2), E65–E70 (2019).
[480]L. Sperling, "Characterization of polymer conformation and morphology through small-angle neutron scattering—A literature review," Polym. Eng. Sci. **24**(1), 1–21 (1984).
[481]X. Tang, C. Liu, J. Chen, R. Kumar, C. C. Bowland, T. Saito, B. E. Dial, J. K. Keum, C. Do, and X. C. Chen, "Probing the interface structure of block copolymer compatibilizers in semicrystalline polymer blends," J. Appl. Polym. Sci. **141**(14), e55178 (2024).
[482]O. Bunk, M. Bech, T. Jensen, R. Feidenhans, T. Binderup, A. Menzel, and F. Pfeiffer, "Multimodal X-ray scatter imaging," New J. Phys. **11**(12), 123016 (2009).
[483]İH. Uzun, M. A. Malkoç, A. Keleş, and A. T. Öğreten, "3D micro-CT analysis of void formations and push-out bonding strength of resin cements used for fiber post cementation," J. Adv. Prosthodont. **8**(2), 101–109 (2016).
[484]Y. Liu, O. C. Esan, Z. Pan, and L. An, "Machine learning for advanced energy materials," Energy AI **3**, 100049 (2021).
[485]M. Zeng, S. Yuan, D. Huang, and Z. Cheng, "Accelerated design of catalytic water-cleaning nanomotors via machine learning," ACS Appl. Mater. Interfaces **11**(43), 40099–40106 (2019).
[486]Y. Liu, B. Guo, X. Zou, Y. Li, and S. Shi, "Machine learning assisted materials design and discovery for rechargeable batteries," Energy Storage Mater. **31**, 434–450 (2020).
[487]W. Shang, M. Zeng, A. N. M. Tanvir, K. Wang, M. Saeidi-Javash, A. Dowling, T. Luo, and Y. Zhang, "Hybrid data-driven discovery of high-performance silver selenide-based thermoelectric composites," Adv. Mater. **35**(47), e2212230 (2023).
[488]K. Wang, M. Zeng, J. Wang, W. Shang, Y. Zhang, T. Luo, and A. W. Dowling, "When physics-informed data analytics outperforms black-box machine learning: A case study in thickness control for additive manufacturing," Digital Chem. Eng. **6**, 100076 (2023).
[489]K. Wang, M. Saeidi-Javash, M. Zeng, Z. Liu, Y. Zhang, T. Luo, and A. W. Dowling, "Gaussian process regression machine learning models for photonic sintering," in *Computer Aided Chemical Engineering*, edited by Y. Yamashita, M. Kano (Elsevier, 2022) Vol. 49, pp. 1819–1824.
[490]M. Saeidi-Javash, K. Wang, M. Zeng, T. Luo, A. W. Dowling, and Y. Zhang, "Machine learning-assisted ultrafast flash sintering of high-performance and flexible silver–selenide thermoelectric devices," Energy Environ. Sci. **15**(12), 5093–5104 (2022).
[491]Z. Si, D. Zhou, J. Yang, and X. Lin, "2D material property characterizations by machine-learning-assisted microscopies," Appl. Phys. A **129**(4), 248 (2023).
[492]L. F. Gerlein, J. A. Benavides-Guerrero, and S. G. Cloutier, "Photonic post-processing of a multi-material transparent conductive electrode architecture for optoelectronic device integration," RSC Adv. **14**(7), 4748–4758 (2024).